

Supplementary Information

The configuration of Northern Hemisphere ice sheets through the Quaternary

Batchelor *et al.*

This document contains details of the data sources used to inform our reconstructions of the maximum, minimum and best-estimate Northern Hemisphere (NH) ice-sheet extents. For each time-slice, the following are included:

- In [Supplementary Figures](#), a raw data map showing the empirical and modelled data that were used to draw the ice-sheet reconstructions, alongside a map showing the hypothesised maximum, minimum and best-estimate ice-sheet extents. [Supplementary Figure 1](#) shows the locations of the places mentioned in this document.
- In [Supplementary Tables](#), a table listing the empirical and modelled data that were used to draw the ice-sheet reconstructions.
- In [Supplementary Notes](#), explanatory text that details the decisions made in reconstructing the maximum, minimum and best-estimate ice-sheet extents. Overall and ice-sheet-wide robustness scores are also provided for each reconstruction. The robustness scores, which range from 0 (low) to 5 (high), are a subjective assessment of the amount and reliability of the source data from which the ice-sheet extent was constructed ([Methods](#)).

Shapefiles of our reconstructions, as well as the digitised and georeferenced empirical and modelled data, are available on the Open Science Framework [<https://osf.io/7jen3/>].

Table of Contents

Supplementary Figures (*reconstructions of NH ice-sheet extent at specified time slices*)

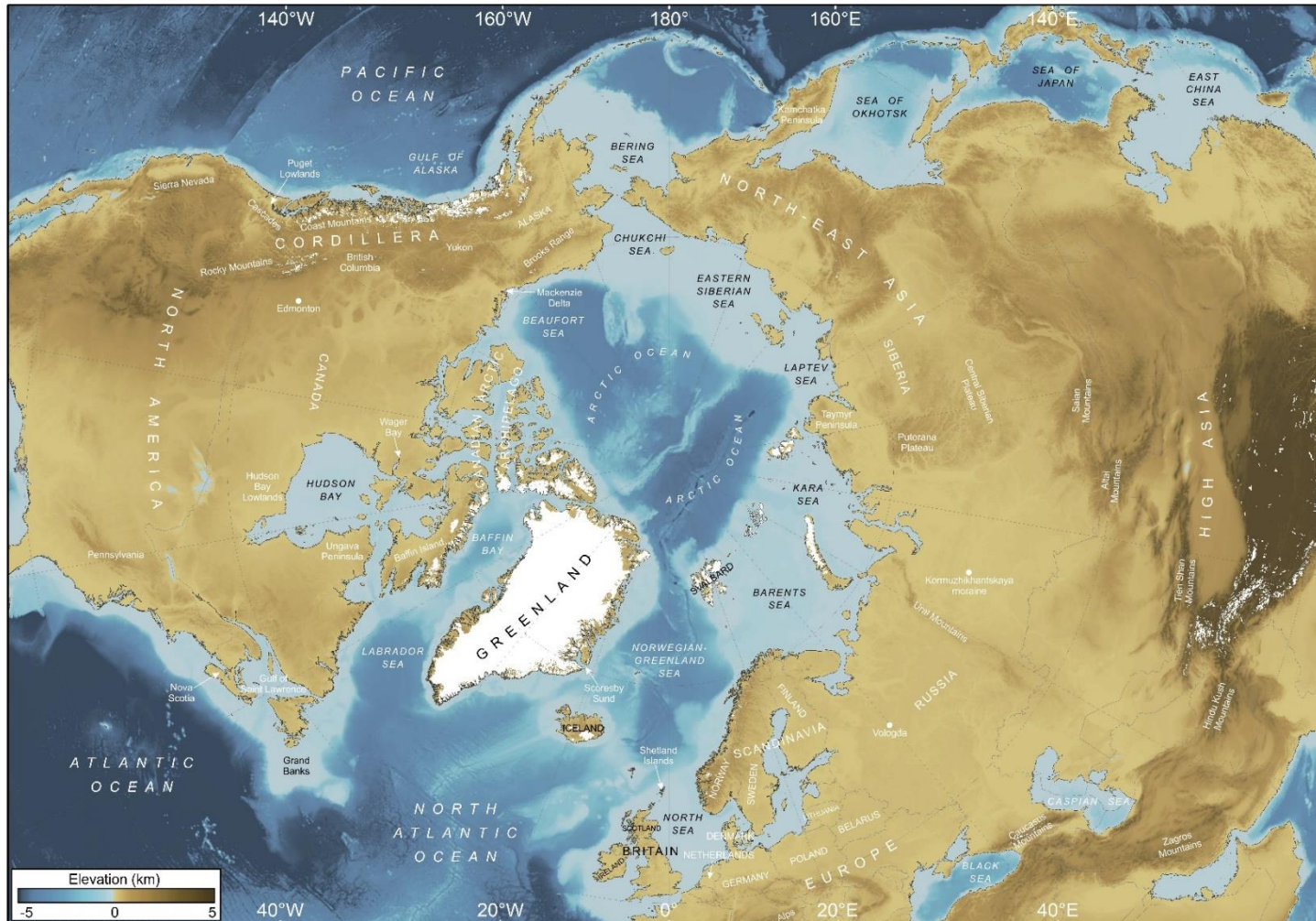
<u>Supplementary Figure 1. Location map showing the places that are referred to in this document.</u>	4
<u>Supplementary Figure 2. 30 ka and 35 ka.</u>	5
<u>Supplementary Figure 3. 40 ka and 45 ka.</u>	6
<u>Supplementary Figure 4. MIS 4 (58–72 ka) and MIS 5a (72–86 ka).</u>	7
<u>Supplementary Figure 5. MIS 5b (86–92 ka) and MIS 5c (92–108 ka).</u>	8
<u>Supplementary Figure 6. MIS 5d (108–117 ka) and MIS 6 (132–190 ka).</u>	9
<u>Supplementary Figure 7. MIS 8 (243–279 ka) and MIS 10 (337–365 ka).</u>	10
<u>Supplementary Figure 8. MIS 12 (429–477 ka) and MIS 16 (622–677 ka).</u>	11
<u>Supplementary Figure 9. MIS 20–24 (790–928 ka) and the early Matuyama Chron (1.78–2.6 Ma).</u>	12
<u>Supplementary Figure 10. Late Gauss Chron (2.6–3.59 Ma).</u>	13

Supplementary Tables (*published evidence for the spatial extent of NH glaciation at specified time slices*)

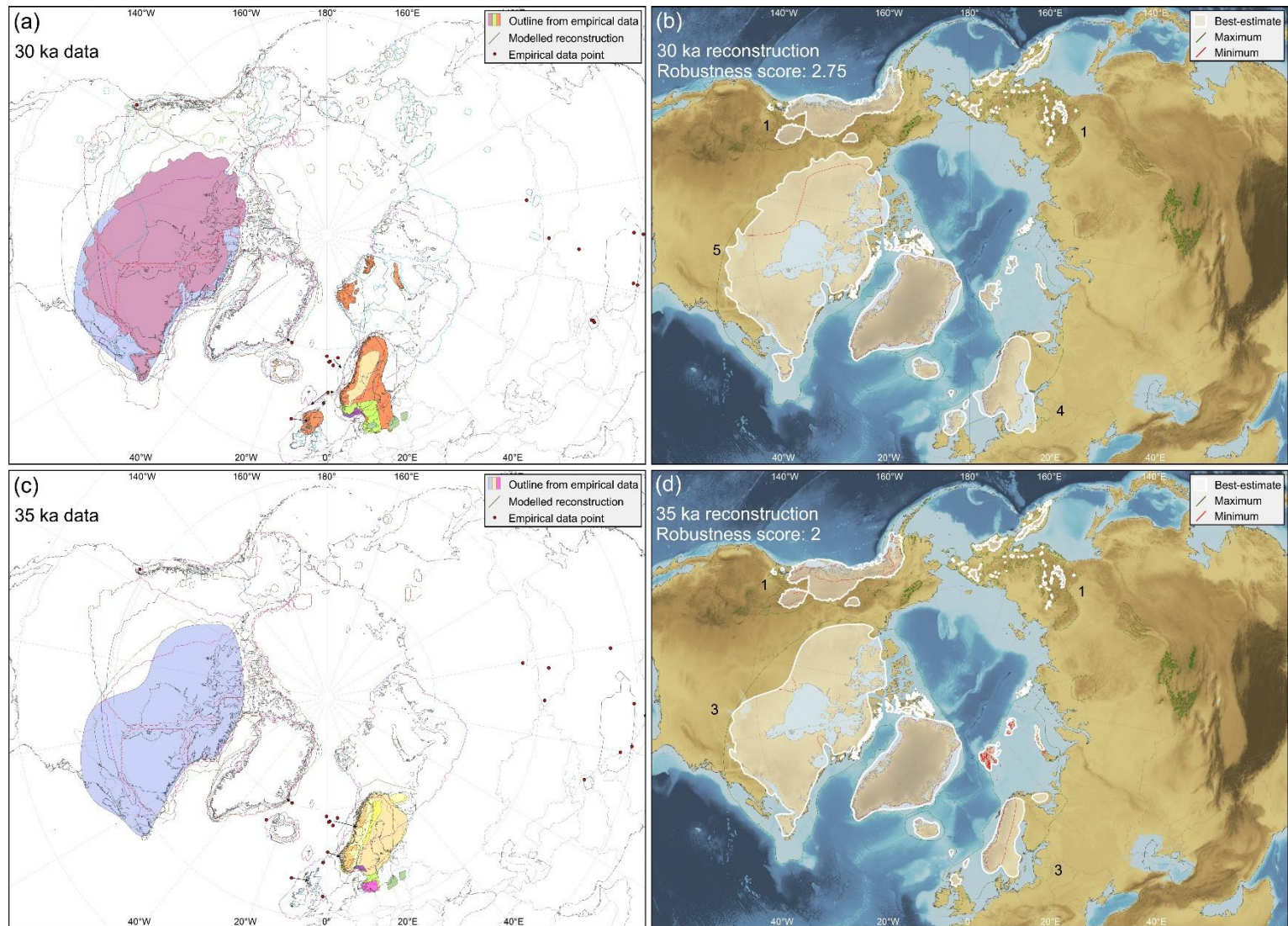
<u>Supplementary Table 1. 30 ka.</u>	14
<u>Supplementary Table 2. 35 ka.</u>	16
<u>Supplementary Table 3. 40 ka</u>	18
<u>Supplementary Table 4. 45 ka.</u>	20
<u>Supplementary Table 5. MIS 4</u>	22
<u>Supplementary Table 6. MIS 5a.</u>	25
<u>Supplementary Table 7. MIS 5b.</u>	27
<u>Supplementary Table 8. MIS 5c.</u>	29
<u>Supplementary Table 9. MIS 5d.</u>	30
<u>Supplementary Table 10. MIS 6.</u>	32
<u>Supplementary Table 11. MIS 8.</u>	35
<u>Supplementary Table 12. MIS 10.</u>	36

<u>Supplementary Table 13. MIS 12.</u>	37
<u>Supplementary Table 14. MIS 16.</u>	38
<u>Supplementary Table 15. MIS 20–24.</u>	39
<u>Supplementary Table 16. The early Matuyama Chron.</u>	40
<u>Supplementary Table 17. The late Gauss Chron.</u>	41
<u>Supplementary Notes</u> (<i>explanatory text that details the decisions made in reconstructing the maximum, minimum and best-estimate ice-sheet extents</i>)	
<u>Supplementary Note 1: The Last Glacial Maximum (LGM)</u>	42
<u>Supplementary Note 2: 30 ka</u>	43
<u>Supplementary Note 3: 35 ka</u>	45
<u>Supplementary Note 4: 40 ka</u>	47
<u>Supplementary Note 5: 45 ka</u>	49
<u>Supplementary Note 6: MIS 4 (58–72 ka)</u>	51
<u>Supplementary Note 7: MIS 5a (72–86 ka)</u>	54
<u>Supplementary Note 8: MIS 5b (86–92 ka)</u>	56
<u>Supplementary Note 9: MIS 5c (92–108 ka)</u>	58
<u>Supplementary Note 10: MIS 5d (108–117 ka)</u>	60
<u>Supplementary Note 11: MIS 6 (132–190 ka)</u>	62
<u>Supplementary Note 12: MIS 8 (243–279 ka)</u>	64
<u>Supplementary Note 13: MIS 10 (337–365 ka)</u>	67
<u>Supplementary Note 14: MIS 12 (429–477 ka)</u>	70
<u>Supplementary Note 15: MIS 16 (622–677 ka)</u>	72
<u>Supplementary Note 16: MIS 20–24 (790–928 ka)</u>	74
<u>Supplementary Note 17: Early Matuyama palaeomagnetic Chron (1.78–2.6 Ma)</u>	76
<u>Supplementary Note 18: Late Gauss palaeomagnetic Chron (2.6–3.59 Ma)</u>	79
<u>Supplementary References</u>	82

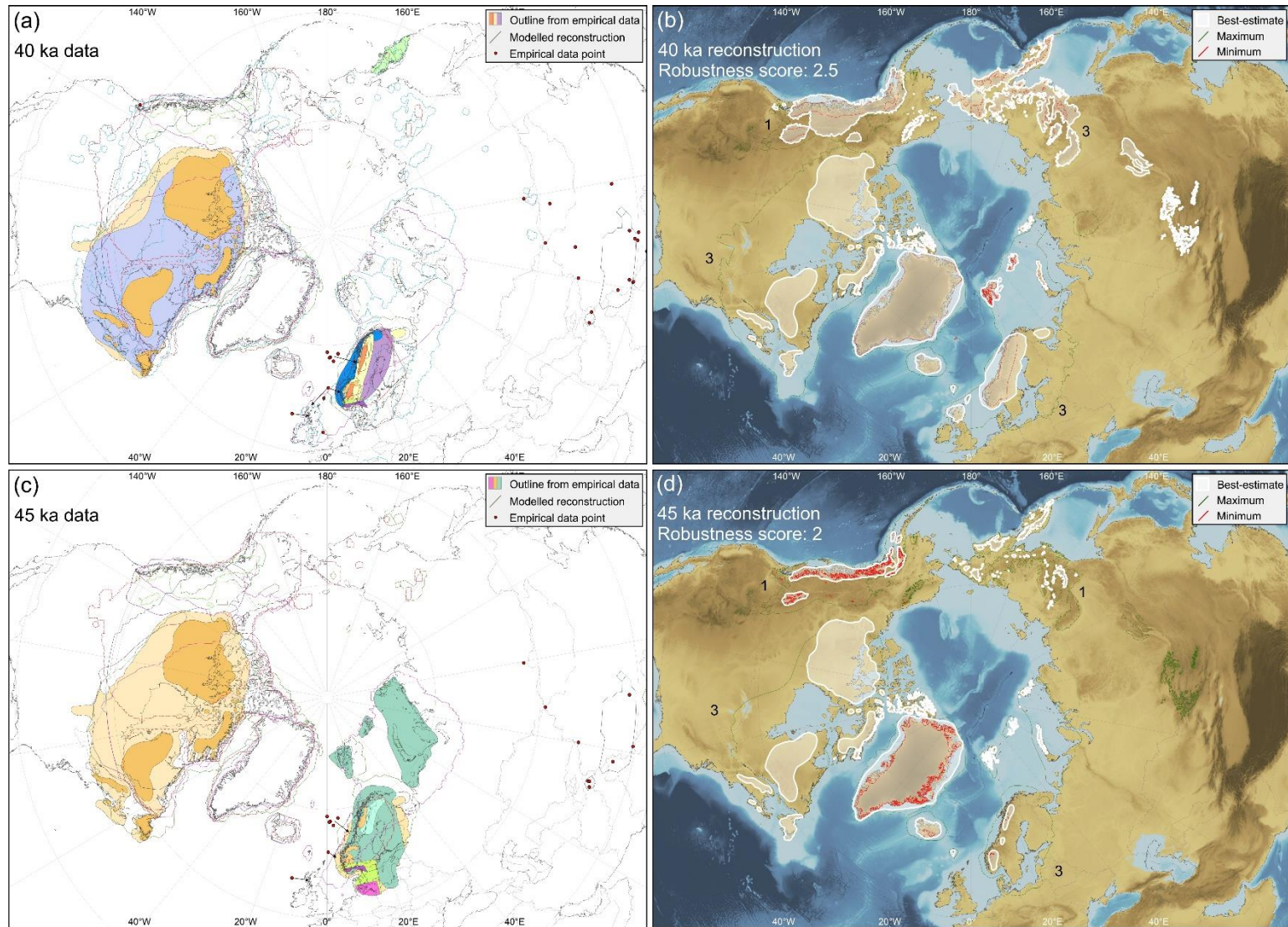
Supplementary Figures



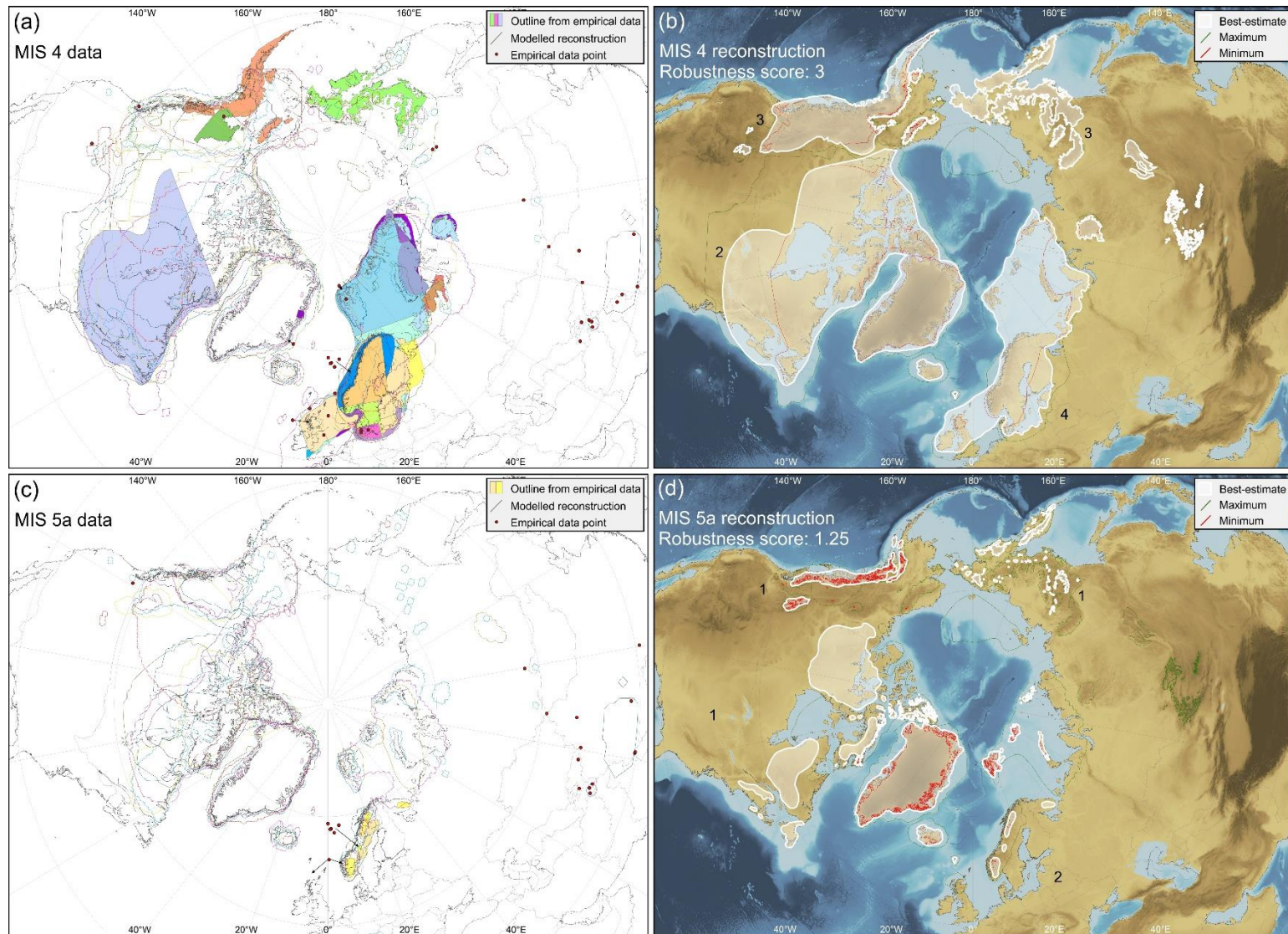
Supplementary Figure 1. Location map showing the places that are referred to in this document. Background is ETOPO1 1 arc-minute global relief model of Earth's surface¹.



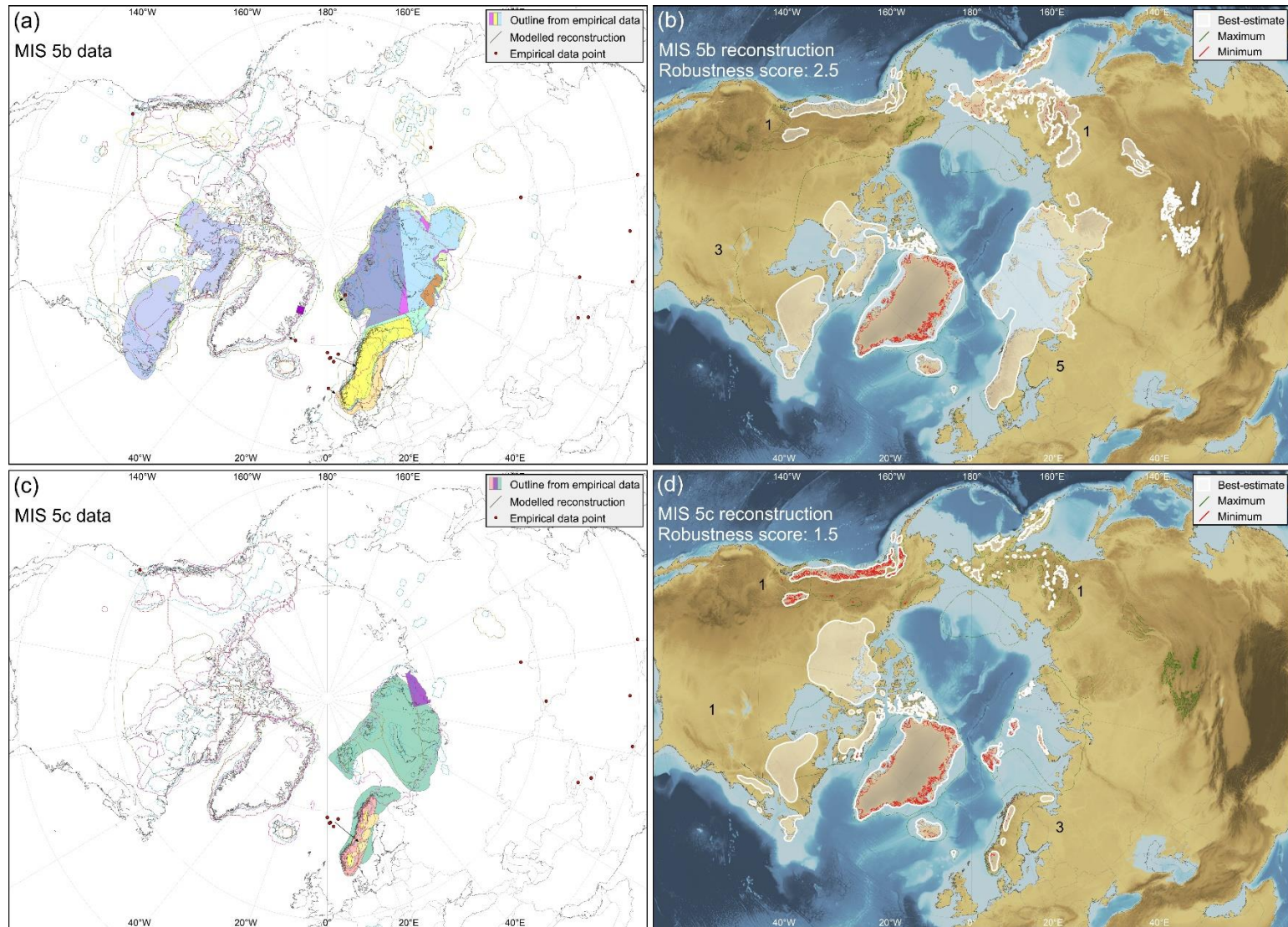
Supplementary Figure 2. Reconstructions of NH ice-sheet extent at 30 ka and 35 ka. **a**, compilation of previously published data on ice-sheet extent at 30 ka. **b**, maximum, minimum and best-estimate ice-sheet reconstruction for 30 ka. **c**, compilation of previously published data on ice-sheet extent at 35 ka. **d**, maximum, minimum and best-estimate ice-sheet reconstruction for 35 ka. Colours in **a** and **c** correspond with those in [Supplementary Tables 1 and 2](#).



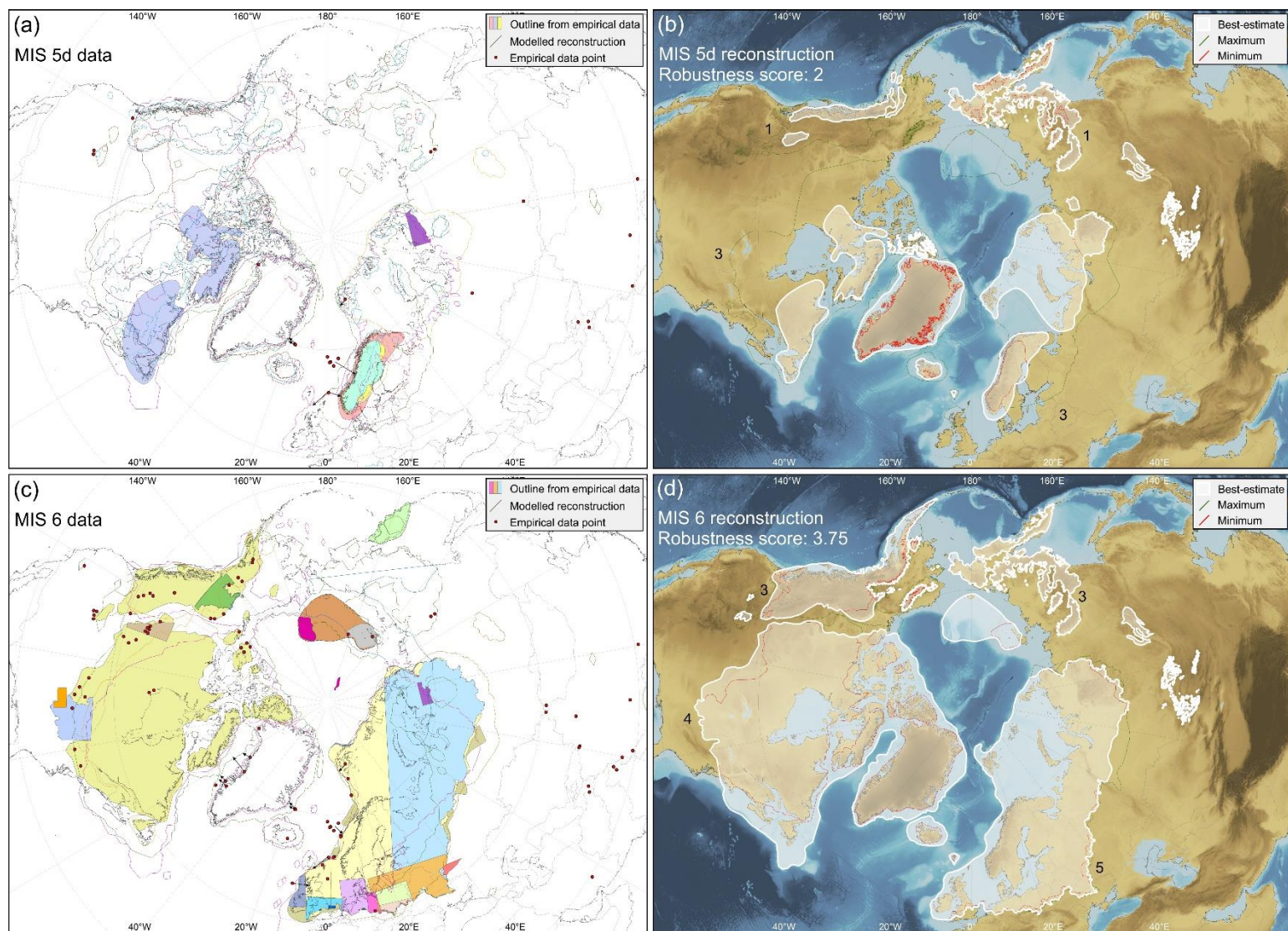
Supplementary Figure 3. Reconstructions of NH ice-sheet extent at 40 ka and 45 ka. See [Supplementary Tables 3 and 4](#) for key. **a**, compilation of published data on ice-sheet extent at 40 ka. **b**, maximum, minimum and best-estimate ice-sheet reconstruction for 40 ka. **c**, compilation of previously published data on ice-sheet extent at 45 ka. **d**, maximum, minimum and best-estimate ice-sheet reconstruction for 45 ka.



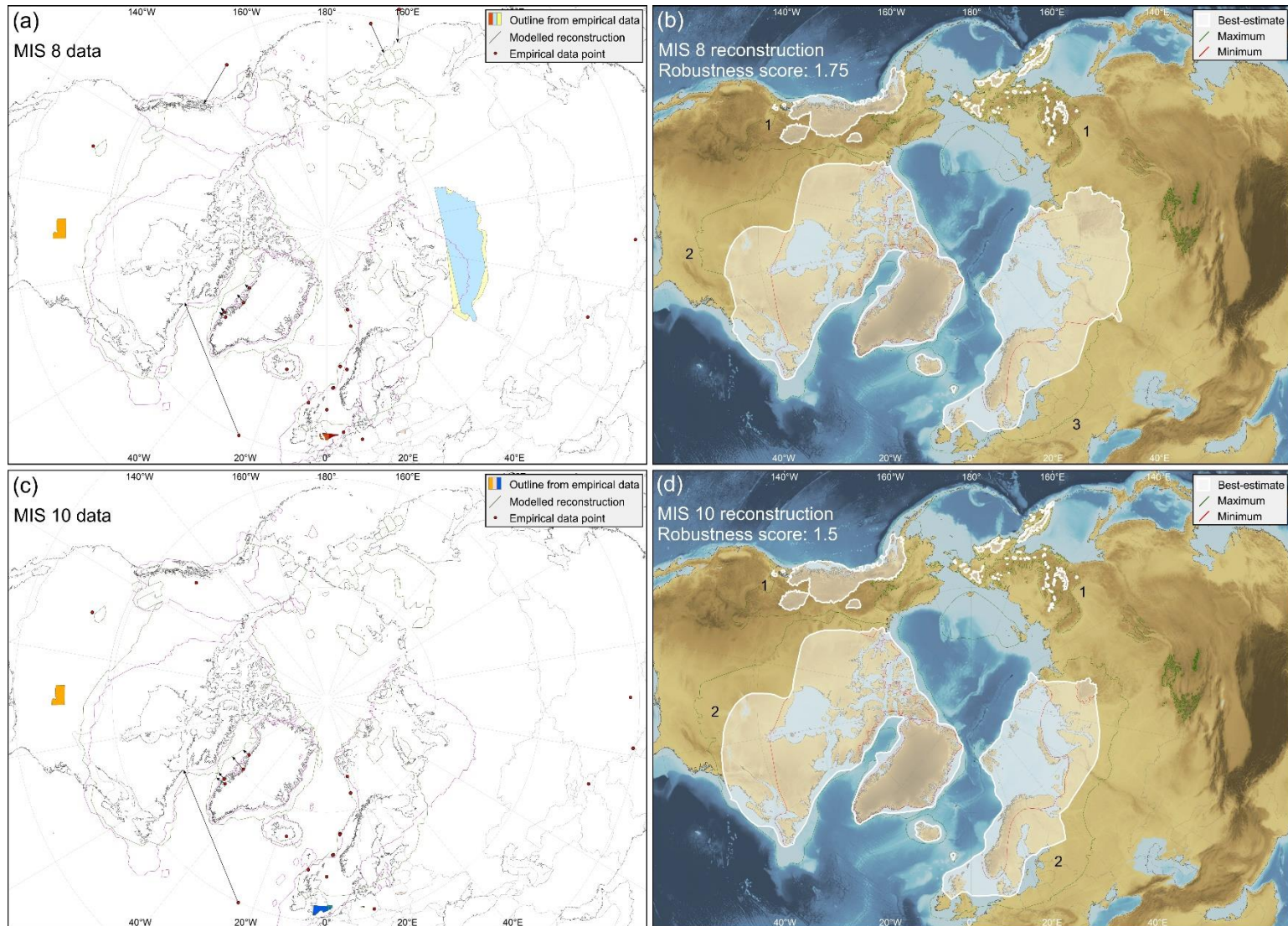
Supplementary Figure 4. Reconstructions of NH ice-sheet extent during MIS 4 (58–72 ka) and MIS 5a (72–86 ka). See [Supplementary Tables 5 and 6](#) for key. **a**, compilation of previously published data on ice-sheet extent during MIS 4. **b**, maximum, minimum and best-estimate ice-sheet reconstruction for MIS 4. **c**, compilation of previously published data on ice-sheet extent during MIS 5a. **d**, maximum, minimum and best-estimate ice-sheet reconstruction for MIS 5a.



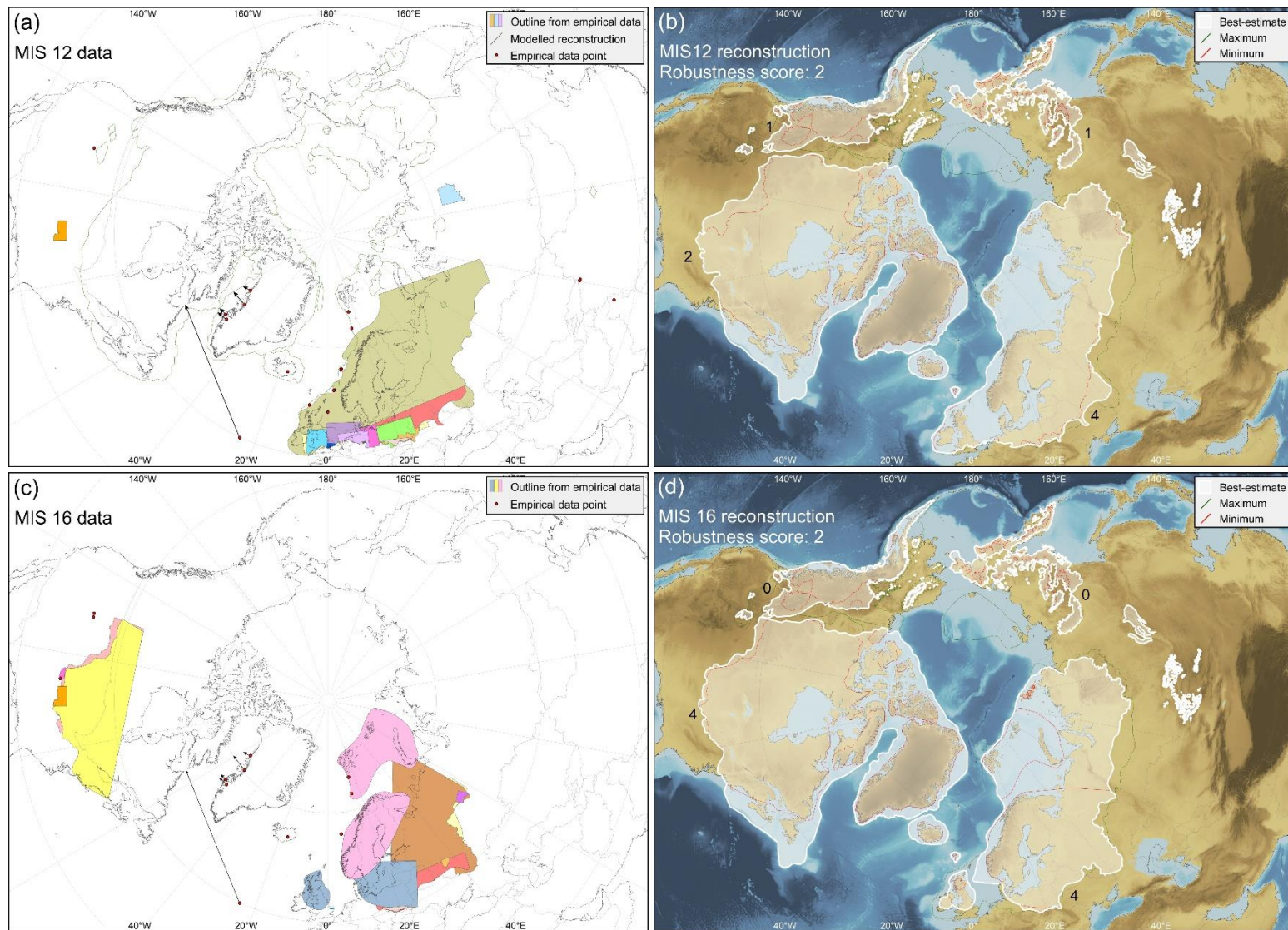
Supplementary Figure 5. Reconstructions of NH ice-sheet extent during MIS 5b (86–92 ka) and MIS 5c (92–108 ka). See [Supplementary Tables 7 and 8](#) for key. **a**, compilation of previously published data on ice-sheet extent during MIS 5b. **b**, maximum, minimum and best-estimate ice-sheet reconstruction for MIS 5b. **c**, compilation of previously published data on ice-sheet extent during MIS 5c. **d**, maximum, minimum and best-estimate ice-sheet reconstruction for MIS 5c.



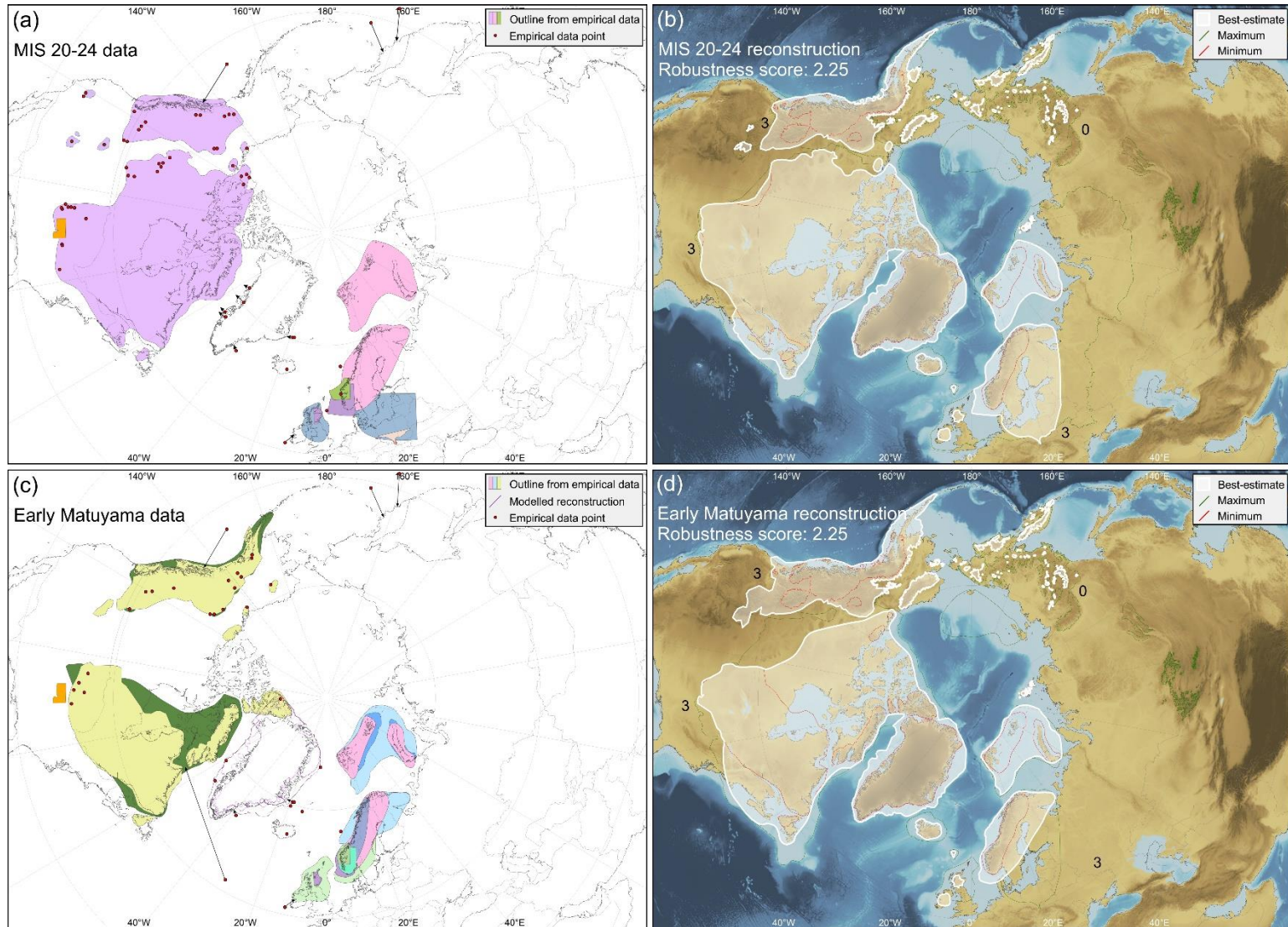
Supplementary Figure 6. Reconstructions of NH ice-sheet extent during MIS 5d (108–117 ka) and MIS 6 (132–190 ka). See [Supplementary Tables 9 and 10](#) for key. **a**, compilation of previously published data on ice-sheet extent during MIS 5d. **b**, maximum, minimum and best-estimate ice-sheet reconstruction for MIS 5d. **c**, compilation of previously published data on ice-sheet extent during MIS 6. **d**, maximum, minimum and best-estimate ice-sheet reconstruction for MIS 6.



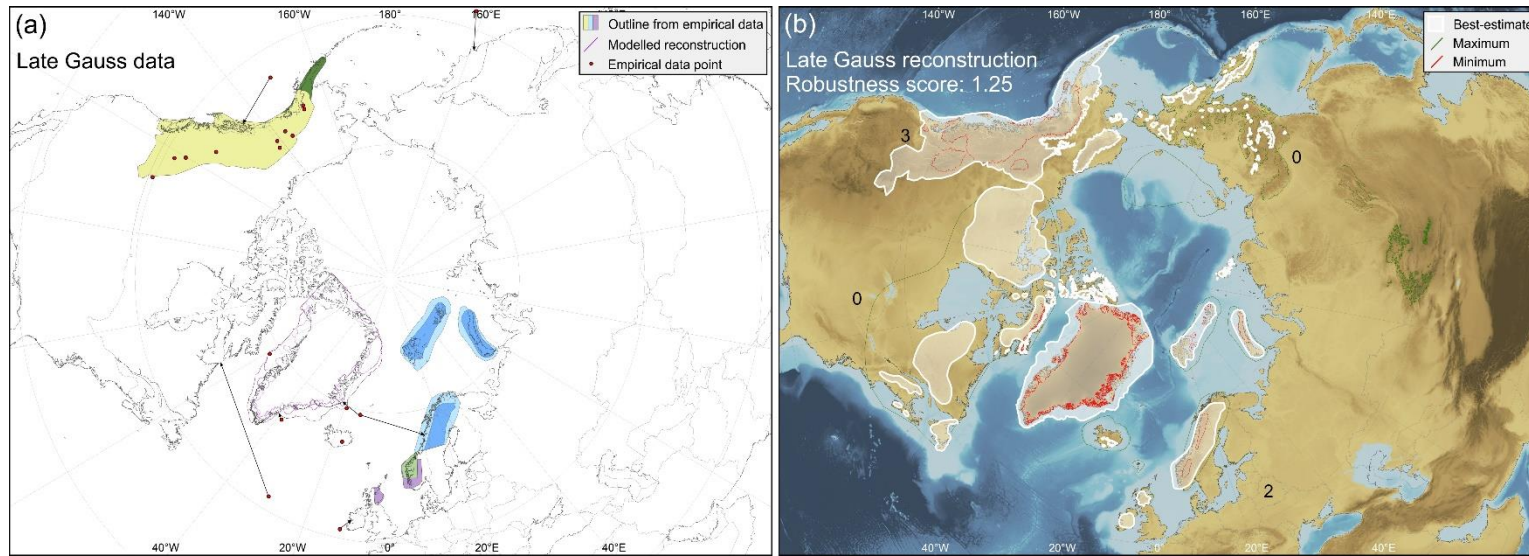
Supplementary Figure 7. Reconstructions of NH ice-sheet extent during MIS 8 (243–279 ka) and MIS 10 (337–365 ka). See [Supplementary Tables 11 and 12](#) for key. **a**, compilation of previously published data on ice-sheet extent during MIS 8. **b**, maximum, minimum and best-estimate ice-sheet reconstruction for MIS 8. **c**, compilation of previously published data on ice-sheet extent during MIS 10. **d**, maximum, minimum and best-estimate ice-sheet reconstruction for MIS 10.



Supplementary Figure 8. Reconstructions of NH ice-sheet extent during MIS 12 (429–477 ka) and MIS 16 (622–677 ka). See [Supplementary Tables 13 and 14](#) for key. **a**, compilation of previously published data on ice-sheet extent during MIS 12. **b**, maximum, minimum and best-estimate ice-sheet reconstruction for MIS 12. **c**, compilation of previously published data on ice-sheet extent during MIS 16. **d**, maximum, minimum and best-estimate ice-sheet reconstruction for MIS 16.



Supplementary Figure 9. Reconstructions of NH ice-sheet extent during MIS 20–24 (790–928 ka) and the early Matuyama magnetic Chron (1.78–2.6 Ma). See [Supplementary Tables 15 and 16](#) for key. **a**, compilation of previously published data on ice-sheet extent during MIS 20–24. **b**, maximum, minimum and best-estimate ice-sheet reconstruction for MIS 20-24. **c**, compilation of previously published data on ice-sheet extent during the early Matuyama Chron. **d**, maximum, minimum and best-estimate ice-sheet reconstruction for the early Matuyama Chron.



Supplementary Figure 10. Reconstructions of NH ice-sheet extent during the late Gauss magnetic Chron (2.6–3.59 Ma). See [Supplementary Table 17](#) for key. **a**, compilation of previously published data on ice-sheet extent during the late Gauss Chron. **b**, maximum, minimum and best-estimate ice-sheet reconstruction for the late Gauss Chron.

Supplementary Tables

30 ka

Key	Reference	Data type	Details
	Dyke <i>et al.</i> , 2002 ²	Empirical outline	LIS; only main ice sheet shown
	Houmark-Nielsen, 2010 ³	Empirical outline	Western EIS; spans MIS 3
	Hughes <i>et al.</i> , 2016 ⁴	Empirical outline	EIS; 30–32 ka
	Kleman <i>et al.</i> , 2010 ⁵	Empirical outline	LIS; late MIS 3
	Larsen <i>et al.</i> , 2009 ⁶	Empirical outline	Western EIS; 29–30 ka
	Marks, 2012 ⁷	Empirical outline	EIS; tentative outlines for 29 ka and 33–37 ka
	Olsen <i>et al.</i> , 2013 ⁸	Empirical outline	Western EIS; 29–30 ka
	Bonelli <i>et al.</i> , 2009 ⁹	Model	NH; spans 0–126 ka with 1 ka increments. Model driven by variations in orbital parameters and CO ₂ concentration.
	de Boer <i>et al.</i> , 2014 ¹⁰	Model	NH; spans 0–410 ka with 1 ka increments. Ice volume and temperature derived from benthic $\delta^{18}\text{O}$ stack.
	Ganopolski and Calov, 2011 ¹¹	Model	NH; spans 0–800 ka with 1 ka increments. Model driven by variations in orbital parameters and CO ₂ concentration.
	Heinemann <i>et al.</i> , 2014 ¹²	Model	NH; spans 0–78 ka with 1 ka increments. Model driven by variations in orbital parameters and CO ₂ concentration.
	Hubbard <i>et al.</i> , 2009 ¹³	Model	Western EIS; timeslices from 35.95–11.65 ka. Model driven by NGRIP ice core $\delta^{18}\text{O}$ curve and sea-level reconstruction.
	Lambeck <i>et al.</i> , 2010 ¹⁴	Model	Western EIS. Model constructed using existing empirical data.
	Patton <i>et al.</i> , 2017 ¹⁵	Model	Iceland; 31 ka. Model driven by temperature, precipitation and sea-level perturbations.
	Seguinot <i>et al.</i> , 2016 ¹⁶	Model	CIS; 30 ka GRIP. Model driven by temperature offsets from proxy records and calibrated against existing empirical data.
	Stokes <i>et al.</i> , 2012 ¹⁷	Model	CIS and LIS. Model calibrated against existing empirical data.
	Zweck and Huybrechts, 2005 ¹⁸	Model	NH; 30–120 ka with 10 k increments. Model parameters chosen to match empirical LGM ice extent.
●	Abramowski <i>et al.</i> , 2006 ¹⁹	Point-source	High Asia; ¹⁰ Be dating
●	Arzhannikhov <i>et al.</i> , 2015 ²⁰	Point-source	NE Asia; ¹⁰ Be dating
●	Baumann <i>et al.</i> , 1995 ²¹	Glacial curve	Western EIS; IRD. 5 data points shown.
●	Chevalier <i>et al.</i> , 2011 ²²	Point-source	High Asia; ¹⁰ Be dating
●	Hall, 2013 ²³	Point-source	Western EIS; geomorphology suggests ice cap over Shetland Islands between 10 and 40 ka
●	Hibbert <i>et al.</i> , 2010 ²⁴	IRD	Western EIS

Key	Reference	Data type	Details
●	Lehmkuhl, 1998 ²⁵	Point-source	High Asia; TL dating
●	Lekens <i>et al.</i> , 2009 ²⁶	Glacial curve	Western EIS; based on seismic data and IRD
●	Li <i>et al.</i> , 2014 ²⁷	Point-source	High Asia; ¹⁰ Be dating
●	Owen and Dortch, 2014 ²⁸	Point-source	High Asia; TCN, OSL and ¹⁴ C dating. 2 data points shown.
●	Owen <i>et al.</i> , 2010 ²⁹	Point-source	High Asia; ¹⁰ Be dating
●	Stein <i>et al.</i> , 1996 ³⁰	IRD	East GIS; IRD, $\delta^{18}\text{O}$ and ¹⁴ C dating
●	Stübner <i>et al.</i> , 2017 ³¹	Point-source	High Asia; ¹⁰ Be dating
●	Thackray, 2008 ³²	Point-source	LIS; ¹⁴ C and ³⁶ Cl dating

Supplementary Table 1. Published evidence for the spatial extent of Northern Hemisphere (NH) glaciation at 30 ka. IRD = ice-rafted debris; OSL = optically-stimulated luminescence; TCN = terrestrial cosmogenic nuclide; TL = thermoluminescence. Key corresponds with colours in [Supplementary Figure 2a](#).

35 ka

Key	Reference	Data type	Details
	Arnold <i>et al.</i> , 2002 ³³	Empirical outline	Western EIS; minimum extent during MIS 3
	Houmark-Nielsen, 2010 ³	Empirical outline	Western EIS; spans MIS 3
	Hughes <i>et al.</i> , 2016 ⁴	Empirical outline	EIS; 34–38 ka; min and max versions
	Kleman <i>et al.</i> , 2010 ⁵	Empirical outline	LIS
	Larsen <i>et al.</i> , 2009 ⁶	Empirical outline	Western EIS; 30–50 ka
	Mangerud <i>et al.</i> , 2011 ³⁴	Empirical outline	Northern EIS; 35–38 ka
	Marks, 2012 ⁷	Empirical outline	EIS; tentative outline for 33–37 ka
	Obst <i>et al.</i> , 2017 ³⁵	Empirical outline	EIS; 30–34k
	Olsen <i>et al.</i> , 2013 ⁸	Empirical outline	Western EIS; 33 ka
	Arnold <i>et al.</i> , 2002 ³³	Model	Western EIS; 36 ka. Model driven by GISP $\delta^{18}\text{O}$ ice core record.
	Bonelli <i>et al.</i> , 2009 ⁹	Model	NH; spans 0–126 ka with 1 ka increments. Model driven by variations in orbital parameters and CO_2 concentration.
	de Boer <i>et al.</i> , 2014 ¹⁰	Model	NH; spans 0–410 ka with 1 ka increments. Ice volume and temperature derived from benthic $\delta^{18}\text{O}$ stack.
	Ganopolski and Calov, 2011 ¹¹	Model	NH; spans 0–800 ka with 1 ka increments. Model driven by variations in orbital parameters and CO_2 concentration.
	Heinemann <i>et al.</i> , 2014 ¹²	Model	NH; spans 0–78 ka with 1 ka increments. Model driven by variations in orbital parameters and CO_2 concentration.
	Hubbard <i>et al.</i> , 2009 ¹³	Model	Western EIS; timeslices from 11.65–35.95 ka. Model driven by NGRIP ice core $\delta^{18}\text{O}$ curve and sea-level reconstruction.
	Lambeck <i>et al.</i> , 2010 ¹⁴	Model	Western EIS. Model constructed using existing empirical data.
●	Abramowski <i>et al.</i> , 2006 ¹⁹	Point-source	High Asia; ^{10}Be dating
●	Arzhannikhov <i>et al.</i> , 2015 ²⁰	Point-source	NE Asia; ^{10}Be dating
●	Baumann <i>et al.</i> , 1995 ²¹	Glacial curve	Western EIS; IRD. 5 data points shown.
●	Chevalier <i>et al.</i> , 2011 ²²	Point-source	High Asia; ^{10}Be dating
●	Hall, 2013 ²³	Point-source	Western EIS; geomorphology suggests ice cap over Shetland Islands between 10 and 40 ka
●	Hibbert <i>et al.</i> , 2010 ²⁴	IRD	Western EIS
●	Lehmkuhl, 1998 ²⁵	Point-source	High Asia; TL dating
●	Lekens <i>et al.</i> , 2009 ²⁶	Glacial curve	Western EIS; based on seismic data and IRD
●	Murton, 2017 ³⁶	Point-source	Western EIS; OSL and palaeomagnetic dating
●	Owen <i>et al.</i> , 2003 ³⁷	Point-source	High Asia; TCN and TL dating
●	Owen <i>et al.</i> , 2009 ³⁸	Point-source	High Asia; TCN and OSL dating
●	Owen <i>et al.</i> , 2010 ²⁹	Point-source	High Asia; ^{10}Be dating

Key	Reference	Data type	Details
●	Rother <i>et al.</i> , 2014 ³⁹	Point-source	NE Asia; TCN dating
●	Stein <i>et al.</i> , 1996 ³⁰	IRD	East GIS; IRD, $\delta^{18}\text{O}$ and ^{14}C dating.
●	Syvitski <i>et al.</i> , 1999 ⁴⁰	Seismic data	Iceland; seismic data
●	Thackray, 2008 ⁴¹	Point-source	LIS; ^{14}C and ^{36}Cl dating

Supplementary Table 2. Published evidence for the spatial extent of NH glaciation at 35 ka.

Key corresponds with colours in [Supplementary Figure 2c](#).

40 ka

Key	Reference	Data type	Details
	Arnold <i>et al.</i> , 2002 ³³	Empirical outline	Western EIS; minimum extent during MIS 3
	Barr and Solomina, 2015 ⁴¹	Empirical outline	NE Asia
	Dredge and Thorleifson, 1987 ⁴²	Empirical outline	LIS; hypotheses for MIS 3
	Houmark-Nielsen, 2010 ³	Empirical outline	Western EIS; spans MIS 3
	Hughes <i>et al.</i> , 2016 ⁴	Empirical outline	EIS; 34–38 ka; min and max versions
	Kleman <i>et al.</i> , 2010 ⁵	Empirical outline	LIS
	Larsen <i>et al.</i> , 2009 ⁶	Empirical outline	Western EIS; 30–50 ka
	van Andel and Tzedakis, 1996 ⁴³	Empirical outline	EIS; min and max versions
	Arnold <i>et al.</i> , 2002 ³³	Model	Western EIS; 36 ka. Model driven by GISP $\delta^{18}\text{O}$ ice core record.
	Bonelli <i>et al.</i> , 2009 ⁹	Model	NH; spans 0–126 ka with 1 ka increments. Model driven by variations in orbital parameters and CO_2 concentration.
	de Boer <i>et al.</i> , 2014 ¹⁰	Model	NH; spans 0–410 ka with 1 ka increments. Ice volume and temperature derived from benthic $\delta^{18}\text{O}$ stack.
	Ganopolski and Calov, 2011 ¹¹	Model	NH; spans 0–800 ka with 1 ka increments. Model driven by variations in orbital parameters and CO_2 concentration.
	Heinemann <i>et al.</i> , 2014 ¹²	Model	NH; spans 0–78 ka with 1 ka increments. Model driven by variations in orbital parameters and CO_2 concentration.
	Lambeck <i>et al.</i> , 2010 ¹⁴	Model	Western EIS. Model constructed using existing empirical data.
	Marshall <i>et al.</i> , 2000 ⁴⁴	Model	LIS and CIS. Model driven by GRIP $\delta^{18}\text{O}$ ice core record and general circulation model.
	Seguinot <i>et al.</i> , 2016 ¹⁶	Model	CIS; 42.9 ka. Model driven by temperature offsets from proxy records and calibrated against existing empirical data.
	Stokes <i>et al.</i> , 2012 ¹⁷	Model	LIS and CIS. Model calibrated against existing empirical data.
	Zweck and Huybrechts, 2005 ¹⁸	Model	NH; 30–120 ka with 10 ka increments. Model parameters chosen to match empirical LGM ice extent.
●	Abramowski <i>et al.</i> , 2006 ¹⁹	Point-source	High Asia; ^{10}Be dating
●	Arzhannikhov <i>et al.</i> , 2015 ²⁰	Point-source	NE Asia; ^{10}Be dating
●	Baumann <i>et al.</i> , 1995 ²¹	Glacial curve	Western EIS; IRD. 5 data points shown.
●	Chevalier <i>et al.</i> , 2011 ²²	Point-source	High Asia; ^{10}Be dating
●	Hall, 2013 ²³	Point-source	Western EIS; geomorphology suggests ice cap over Shetland Islands between 10 and 40 ka

Key	Reference	Data type	Details
●	Hibbert <i>et al.</i> , 2010 ²⁴	IRD	Western EIS
●	Lekens <i>et al.</i> , 2009 ²⁶	Glacial curve	Western EIS; based on seismic data and IRD
●	Li <i>et al.</i> , 2014 ²⁷	Point-source	High Asia; ¹⁰ Be dating
●	Murton, 2017 ³⁶	Point-source	Western EIS; OSL and palaeomagnetic dating
●	Owen and Dortch, 2014 ²⁸	Point-source	High Asia; TCN, OSL and ¹⁴ C dating
●	Owen <i>et al.</i> , 2003 ³⁷	Point-source	High Asia; TCN and TL dating
●	Owen <i>et al.</i> , 2009 ³⁸	Point-source	High Asia; TCN and OSL dating
●	Owen <i>et al.</i> , 2010 ²⁹	Point-source	High Asia; ¹⁰ Be dating
●	Rother <i>et al.</i> , 2014 ³⁹	Point-source	NE Asia; TCN dating
●	Stübner <i>et al.</i> , 2017 ³¹	Point-source	High Asia; ¹⁰ Be dating
●	Thackray, 2008 ³²	Point-source	LIS; ¹⁴ C and ³⁶ Cl dating
●	Zhao <i>et al.</i> , 2009 ⁴⁵	Point-source	High Asia; ESR dating
●	Zhao <i>et al.</i> , 2013 ⁴⁶	Point-source	High Asia; ESR and OSL dating

Supplementary Table 3. Published evidence for the spatial extent of NH glaciation at 40 ka.

ERS = electron spin resonance. Key corresponds with colours in [Supplementary Figure 3a](#).

45 ka

Key	Reference	Data type	Details
	Arnold <i>et al.</i> , 2002 ³³	Empirical outline	Western EIS; minimum extent during MIS 3
	Dredge and Thorleifson, 1987 ⁴²	Empirical outline	LIS; hypotheses for MIS 3
	Helmens, 2014 ⁴⁷	Empirical outline	Western EIS; early MIS 3
	Houmark-Nielsen, 2010 ³	Empirical outline	Western EIS; spans MIS 3
	Larsen <i>et al.</i> , 2006 ⁴⁶	Empirical outline	EIS; 45–55 ka
	Larsen <i>et al.</i> , 2009 ⁶	Empirical outline	Western EIS; 30–50 ka
	Obst <i>et al.</i> , 2017 ³⁵	Empirical outline	Western EIS; 46–56 ka
	Olsen <i>et al.</i> , 2013 ⁸	Empirical outline	Western EIS; 44 ka
	Arnold <i>et al.</i> , 2002 ³¹	Model	Western EIS; 36 ka. Model driven by GISP $\delta^{18}\text{O}$ ice core record.
	Bonelli <i>et al.</i> , 2009 ⁹	Model	NH; spans 0–126 ka with 1 ka increments. Model driven by variations in orbital parameters and CO_2 concentration.
	de Boer <i>et al.</i> , 2014 ¹⁰	Model	NH; spans 0–410 ka with 1 ka increments. Ice volume and temperature derived from benthic $\delta^{18}\text{O}$ stack.
	Ganopolski and Calov, 2011 ¹¹	Model	NH; spans 0–800 ka with 1 ka increments. Model driven by variations in orbital parameters and CO_2 concentration.
	Heinemann <i>et al.</i> , 2014 ¹²	Model	NH; spans 0–78 ka with 1 ka increments. Model driven by variations in orbital parameters and CO_2 concentration.
	Lambeck <i>et al.</i> , 2010 ¹⁴	Model	Western EIS. Model constructed using existing empirical data.
	Seguinot <i>et al.</i> , 2016 ¹⁶	Model	CIS; 45.9 ka. Model driven by temperature offsets from proxy records and calibrated against existing empirical data.
	Stokes <i>et al.</i> , 2012 ¹⁷	Model	LIS and CIS. Model calibrated against existing empirical data.
●	Abramowski <i>et al.</i> , 2006 ¹⁹	Point-source	High Asia; ^{10}Be dating
●	Arzhannikhov <i>et al.</i> , 2015 ²⁰	Point-source	NE Asia; ^{10}Be dating
●	Baumann <i>et al.</i> , 1995 ²¹	Glacial curve	Western Norway; IRD. 5 data points shown.
●	Hibbert <i>et al.</i> , 2010 ²⁴	IRD	Western EIS
●	Lekens <i>et al.</i> , 2009 ²⁶	Glacial curve	Western EIS; based on seismic data and IRD
●	Owen and Dortch, 2014 ²⁸	Point-source	High Asia; TCN, OSL and ^{14}C dating. 2 data points shown.
●	Owen <i>et al.</i> , 2006 ⁴⁹	Point-source	High Asia; TCN dating
●	Owen <i>et al.</i> , 2010 ²⁹	Point-source	High Asia; ^{10}Be dating
●	Stübner <i>et al.</i> , 2017 ³¹	Point-source	High Asia; ^{10}Be dating
●	Zhao <i>et al.</i> , 2009 ⁴⁵	Point-source	High Asia; ESR dating
●	Zhao <i>et al.</i> , 2013 ⁴⁶	Point-source	High Asia; ESR and OSL dating

Supplementary Table 4. Published evidence for the spatial extent of NH glaciation at 45 ka.
IRSL = infrared stimulated luminescence. Key corresponds with colours in [Supplementary Figure 3c](#).

MIS 4 (58–72 ka)

Key	Reference	Data type	Details
	Arnold <i>et al.</i> , 2002 ³³	Empirical outline	Western EIS
	Astakhov, 2018 ⁵²	Empirical outline	Eastern EIS; 70–90 ka
	Astakhov <i>et al.</i> , 2016 ⁵³	Empirical outline	Eastern EIS; 50–60 ka
	Carr <i>et al.</i> , 2006 ⁵⁴	Empirical outline	Western EIS; tentative extent
	Glushkova, 2011 ⁵⁵	Empirical outline	NE Asia
	Helmens, 2014 ⁴⁷	Empirical outline	EIS
	Hjort, 1981 ⁵⁶	Empirical outline	Northeast GIS; tentative glacial limits
	Houmark-Nielsen, 2010 ³	Empirical outline	Western EIS; 46–56 ka
	Kaufman <i>et al.</i> , 2011 ⁵⁷	Empirical outline	CIS; outline may be MIS 6 in places
	Kleman <i>et al.</i> , 2010 ⁵	Empirical outline	LIS; includes extrapolations based on topography
	Kleman <i>et al.</i> , 2013 ⁵⁸	Empirical outline	EIS
	Larsen <i>et al.</i> , 2006 ⁴⁸	Empirical outline	EIS; 65–70 ka
	Larsen <i>et al.</i> , 2009 ⁶	Empirical outline	Western EIS; 50–55 ka
	Lundqvist, 2004 ⁵⁹	Empirical outline	Western EIS; 65 ka
	Mangerud <i>et al.</i> , 2011 ³⁴	Empirical outline	Western EIS; 55–60 ka
	Möller <i>et al.</i> , 2015 ⁶⁰	Empirical outline	Eastern EIS
	Obst <i>et al.</i> , 2017 ³⁵	Empirical outline	Western EIS; 46–56 ka
	Olsen <i>et al.</i> , 2013 ⁸	Empirical outline	Western EIS; 65 ka
	Rolfe <i>et al.</i> , 2012 ⁶¹	Empirical outline	Western EIS; tentative extent
	Svendsen <i>et al.</i> , 2004 ⁶²	Empirical outline	EIS
	Svendsen <i>et al.</i> , 2014 ⁶³	Empirical outline	Eastern EIS
	Turner <i>et al.</i> , 2016 ⁶⁴	Empirical outline	CIS; MIS 4 and MIS 6 extents not differentiated
	van Andel and Tzedakis, 1996 ⁴³	Empirical outline	Western EIS; includes min and max versions
	Bonelli <i>et al.</i> , 2009 ⁹	Model	NH; spans 0–126 ka with 1 ka increments. Model driven by variations in orbital parameters and CO ₂ concentration.
	de Boer <i>et al.</i> , 2014 ¹⁰	Model	NH; spans 0–410 ka with 1 ka increments. Ice volume and temperature derived from benthic $\delta^{18}\text{O}$ stack.
	Ganopolski and Calov, 2011 ¹¹	Model	NH; spans 0–800 ka with 1 ka increments. Model driven by variations in orbital parameters and CO ₂ concentration.
	Heinemann <i>et al.</i> , 2014 ¹²	Model	NH; spans 0–78 ka with 1 ka increments. Model driven by variations in orbital parameters and CO ₂ concentration.
	Kleman <i>et al.</i> , 2002 ⁶⁵	Model	LIS and CIS; 70 ka. Model driven by GRIP $\delta^{18}\text{O}$ ice core record and tuned to fit existing empirical data.
	Kleman <i>et al.</i> , 2013 ⁵⁸	Model	NH; 64 ka. Model constrained by existing empirical data.
	Lambeck <i>et al.</i> , 2010 ¹⁴	Model	Western EIS. Model constructed using existing empirical data.

Key	Reference	Data type	Details
	Marshall <i>et al.</i> , 2000 ⁴⁴	Model	LIS and CIS; 60 ka. Model driven by GRIP $\delta^{18}\text{O}$ ice core record and general circulation model.
	Seguinot <i>et al.</i> , 2016 ¹⁶	Model	CIS; 60 ka. Model driven by temperature offsets from proxy records and calibrated against existing empirical data.
	Stokes <i>et al.</i> , 2012 ¹⁷	Model	CIS and LIS. Model calibrated against existing empirical data.
	Zweck and Huybrechts, 2005 ¹⁸	Model	NH; 30–120 ka with 10 ka increments. Model parameters chosen to match empirical LGM ice extent.
●	Abramowski <i>et al.</i> , 2006 ¹⁹	Point-source	High Asia; ¹⁰ Be dating
●	Arzhannikhov <i>et al.</i> , 2015 ²⁰	Point-source	NE Asia; ¹⁰ Be dating
●	Baumann <i>et al.</i> , 1995 ²¹	Glacial curve	Western EIS; IRD. 5 data points shown.
●	Chevalier <i>et al.</i> , 2011 ²²	Point-source	High Asia; ¹⁰ Be dating
●	Davies, 2008 ⁶⁶	Point-source	Western EIS; OSL dating
●	Eccleshall <i>et al.</i> , 2016 ⁶⁷	Glacial curve	EIS; OSL dating
●	Grin <i>et al.</i> , 2016 ⁶⁸	Point-source	High Asia; overview of regional glaciations
●	Hall and Shroba, 1995 ⁶⁹	Point-source	US mountains; soil properties
●	Hibbert <i>et al.</i> , 2010 ²⁴	IRD	Western EIS
●	Houmark-Nielsen, 2010 ³	Point-source	Western EIS; OSL and ¹⁴ C dating. 3 data points shown.
●	Li <i>et al.</i> , 2014 ²⁷	Point-source	High Asia; ¹⁰ Be dating
●	Owen and Dortch, 2014 ²⁸	Point-source	High Asia; TCN, OSL and ¹⁴ C dating. 2 data points shown.
●	Owen <i>et al.</i> , 2006 ⁴⁹	Point-source	High Asia; TCN dating
●	Owen <i>et al.</i> , 2010 ²⁹	Point-source	High Asia; ¹⁰ Be dating
●	Sejrup <i>et al.</i> , 2000 ⁷⁰	Glacial curve	Western EIS; from seismic data
●	Sejrup <i>et al.</i> , 2005 ⁷¹	Glacial curve	Western EIS; glacial curves from seismic profiles
●	Stauch and Lehmkühl, 2010 ⁵⁰	Point-source	NE Asia; IRSL dating
●	Stein <i>et al.</i> , 1996 ³⁰	IRD	East GIS; IRD, $\delta^{18}\text{O}$ and ¹⁴ C dating.
●	Stewart and Lonergan, 2011 ⁷²	Seismic data	Western EIS; seismic data
●	Stübner <i>et al.</i> , 2017 ³¹	Point-source	High Asia; ¹⁰ Be dating
●	Thackray, 2008 ³²	Point-source	LIS; ¹⁴ C and ³⁶ Cl dating
●	Ward <i>et al.</i> , 2007 ⁵¹	Point-source	CIS; TCN dating
●	Winkelmann <i>et al.</i> , 2008 ⁷³	Glacial curve	EIS; based on IRD
●	Zech <i>et al.</i> , 2011 ⁷⁴	Point-source	NE Asia; IRSL dating
●	Zech <i>et al.</i> , 2013 ⁷⁵	Point-source	High Asia; ¹⁰ Be dating
●	Zhao <i>et al.</i> , 2009 ⁴⁵	Point-source	High Asia; ERS dating
●	Zhao <i>et al.</i> , 2013 ⁴⁶	Point-source	High Asia; ERS and OSL dating

Supplementary Table 5. Published evidence for the spatial extent of NH glaciation during MIS 4. Key corresponds with colours in [Supplementary Figure 4a](#).

MIS 5a (72–86 ka)

Key	Reference	Data type	Details
	Mangerud <i>et al.</i> , 2011 ³⁴	Empirical outline	Western EIS; Odderade interstadial, 80 ka
	Olsen <i>et al.</i> , 2013 ⁸	Empirical outline	Western EIS; 80 ka
	Bonelli <i>et al.</i> , 2009 ⁹	Model	NH; spans 0–126 ka with 1 ka increments. Model driven by variations in orbital parameters and CO ₂ concentration.
	de Boer <i>et al.</i> , 2014 ¹⁰	Model	NH; spans 0–410 ka with 1 ka increments. Ice volume and temperature derived from benthic $\delta^{18}\text{O}$ stack.
	Ganopolski and Calov, 2011 ¹¹	Model	NH; spans 0–800 ka with 1 ka increments. Model driven by variations in orbital parameters and CO ₂ concentration.
	Heinemann <i>et al.</i> , 2014 ¹²	Model	NH; spans 0–78 ka with 1 ka increments. Model driven by variations in orbital parameters and CO ₂ concentration.
	Kleman <i>et al.</i> , 2002 ⁶⁵	Model	LIS and CIS; 84 ka. Model driven by GRIP $\delta^{18}\text{O}$ ice core record and tuned to fit existing empirical data.
	Lambeck <i>et al.</i> , 2006 ⁷⁶	Model	Western EIS; 85 ka. Model constructed using existing empirical data.
	Marshall <i>et al.</i> , 2000 ⁴⁴	Model	LIS and CIS; 80 ka. Model driven by GRIP $\delta^{18}\text{O}$ ice core record and general circulation model.
	Stokes <i>et al.</i> , 2012 ¹⁷	Model	CIS and LIS; 80 ka. Model calibrated against existing empirical data.
	Zweck and Huybrechts, 2005 ¹⁸	Model	NH; 30–120 ka with 10 ka increments. Model parameters chosen to match empirical LGM ice extent.
●	Abramowski <i>et al.</i> , 2006 ¹⁹	Point-source	High Asia; ¹⁰ Be dating
●	Arzhannikhov <i>et al.</i> , 2015 ²⁰	Point-source	NE Asia; ¹⁰ Be dating
●	Baumann <i>et al.</i> , 1995 ²¹	Glacial curve	Western EIS; IRD. 5 data points shown.
●	Blomdin <i>et al.</i> , 2016 ⁷⁷	Point-source	High Asia; ¹⁰ Be dating
●	Chevalier <i>et al.</i> , 2011 ²²	Point-source	High Asia; ¹⁰ Be dating
●	Fu <i>et al.</i> , 2013 ⁷⁸	Point-source	High Asia; ¹⁰ Be dating
●	Grin <i>et al.</i> , 2016 ⁶⁸	Point-source	High Asia; overview of regional glaciations
●	Lekens <i>et al.</i> , 2009 ²⁶	Glacial curve	Western EIS; based on seismic data and IRD
●	Li <i>et al.</i> , 2014 ²⁷	Point-source	High Asia; ¹⁰ Be dating
●	Owen and Dortch, 2014 ²⁸	Point-source	High Asia; TCN, OSL and ¹⁴ C dating. 2 data points shown.
●	Owen <i>et al.</i> , 2010 ²⁹	Point-source	High Asia; ¹⁰ Be dating
●	Stübner <i>et al.</i> , 2017 ³¹	Point-source	High Asia; ¹⁰ Be dating
●	Thackray, 2008 ³²	Point-source	LIS; ¹⁴ C and ³⁶ Cl dating
●	Zhao <i>et al.</i> , 2013 ⁴⁶	Point-source	High Asia; ERS and OSL dating
●	Zhao <i>et al.</i> , 2015 ⁸⁰	Point-source	High Asia; ERS dating

Supplementary Table 6. Published evidence for the spatial extent of NH glaciation during MIS 5a. Key corresponds with colours in [Supplementary Figure 4c](#).

MIS 5b (86–92 ka)

Key	Reference	Data type	Details
	Astakhov, 2004 ⁸¹	Empirical outline	Eastern EIS; Early Weichselian limit
	Astakhov, 2018 ⁵²	Empirical outline	Eastern EIS; 70–90 ka
	Astakhov <i>et al.</i> , 2016 ⁵³	Empirical outline	Eastern EIS; 80–90 ka
	Helmens, 2014 ⁴⁷	Empirical outline	Western EIS
	Hjort, 1981 ⁵⁶	Empirical outline	Tentative glacial limits in northern East GIS
	Kleman <i>et al.</i> , 2010 ⁵	Empirical outline	LIS; MIS 5b or d
	Mangerud <i>et al.</i> , 2011 ³⁴	Empirical outline	EIS; 90 ka
	Olsen <i>et al.</i> , 2013 ⁸	Empirical outline	Western EIS; 90 ka
	Svendsen <i>et al.</i> , 2004 ⁶²	Empirical outline	EIS; 90 ka
	Bonelli <i>et al.</i> , 2009 ⁹	Model	NH; spans 0–126 ka with 1 ka increments. Model driven by variations in orbital parameters and CO ₂ concentration.
	de Boer <i>et al.</i> , 2014 ¹⁰	Model	NH; spans 0–410 ka with 1 ka increments. Ice volume and temperature derived from benthic $\delta^{18}\text{O}$ stack.
	Ganopolski and Calov, 2011 ¹¹	Model	NH; spans 0–800 ka with 1 ka increments. Model driven by variations in orbital parameters and CO ₂ concentration.
	Kleman <i>et al.</i> , 2002 ⁶⁵	Model	LIS and CIS; 90 ka. Model driven by GRIP $\delta^{18}\text{O}$ ice core record and tuned to fit existing empirical data.
	Kleman <i>et al.</i> , 2013 ⁵⁸	Model	NH; 86.2 ka. Model constrained by existing empirical data.
	Lambeck <i>et al.</i> , 2006 ⁷⁶	Model	Western EIS; 94 ka. Model constructed using existing empirical data.
	Stokes <i>et al.</i> , 2012 ¹⁷	Model	CIS and LIS; 90 ka. Model calibrated against existing empirical data.
	Zweck and Huybrechts, 2005 ¹⁸	Model	NH; 30–120 ka with 10 ka increments. Model parameters chosen to match empirical LGM ice extent.
●	Arzhannikhov <i>et al.</i> , 2015 ²⁰	Point-source	NE Asia; ¹⁰ Be dating
●	Baumann <i>et al.</i> , 1995 ²¹	Glacial curve	Western EIS; IRD. 5 data points shown.
●	Eccleshall <i>et al.</i> , 2016 ⁶⁷	Glacial curve	Western EIS; glacial curve based on OSL dating
●	Fu <i>et al.</i> , 2013 ⁷⁸	Point-source	High Asia; ¹⁰ Be dating
●	Funder <i>et al.</i> , 1998 ⁸²	Point-source	Eastern GIS; sedimentology, IRD and luminescence dating
●	Grin <i>et al.</i> , 2016 ⁶⁸	Point-source	High Asia; overview of regional glaciations
●	Lekens <i>et al.</i> , 2009 ²⁶	Glacial curve	Western EIS; based on seismic data and IRD
●	Owen and Dortch, 2014 ²⁸	Point-source	High Asia; TCN, OSL and ¹⁴ C dating. 2 data points shown.
●	Owen <i>et al.</i> , 2010 ²⁹	Point-source	High Asia; ¹⁰ Be dating
●	Stauch and Lehmkühl, 2010 ⁵⁰	Point-source	NE Asia; IRSL dating
●	Thackray, 2008 ³²	Point-source	LIS; ¹⁴ C and ³⁶ Cl dating

Key	Reference	Data type	Details
●	Zhao <i>et al.</i> , 2015 ⁸⁰	Point-source	High Asia; ERS dating

Supplementary Table 7. Published evidence for the spatial extent of NH glaciation during MIS 5b. Key corresponds with colours in [Supplementary Figure 5a](#).

MIS 5c (92–108 ka)

Key	Reference	Data type	Details
	Larsen <i>et al.</i> , 2006 ⁴⁸	Empirical outline	EIS; 90–100 ka
	Lundqvist, 2004 ⁵⁹	Empirical outline	EIS; 100 ka
	Mangerud <i>et al.</i> , 2011 ³⁴	Empirical outline	EIS; 100 ka
	Möller <i>et al.</i> , 2015 ⁶⁰	Empirical outline	Eastern EIS; MIS 5c–d
	Olsen <i>et al.</i> , 2013 ⁸	Empirical outline	Western EIS; 100 ka
	Bonelli <i>et al.</i> , 2009 ⁹	Model	NH; spans 0–126 ka with 1 ka increments. Model driven by variations in orbital parameters and CO ₂ concentration.
	de Boer <i>et al.</i> , 2014 ¹⁰	Model	NH; spans 0–410 ka with 1 ka increments. Ice volume and temperature derived from benthic δ ¹⁸ O stack.
	Ganopolski and Calov, 2011 ¹¹	Model	NH; spans 0–800 ka with 1 ka increments. Model driven by variations in orbital parameters and CO ₂ concentration.
	Lambeck <i>et al.</i> , 2006 ⁷⁶	Model	EIS; 106 ka. Model constructed using existing empirical data.
	Stokes <i>et al.</i> , 2012 ¹⁷	Model	CIS and LIS; 100 ka. Model calibrated against existing empirical data.
	Zweck and Huybrechts, 2005 ¹⁸	Model	NH; 30–120 ka with 10 ka increments. Model parameters chosen to match empirical LGM ice extent.
●	Abramowski <i>et al.</i> , 2006 ¹⁹	Point-source	High Asia; ¹⁰ Be dating
●	Arzhannikhov <i>et al.</i> , 2015 ²⁰	Point-source	NE Asia; ¹⁰ Be dating
●	Baumann <i>et al.</i> , 1995 ²¹	Glacial curve	Western EIS; IRD. 5 data points shown.
●	Fu <i>et al.</i> , 2013 ⁷⁸	Point-source	High Asia; ¹⁰ Be dating
●	Grin <i>et al.</i> , 2016 ⁶⁸	Point-source	High Asia; overview of regional glaciations
●	Lehmkuhl, 1998 ²⁵	Point-source	High Asia; TL dating
●	Owen and Dortch, 2014 ²⁸	Point-source	High Asia; TCN, OSL and ¹⁴ C dating
●	Owen <i>et al.</i> , 2010 ²⁹	Point-source	High Asia; ¹⁰ Be dating
●	Thackray, 2008 ³²	Point-source	LIS; ¹⁴ C and ³⁶ Cl dating

Supplementary Table 8. Published evidence for the spatial extent of NH glaciation during MIS 5c. Key corresponds with colours in [Supplementary Figure 5c](#).

MIS 5d (108–117 ka)

Key	Reference	Data type	Details
	Helmens, 2014 ⁴⁷	Empirical outline	EIS
	Kleman <i>et al.</i> , 2010 ⁵	Empirical outline	LIS; MIS 5b or 5d
	Lundqvist, 2004 ⁵⁹	Empirical outline	EIS; 110 ka
	Mangerud <i>et al.</i> , 2011 ³⁴	Empirical outline	EIS; 110 ka
	Möller <i>et al.</i> , 2015 ⁶⁰	Empirical outline	Eastern EIS; MIS 5c–d
	Olsen <i>et al.</i> , 2013 ⁸	Empirical outline	Western EIS; 110 ka
	Bonelli <i>et al.</i> , 2009 ⁹	Model	NH; spans 0–126 ka with 1 ka increments. Model driven by variations in orbital parameters and CO ₂ concentration.
	de Boer <i>et al.</i> , 2014 ¹⁰	Model	NH; spans 0–410 ka with 1 ka increments. Ice volume and temperature derived from benthic $\delta^{18}\text{O}$ stack.
	Ganopolski and Calov, 2011 ¹¹	Model	NH; spans 0–800 ka with 1 ka increments. Model driven by variations in orbital parameters and CO ₂ concentration.
	Lambeck <i>et al.</i> , 2006 ⁷⁶	Model	EIS; 106 ka. Model constructed using existing empirical data.
	Marshall <i>et al.</i> , 2000 ⁴⁴	Model	LIS and CIS; 110 ka. Model driven by GRIP $\delta^{18}\text{O}$ ice core record and general circulation model.
	Stokes <i>et al.</i> , 2012 ¹⁷	Model	CIS and LIS; 110 ka. Model calibrated against existing empirical data.
	Zweck and Huybrechts, 2005 ¹⁸	Model	NH; 30–120 ka with 10 ka increments. Model parameters chosen to match empirical LGM ice extent.
●	Arzhannikhov <i>et al.</i> , 2015 ²⁰	Point-source	NE Asia; ¹⁰ Be dating
●	Baumann <i>et al.</i> , 1995 ²¹	Glacial curve	Western EIS; IRD. 5 data points shown.
●	Chadwick <i>et al.</i> , 1997 ⁸³	Point-source	US mountains; ¹⁴ C and ³⁶ Cl dating
●	Eccleshall <i>et al.</i> , 2016 ⁶⁷	Glacial curve	Western EIS; based on OSL dating
●	Fu <i>et al.</i> , 2013 ⁷⁸	Point-source	High Asia; ¹⁰ Be dating
●	Funder, 1989 ⁸⁴	Point-source	Northwest GIS; sedimentology, luminescence and ¹⁴ C dating.
●	Funder <i>et al.</i> , 1998 ⁸²	Point-source	Eastern GIS; glaciation at around 114 ka, from sedimentology, IRD and luminescence dating.
●	Grin <i>et al.</i> , 2016 ⁶⁸	Point-source	High Asia; overview of regional glaciations
●	Karabanov <i>et al.</i> , 1998 ⁸⁵	Point-source	Russia, TL dating
●	Lekens <i>et al.</i> , 2009 ²⁶	Glacial curve	Western EIS; based on seismic data and IRD
●	Owen and Dortch, 2014 ²⁸	Point-source	High Asia; TCN, OSL and ¹⁴ C dating. 2 data points shown.
●	Owen <i>et al.</i> , 2010 ²⁹	Point-source	High Asia; ¹⁰ Be dating
●	Phillips <i>et al.</i> , 1997 ⁸⁶	Point-source	US mountains; ¹⁴ C and ³⁶ Cl dating
●	Stauch and Lehmkühl, 2010 ⁵⁰	Point-source	NE Asia; IRSL dating
●	Stein <i>et al.</i> , 1996 ³⁰	IRD	East GIS; IRD, $\delta^{18}\text{O}$ and ¹⁴ C dating

Key	Reference	Data type	Details
●	Stübner <i>et al.</i> , 2017 ³¹	Point-source	High Asia; ¹⁰ Be dating
●	Thackray, 2008 ³²	Point-source	LIS; ¹⁴ C and ³⁶ Cl dating
●	Zech <i>et al.</i> , 2011 ⁷⁴	Point-source	NE Asia; IRSL dating

Supplementary Table 9. Published evidence for the spatial extent of NH glaciation during MIS 5d. Key corresponds with colours in [Supplementary Figure 6a](#).

MIS 6 (132–190 ka)

Key	Reference	Data type	Details
	Astakhov <i>et al.</i> , 2016 ⁵³	Empirical outline	Eastern EIS
	Balco and Rovey, 2010 ⁸⁷	Empirical outline	LIS; TCN dating suggests 3 ice advances between 0.2 and 0.75 Ma
	Barendregt <i>et al.</i> , 2014 ⁸⁸	Empirical outline	LIS and CIS; constrained by palaeomagnetic data
	Barr and Solomina, 2015 ⁴¹	Empirical outline	NE Asia
	Basilian <i>et al.</i> , 2008 ⁸⁹	Empirical outline	Arctic Ocean
	Böse <i>et al.</i> , 2012 ⁹⁰	Empirical outline	Western EIS
	Curry <i>et al.</i> , 2011 ⁹¹	Empirical outline	LIS
	Ehlers <i>et al.</i> , 1990 ⁹²	Empirical outline	EIS
	Ehlers <i>et al.</i> , 2011 ⁹³	Empirical outline	EIS
	Eissmann, 2002 ⁹⁴	Empirical outline	EIS
	Gibbard and Clark, 2011 ⁹⁵	Empirical outline	Western EIS
	Gozhik <i>et al.</i> , 2010 ⁹⁶	Empirical outline	EIS
	Hamblin <i>et al.</i> , 2005 ⁹⁷	Empirical outline	Western EIS
	Hughes and Gibbard, 2018 ⁹⁸	Empirical outline	EIS
	Jackson <i>et al.</i> , 2011 ⁹⁹	Empirical outline	LIS
	Jakobsson <i>et al.</i> , 2008 ¹⁰⁰	Empirical outline	Arctic Ocean
	Laban and van der Meer, 2011 ¹⁰¹	Empirical outline	Western EIS
	Marks, 2005 ¹⁰²	Empirical outline	EIS; Saalian 1 (Odranian)
	Marks, 2011 ¹⁰³	Empirical outline	Eastern EIS
	Marks <i>et al.</i> , 2018 ¹⁰⁴	Empirical outline	EIS
	Möller <i>et al.</i> , 2015 ⁶⁰	Empirical outline	Eastern EIS; Urdachsk and Sampesa moraines
	Niessen <i>et al.</i> , 2013 ¹⁰⁵	Empirical outline	Arctic Ocean
	Roskosch <i>et al.</i> , 2015 ¹⁰⁶	Empirical outline	EIS
	Svendsen <i>et al.</i> , 2004 ⁶²	Empirical outline	EIS
	Turner <i>et al.</i> , 2016 ⁶⁴	Empirical outline	CIS; MIS 4 and/or 6
	Colleoni <i>et al.</i> , 2016 ¹⁰⁷	Model	NE Asia. Ice-sheet model forced by coupled atmosphere-ocean-sea-ice-land model.
	de Boer <i>et al.</i> , 2014 ¹⁰	Model	NH; spans 0–410 ka with 1 ka increments. Ice volume and temperature derived from benthic $\delta^{18}\text{O}$ stack.
	Ganopolski and Calov, 2011 ¹¹	Model	NH; spans 0–800 ka with 1 ka increments. Model driven by variations in orbital parameters and CO ₂ concentration.
	Lambeck <i>et al.</i> , 2006 ⁷⁶	Model	EIS; 106 ka. Model constructed using existing empirical data.
	Peltier, 2004 ¹⁰⁸	Model	LIS; Colleoni <i>et al.</i> (2016) ¹⁰⁶ use the 13 ka LIS of Peltier (2004) ¹⁰⁷ to show a small LIS during MIS 6.
●	Anderson <i>et al.</i> , 2012 ¹⁰⁹	Point-source	US Mountains; geomorphological mapping

Key	Reference	Data type	Details
●	Barendregt <i>et al.</i> , 2014 ⁸⁸	Point-source	LIS and CIS; spans 0.13–0.78 Ma. 37 data points shown.
●	Baumann <i>et al.</i> , 1995 ²¹	Glacial curve	Western EIS; IRD. 5 data points shown.
●	Chadwick <i>et al.</i> , 1997 ⁸³	Point-source	US mountains; ¹⁴ C and ³⁶ Cl dating
●	Chevalier <i>et al.</i> , 2011 ²²	Point-source	High Asia; ¹⁰ Be dating
●	Dahlgren <i>et al.</i> , 2002 ¹¹⁰	Glacial curve	Western EIS; based on seismic data
●	Eccleshall <i>et al.</i> , 2016 ⁶⁷	Glacial curve	Western EIS; based on OSL dating
●	Eissmann, 2002 ⁹⁴	Point-source	Western EIS; stratigraphy
●	Fu <i>et al.</i> , 2013 ⁷⁸	Point-source	High Asia; ¹⁰ Be dating
●	Funder, 1989 ⁸⁴	Point-source	Northwest GIS; sedimentology, luminescence and ¹⁴ C dating.
●	Funder <i>et al.</i> , 1998 ⁸²	Point-source	Eastern GIS; sedimentology, IRD and luminescence dating.
●	Geirsdóttir <i>et al.</i> , 2007 ¹¹¹	Point-source	Iceland; sedimentology and K–Ar dating
●	Hall and Shroba, 1995 ⁶⁹	Point-source	US mountains; soil properties
●	Hibbert <i>et al.</i> , 2010 ²⁴	IRD	Western EIS
●	Hjelstuen <i>et al.</i> , 2005 ¹¹²	Seismic data	Western EIS; seismic stratigraphy
●	Kuhle, 2007 ¹¹³	Point-source	High Asia; geomorphological mapping
●	Lehmkuhl, 1998 ²⁵	Point-source	High Asia; TL dating
●	Lekens <i>et al.</i> , 2009 ²⁶	Glacial curve	Western EIS; based on seismic data and IRD
●	Li <i>et al.</i> , 2014 ²⁷	Point-source	High Asia; ¹⁰ Be dating
●	Licciardi and Pierce, 2008 ¹¹⁴	Point-source	US mountains; ¹⁰ Be dating
●	Montelli <i>et al.</i> , 2017 ¹¹⁵	Seismic data	Western EIS; seismic stratigraphy
●	Nielsen and Kuijpers, 2013 ¹¹⁶	Seismic data	Southwest GIS; seismic stratigraphy
●	Nikolskiy <i>et al.</i> , 2017 ¹¹⁷	Point-source	NE Asia; <190–210 ka
●	O'Regan <i>et al.</i> , 2017 ¹¹⁸	Seismic data	NE Asia; seismic stratigraphy
●	Owen and Dortch, 2014 ²⁸	Point-source	High Asia; TCN, OSL and ¹⁴ C dating. 2 data points shown.
●	Owen <i>et al.</i> , 2006 ⁴⁹	Point-source	High Asia; TCN dating
●	Owen <i>et al.</i> , 2010 ²⁹	Point-source	High Asia; ¹⁰ Be dating
●	Phillips <i>et al.</i> , 1997 ⁸⁶	Point-source	US Mountains; ¹⁰ Be and ³⁶ Cl dating
●	Sejrup <i>et al.</i> , 2000 ⁷⁰	Glacial curve	Western EIS; from seismic data
●	Sejrup <i>et al.</i> , 2005 ⁷¹	Glacial curve	Western EIS; from seismic data
●	Stauch and Lehmkuhl, 2010 ⁵⁰	Point-source	NE Asia; IRSL dating
●	Stein <i>et al.</i> , 1996 ³⁰	IRD	East GIS; IRD, $\delta^{18}\text{O}$ and ¹⁴ C dating.
●	Stewart and Lonergan, 2011 ⁷²	Seismic data	Western EIS; seismic stratigraphy
●	Strunk <i>et al.</i> , 2017 ¹¹⁹	Glacial curve	West GIS; modelling and ¹⁰ Be– ²⁶ Al dating. 4 data points shown.
●	Stübner <i>et al.</i> , 2017 ³¹	Point-source	High Asia; ¹⁰ Be dating
●	Vorren and Laberg, 1997 ¹²⁰	Seismic data	EIS
●	Zech <i>et al.</i> , 2011 ⁷⁴	Point-source	NE Asia; Sedimentology and IRSL dating

Key	Reference	Data type	Details
●	Zhao <i>et al.</i> , 2009 ⁴⁵	Point-source	High Asia; ESR dating
●	Zhao <i>et al.</i> , 2013 ⁴⁶	Point-source	High Asia; ESR and OSL dating
●	Zhao <i>et al.</i> , 2015 ⁸⁰	Point-source	High Asia; ESR dating

Supplementary Table 10. Published evidence for the spatial extent of NH glaciation during MIS 6. Key corresponds with colours in [Supplementary Figure 6c](#).

MIS 8 (243–279 ka)

Key	Reference	Data type	Details
	Astakhov <i>et al.</i> , 2016 ⁵³	Empirical outline	Eastern EIS; Samarovo limit
	Balco and Rovey, 2010 ⁸⁷	Empirical outline	LIS; TCN dating suggests 3 ice advances between 0.2 and 0.75 Ma
	Hughes and Gibbard, 2018 ⁹⁸	Empirical outline	EIS
	Marks, 2011 ¹⁰³	Empirical outline	EIS; Krznanian limit
	White <i>et al.</i> , 2010 ¹²¹	Empirical outline	Western EIS
	White <i>et al.</i> , 2017 ¹²²	Empirical outline	Western EIS
	de Boer <i>et al.</i> , 2014 ¹⁰	Model	NH; spans 0–410 ka with 1 ka increments. Ice volume and temperature derived from benthic $\delta^{18}\text{O}$ stack.
	Ganopolski and Calov, 2011 ¹¹	Model	NH; spans 0–800 ka with 1 ka increments. Model driven by variations in orbital parameters and CO_2 concentration.
●	Beets <i>et al.</i> , 2005 ¹²³	Point-source	Western EIS; seismic profiles and AAR dating
●	Chevalier <i>et al.</i> , 2011 ²²	Point-source	High Asia; ^{10}Be dating
●	Dahlgren <i>et al.</i> , 2002 ¹¹⁰	Glacial curve	Western EIS; based on seismic data
●	Geirsdóttir <i>et al.</i> , 2007 ¹¹¹	Point-source	Iceland; sedimentology and K–Ar dating
●	Hjelstuen <i>et al.</i> , 2005 ¹¹²	Seismic data	Western EIS; seismic stratigraphy
●	Hodell <i>et al.</i> , 2008 ¹²⁴	IRD	LIS; age model from IRD and ^{14}C dating
●	Krissek, 1995 ¹²⁵	IRD	CIS and NE Asia; marine-calving margin at 0.27–0.29 Ma
●	Montelli <i>et al.</i> , 2017 ¹¹⁵	Seismic data	Western EIS; seismic stratigraphy
●	Owen and Dortch, 2014 ²⁸	Point-source	High Asia; TCN, OSL and ^{14}C dating
●	Phillips <i>et al.</i> , 1997 ⁸⁶	Point-source	US Mountains; ^{10}Be and ^{36}Cl dating
●	Roskosch <i>et al.</i> , 2015 ¹⁰⁶	Point-source	Western EIS; OSL dating
●	Sejrup <i>et al.</i> , 2000 ⁷⁰	Glacial curve	Western EIS; from seismic data
●	Sejrup <i>et al.</i> , 2005 ⁷¹	Glacial curve	Western EIS; from seismic profiles
●	Stewart and Lonergan, 2011 ⁷²	Seismic data	Western EIS; seismic stratigraphy
●	Strunk <i>et al.</i> , 2017 ¹¹⁹	Glacial curve	West GIS; modelling and ^{10}Be – ^{26}Al dating. 4 data points shown.
●	Vorren and Laberg, 1997 ¹²⁰	Seismic data	EIS

Supplementary Table 11. Published evidence for the spatial extent of NH glaciation during MIS 8. Key corresponds with colours in [Supplementary Figure 7a](#).

MIS 10 (337–365 ka)

Key	Reference	Data type	Details
	Balco and Rovey, 2010 ⁸⁷	Empirical outline	LIS; TCN dating suggests 3 ice advances between 0.2 and 0.75 Ma
	Böse <i>et al.</i> , 2012 ⁹⁰	Empirical outline	Western EIS
	Hamblin <i>et al.</i> , 2005 ⁹⁷	Empirical outline	Western EIS
	Marks, 2011 ¹⁰³	Empirical outline	EIS; Krznanian limit
	Roskosch <i>et al.</i> , 2015 ¹⁰⁶	Empirical outline	Western EIS
	de Boer <i>et al.</i> , 2014 ¹⁰	Model	NH; spans 0–410 ka with 1 ka increments. Ice volume and temperature derived from benthic $\delta^{18}\text{O}$ stack.
	Ganopolski and Calov, 2011 ¹¹	Model	NH; spans 0–800 ka with 1 ka increments. Model driven by variations in orbital parameters and CO_2 concentration.
●	Dahlgren <i>et al.</i> , 2002 ¹¹⁰	Glacial curve	Western EIS; based on seismic data
●	Eissmann, 2002 ⁹⁴	Point-source	Western EIS; stratigraphic sections
●	Geirsdóttir <i>et al.</i> , 2007 ¹¹¹	Point-source	Iceland; sedimentology and K–Ar dating
●	Hjelstuen <i>et al.</i> , 2005 ¹¹²	Seismic data	Western EIS; seismic stratigraphy
●	Hodell <i>et al.</i> , 2008 ¹²⁴	IRD	LIS; age model from IRD and ^{14}C dating
●	Montelli <i>et al.</i> , 2017 ¹¹⁵	Seismic data	Western EIS; seismic stratigraphy
●	Owen and Dortch, 2014 ²⁸	Point-source	High Asia; TCN, OSL and ^{14}C dating. 2 data points shown.
●	Owen <i>et al.</i> , 2009 ³⁸	Point-source	High Asia; TCN and OSL dating
●	Owen <i>et al.</i> , 2010 ²⁹	Point-source	High Asia; TCN dating
●	Phillips <i>et al.</i> , 1997 ⁸⁶	Point-source	US Mountains; ^{10}Be and ^{36}Cl dating
●	Sejrup <i>et al.</i> , 2000 ⁷⁰	Glacial curve	Western EIS; from seismic data
●	Sejrup <i>et al.</i> , 2005 ⁷¹	Glacial curve	Western EIS; from seismic data
●	Spooner <i>et al.</i> , 1996 ¹²⁶	Point-source	CIS; stratigraphy and palaeomagnetic data
●	Stewart and Lonergan, 2011 ⁷²	Seismic data	Western EIS; seismic stratigraphy
●	Strunk <i>et al.</i> , 2017 ¹¹⁹	Glacial curve	West GIS; modelling and ^{10}Be – ^{26}Al dating. 4 data points shown.
●	Vorren and Laberg, 1997 ¹²⁰	Seismic data	EIS

Supplementary Table 12. Published evidence for the spatial extent of NH glaciation during MIS 10. Key corresponds with colours in [Supplementary Figure 7c](#).

MIS 12 (429–477 ka)

Key	Reference	Data type	Details
	Astakhov <i>et al.</i> , 2016 ⁵³	Empirical outline	Eastern EIS; Lebed glaciation
	Balco and Rovey, 2010 ⁸⁷	Empirical outline	LIS; TCN dating suggests 3 ice advances between 0.2 and 0.75 Ma
	Böse <i>et al.</i> , 2012 ⁹⁰	Empirical outline	Western EIS
	Ehlers <i>et al.</i> , 1990 ⁹²	Empirical outline	EIS; older Saalian
	Ehlers <i>et al.</i> , 2011 ⁹³	Empirical outline	EIS; Elsterian glaciation
	Eissmann, 2002 ⁹⁴	Empirical outline	EIS; Don lobe is shown as MIS 12
	Gibbard and Clark, 2011 ⁹⁵	Empirical outline	EIS
	Gozhik <i>et al.</i> , 2010 ⁹⁶	Empirical outline	EIS
	Hamblin <i>et al.</i> , 2005 ⁹⁷	Empirical outline	Western EIS
	Hughes and Gibbard, 2018 ⁹⁸	Empirical outline	EIS
	Krzyszowski <i>et al.</i> , 2015 ¹²⁷	Empirical outline	EIS; Elsterian T2 till
	Laban and van der Meer, 2011 ¹⁰¹	Empirical outline	EIS
	Marks, 2011 ¹⁰³	Empirical outline	EIS; Sanian 2 limit
	Marks <i>et al.</i> , 2018 ¹⁰⁴	Empirical outline	EIS; Elsterian, Sanian 2 and Berezinian limits
	Roskosch <i>et al.</i> , 2015 ¹⁰⁶	Empirical outline	EIS
	Ganopolski and Calov, 2011 ¹¹	Model	NH; spans 0–800 ka with 1 ka increments. Model driven by variations in orbital parameters and CO ₂ concentration.
●	Dahlgren <i>et al.</i> , 2002 ¹¹⁰	Glacial curve	Western EIS; based on seismic data
●	Geirsdóttir <i>et al.</i> , 2007 ¹¹¹	Point-source	Iceland; sedimentology and K–Ar dating
●	Hjelstuen <i>et al.</i> , 2005 ¹¹²	Seismic data	Western EIS; seismic stratigraphy
●	Hodell <i>et al.</i> , 2008 ¹²⁴	IRD	LIS; age model from IRD and ¹⁴ C dating
●	Montelli <i>et al.</i> , 2017 ¹¹⁵	Seismic data	Western EIS; seismic stratigraphy
●	Owen <i>et al.</i> , 2006 ⁴⁹	Point-source	High Asia; TCN dating
●	Phillips <i>et al.</i> , 1997 ⁸⁶	Point-source	US Mountains; ¹⁰ Be and ³⁶ Cl dating
●	Sejrup <i>et al.</i> , 2000 ⁷⁰	Glacial curve	Western EIS; from seismic data
●	Sejrup <i>et al.</i> , 2005 ⁷¹	Glacial curve	Western EIS; glacial curves from seismic profiles
●	Stewart and Lonergan, 2011 ⁷²	Seismic data	Western EIS; seismic stratigraphy
●	Strunk <i>et al.</i> , 2017 ¹¹⁹	Glacial curve	West GIS; modelling and ¹⁰ Be– ²⁶ Al dating. 4 data points shown.
●	Vorren and Laberg, 1997 ¹²⁰	Seismic data	EIS
●	Zhao <i>et al.</i> , 2009 ⁴⁵	Point-source	High Asia; ESR dating
●	Zhao <i>et al.</i> , 2015 ⁸⁰	Point-source	High Asia; ERS dating

Supplementary Table 13. Published evidence for the spatial extent of NH glaciation during MIS 12. Key corresponds with colours in [Supplementary Figure 8a](#).

MIS 16 (622–677 ka)

Key	Reference	Data type	Details
	Aber, 1991 ¹²⁸	Empirical outline	LIS; Pre-Illinoian glaciation
	Astakhov, 2004 ⁸¹	Empirical outline	Eastern EIS; Donian glaciation
	Astakhov <i>et al.</i> , 2016 ⁵³	Empirical outline	Eastern EIS; Donian glaciation
	Balco and Rovey, 2010 ⁸⁷	Empirical outline	LIS; TCN dating suggests 3 ice advances between 0.75 and 0.2 Ma
	Colgan, 1999 ¹²⁹	Empirical outline	LIS; Pre-Illinoian glaciation
	Gozhik <i>et al.</i> , 2010 ⁹⁶	Empirical outline	EIS; Donian/ Sanian 1 glaciation
	Hamblin <i>et al.</i> , 2005 ⁹⁷	Empirical outline	Western EIS; Happendburg Formation
	Hughes and Gibbard, 2018 ⁹⁸	Empirical outline	EIS; Donian glaciation
	Marks, 2011 ¹⁰³	Empirical outline	EIS; Sanian 1 glaciation
	Marks <i>et al.</i> , 2018 ¹⁰⁴	Empirical outline	EIS; Donian/ Sanian 1 glaciation
	Olsen <i>et al.</i> , 2013 ⁸	Empirical outline	EIS; transitional phase at 0.5–1.5 Ma
	Toucanne <i>et al.</i> , 2009 ¹³⁰	Empirical outline	EIS; pre-MIS 12 glaciations, based on IRD
●	Chadwick <i>et al.</i> , 1997 ⁸³	Point-source	LIS; ¹⁰ Be and ³⁶ Cl dating
●	Colgan, 1999 ¹²⁹	Point-source	LIS; sedimentology and palaeomagnetism
●	Geirsdóttir <i>et al.</i> , 2007 ¹¹¹	Point-source	Iceland; sedimentology and K–Ar dating
●	Hodell <i>et al.</i> , 2008 ¹²⁴	IRD	LIS; age model from IRD and ¹⁴ C dating
●	Montelli <i>et al.</i> , 2017 ¹¹⁵	Seismic data	Western EIS; seismic stratigraphy
●	Phillips <i>et al.</i> , 1997 ⁸⁶	Point-source	US Mountains; ¹⁰ Be and ³⁶ Cl dating
●	Strunk <i>et al.</i> , 2017 ¹¹⁹	Glacial curve	West GIS; modelling and ¹⁰ Be– ²⁶ Al dating. 4 data points shown.
●	Vorren and Laberg, 1997 ¹²⁰	Seismic data	EIS

Supplementary Table 14. Published evidence for the spatial extent of NH glaciation during MIS 16. Key corresponds with colours in [Supplementary Figure 8c](#).

MIS 20–24 (790–928 ka)

Key	Reference	Data type	Details
	Andriashek and Barendregt, 2017 ¹³¹	Empirical outline	LIS; MIS 20, around 0.8 Ma. 40 data points shown.
	Balco and Rovey, 2010 ⁸⁷	Empirical outline	LIS; TCN dating indicates ice advance around 0.8 Ma
	Batchelor <i>et al.</i> , 2017 ¹³²	Empirical outline	Western EIS; hypothesised ice sheet <i>c.</i> 1 Ma
	Gozhik <i>et al.</i> , 2010 ⁹⁶	Empirical outline	EIS; Nidanian glaciation is MIS 20 or 22
	Marks, 2011 ¹⁰³	Empirical outline	EIS; Nidanian glaciation, around 0.9 Ma
	Olsen <i>et al.</i> , 2013 ⁸	Empirical outline	EIS; transitional phase at 0.5–1.5 Ma
	Ottesen <i>et al.</i> , 2018 ¹³³	Empirical outline	Western EIS; ice sheet <i>c.</i> 1 Ma
	Toucanne <i>et al.</i> , 2009 ¹³⁰	Empirical outline	EIS; pre-MIS 12 glaciations, based on IRD
●	Anderson <i>et al.</i> , 2012 ¹⁰⁹	Point-source	US mountains; mapped glacial deposits
●	Andriashek and Barendregt, 2017 ¹³¹	Point-source	LIS; palaeomagnetic dating
●	Bierman <i>et al.</i> , 2016 ¹³⁴	IRD	Southeast GIS; IRD peak at 0.8 Ma. 2 data points shown.
●	Geirsdóttir <i>et al.</i> , 2007 ¹¹¹	Point-source	Iceland; sedimentology and K–Ar dating
●	Krissek, 1995 ¹²⁵	IRD	CIS and NE Asia; marine-calving margin at 0.92–0.93 Ma. 3 data points shown.
●	Laberg <i>et al.</i> , 2013 ¹³⁵	Seismic data	East GIS; multiple shelf-break glaciations between 0.8 and 1.8 Ma
●	Montelli <i>et al.</i> , 2017 ¹¹⁵	Seismic data	Western EIS; seismic stratigraphy
●	Sejrup <i>et al.</i> , 1991 ¹³⁶	Point-source	Western EIS; palaeomagnetic dating suggests grounded ice sheet at around 0.85 Ma
●	Sejrup <i>et al.</i> , 2000 ⁷⁰	Glacial curve	Western EIS; from seismic data
●	Strunk <i>et al.</i> , 2017 ¹¹⁹	Glacial curve	West GIS; modelling and ¹⁰ Be– ²⁶ Al dating. 4 data points shown.
●	Thierens <i>et al.</i> , 2012 ¹³⁷	IRD	West EIS; 0.65–1.2 Ma

Supplementary Table 15. Published evidence for the spatial extent of NH glaciation during MIS 20–24. Key corresponds with colours in [Supplementary Figure 9a](#).

Early Matuyama palaeomagnetic Chron (1.78–2.6 Ma)

Key	Reference	Data type	Details
	Balco and Rovey, 2010 ⁸⁷	Empirical outline	LIS; TCN dating indicates ice advance around 2.4 Ma
	Barendregt and Duk-Rodkin, 2011 ¹³⁸	Empirical outline	LIS and CIS; 1.78–2.6 Ma, palaeomagnetic dating
	Barendregt <i>et al.</i> , 2014 ⁸⁸	Empirical outline	LIS and CIS; 1.78–2.6 Ma, palaeomagnetic dating
	Batchelor <i>et al.</i> , 2017 ¹³²	Empirical outline	Western EIS: ice sheet at onset of Quaternary
	Dowdeswell and Ottesen, 2013 ¹³⁹	Seismic data	Western EIS
	Kleman <i>et al.</i> , 2008 ¹⁴⁰	Empirical outline	EIS; 1.0–2.6 Ma
	Knies <i>et al.</i> , 2009 ¹⁴¹	Empirical outline	EIS; maximum and minimum versions based on compilation of empirical data
	Olsen <i>et al.</i> , 2013 ⁸	Empirical outline	EIS; onshore phase at 1.5–2.5 Ma
	Ottesen <i>et al.</i> , 2018 ¹³³	Empirical outline	Western EIS; ice sheet <i>c.</i> 1.6 Ma
	Rea <i>et al.</i> , 2018 ¹⁴²	Empirical outline	EIS; seismic data, from 2.53 Ma
	Solgaard <i>et al.</i> , 2011 ¹⁴³	Model	GIS: 3 models for ice expansion at 2.4–3 Ma. Ice flow model constrained by geological observations and climate reconstructions.
●	Bailey <i>et al.</i> , 2013 ¹⁴⁴	IRD	IRD peak at 2.52 Ma traced to Archaean basement rocks of GIS
●	Barendregt <i>et al.</i> , 2014 ⁸⁸	Point-source	LIS; palaeomagnetic dating. 20 data points shown.
●	Berger and Jokat, 2009 ¹⁴⁵	Seismic data	Northeast GIS; onset of margin progradation around 2.5 Ma
●	Bierman <i>et al.</i> , 2016 ¹³⁴	IRD	Southeast GIS; IRD peak at 1.9 Ma. 2 data points shown.
●	Butt <i>et al.</i> , 2001 ¹⁴⁶	Seismic data	East GIS; seismic data and palaeomagnetic dating
●	Geirsdóttir <i>et al.</i> , 2007 ¹¹¹	Point-source	Iceland; sedimentology and K–Ar dating
●	Hidy <i>et al.</i> , 2013 ¹⁴⁷	Point-source	CIS; TCN dating
●	Hofmann <i>et al.</i> , 2016 ¹⁴⁸	Seismic data	West GIS; seismic stratigraphy
●	Jansen <i>et al.</i> , 2000 ¹⁴⁹	IRD	West EIS; IRD peaks at 2.1 and 2.4 Ma
●	Krissek, 1995 ¹²⁵	IRD	CIS and NE Asia; marine-calving margin at 2.6 Ma. 3 data points shown.
●	Laberg <i>et al.</i> , 2013 ¹³⁵	Seismic data	East GIS; seismic data and palaeomagnetic dating
●	Montelli <i>et al.</i> , 2017 ¹¹⁵	Seismic data	Western EIS; seismic stratigraphy
●	Nielsen and Kuijpers, 2013 ¹¹⁶	Seismic data	Southwest GIS; age of 2.5 Ma suggested from seismic stratigraphy
●	Thierens <i>et al.</i> , 2012 ¹³⁷	IRD	West EIS; marine-calving margin at 2.5 Ma

Supplementary Table 16. Published evidence for the spatial extent of NH glaciation during the early Matuyama Chron. Key corresponds with colours in [Supplementary Figure 9c](#).

Late Gauss palaeomagnetic Chron (2.6–3.59 Ma)

Key	Reference	Data type	Details
	Barendregt and Duk-Rodkin, 2011 ¹³⁸	Empirical outline	CIS; 1.78–2.6 Ma, palaeomagnetic dating
	Barendregt <i>et al.</i> , 2014 ⁸⁸	Empirical outline	CIS; 2.6–3.6 Ma
	Batchelor <i>et al.</i> , 2017 ¹³²	Empirical outline	Western EIS; ice sheet at onset of Quaternary
	Knies <i>et al.</i> , 2009 ¹⁴¹	Empirical outline	EIS; maximum and minimum versions based on compilation of empirical data
	Ottesen <i>et al.</i> , 2018 ¹³³	Empirical outline	Western EIS; ice sheet at onset of Quaternary
	Solgaard <i>et al.</i> , 2011 ¹⁴³	Model	GIS: 3 models for ice expansion at 2.4–3 Ma. Ice flow model constrained by geological observations and climate reconstructions.
●	Bailey <i>et al.</i> , 2013 ¹⁴⁴	IRD	IRD peak at 2.64 Ma traced to Archaean basement rocks of GIS
●	Barendregt <i>et al.</i> , 2014 ⁸⁸	Point-source	CIS; palaeomagnetic dating. 9 data points shown.
●	Bierman <i>et al.</i> , 2016 ¹³⁴	IRD	Southeast GIS; IRD peak at 2.8 Ma
●	Butt <i>et al.</i> , 2001 ¹⁴⁶	Seismic data	East GIS; seismic data and palaeomagnetic dating
●	Geirsdóttir <i>et al.</i> , 2007 ¹¹¹	Point-source	Iceland; sedimentology and K–Ar dating
●	Hidy <i>et al.</i> , 2013 ¹⁴⁷	Point-source	CIS; TCN dating
●	Hofmann <i>et al.</i> , 2016 ¹⁴⁸	Seismic data	West GIS; seismic stratigraphy
●	Jansen <i>et al.</i> , 2000 ¹⁴⁹	IRD	West EIS; IRD peaks at 3.3 and 2.74 Ma
●	Krissek, 1995 ¹²⁵	IRD	CIS and NE Asia; marine-calving margin at 2.6 Ma. 3 data points shown.
●	Thierens <i>et al.</i> , 2012 ¹³⁷	IRD	West EIS; marine-calving margin at 2.6 Ma

Supplementary Table 17. Published evidence for the spatial extent of NH glaciation during the late Gauss Chron. Key corresponds with colours in [Supplementary Figure 10a](#).

Supplementary Notes

Supplementary Note 1: The Last Glacial Maximum (LGM)

The Last Glacial Maximum (LGM) best-estimate reconstruction is based on the LGM extent of Ehlers *et al.*⁹³, which was derived from a compilation of published empirical datasets. In this reconstruction, the Greenland Ice Sheet (GIS) is shown at the shelf break, following marine geophysical work that has identified subglacially formed landforms on the outermost shelf¹⁵¹⁻¹⁵³. Grounded ice is also extended to the shelf break on Grand Banks and beyond Baffin Island, British Columbia and western Britain^{4,154}. A lobe of the Cordilleran Ice Sheet (CIS) is shown to enter the Puget Lowlands during this time¹⁵⁵. The LGM outline of Barr and Clark¹⁵⁶, which is more detailed than that of Ehlers *et al.*⁹³, is used in north-east (NE) Asia.

Robustness score

Mean robustness score: 5 (ice-sheet-wide empirical outlines)

Supplementary Note 2: 30 ka

The reader should refer to [Supplementary Figure 2a](#) for a map of previously published data on ice-sheet extent at 30 ka, [Supplementary Figure 2b](#) for a map of the maximum, minimum and best-estimate ice-sheet reconstructions, and [Supplementary Table 1](#) for details of the data sources used to inform these reconstructions.

Maximum estimate of the 30 ka ice-sheet extent

The maximum ice extent in Europe at 30 ka is based mainly on empirical data and the ice-sheet extent at the LGM. The empirical outlines of Larsen *et al.*⁶, Hughes *et al.*⁴ and Marks⁷ are followed over western Europe and Scandinavia. The EIS is extended to the east to include Finland because of the geometry of the ice in northern Poland. Hughes *et al.*⁴ keep Finland ice-free in their reconstruction for 30–32 ka, but note that they find it likely that ice expansion to the south was matched by ice growth to the east. Over northern Siberia, the LGM extent is used for the Barents-Kara Sea, and the maximum MIS 4 extent is used for the Putorana Plateau in central Siberia. Ice is shown to extend to the shelf break beyond northern Britain and Norway, as suggested by ice-rafted debris (IRD) records^{21,25}. Ice is shown in the North Sea, and ice in Greenland and Iceland is shown at the shelf break. Ice is also shown at the shelf break along the northern, northwestern and eastern margin of the Laurentide Ice Sheet (LIS). The southern and western margin of the LIS is the larger of the two empirically derived outlines of Dyke *et al.*² and Kleman *et al.*⁵. The CIS is shown at its LGM extent⁹³. The maximum Quaternary ice-sheet extent template is used in NE Asia, which is a combination of the maximum Quaternary limits of Glushkova⁵⁵ and Barr and Clark¹⁵⁶ (see [Methods](#)).

Minimum estimate of the 30 ka ice-sheet extent

The minimum ice extent in Europe at 30 ka is based on the outline of Hughes *et al.*⁴ for 30–32 ka, which is a compilation of empirical evidence. Ice in Greenland and Iceland is shown at the present-day coastline. The LIS is the smaller of the two empirically derived outlines of Dyke *et al.*² and Kleman *et al.*⁵. The minimum ice extent was further reduced in west-central Canada by ~500 km to account for the possibility of an ice-free interval in that area as indicated by thermoluminescence dating of non-glacial sediments¹⁵⁷. The CIS extent is based on the 30 ka regional model of Seguinot *et al.*¹⁶. The LGM extent of Barr and Clark¹⁵⁶ is used in NE Asia.

47 **Best-estimate of the 30 ka ice-sheet extent**

48 The minimum ice extent in Europe at 30 ka, which is the empirically derived
49 reconstruction of Hughes *et al.*⁴, is generally used as the best-estimate for the 30 ka ice-sheet
50 reconstruction. The exception is that the ice sheet is extended to the shelf break in the
51 northern North Sea to account for the probable operation of the Norwegian Channel Ice
52 Stream during this time^{26,70,158}. Our best-estimate reconstruction does not include the tentative
53 outlines of Marks⁷ in Poland and Lithuania, which span 33–37 ka. Ice in Greenland is shown
54 in a mid-shelf position, following the suggestion that the ice sheet was on the continental
55 shelf during this time⁸². Ice in Iceland is shown at the present-day coastline. The detailed
56 empirically derived reconstruction of Dyke *et al.*² is followed for the best-estimate LIS at 30
57 ka. Although the 1-sigma errors on Berger and Nielsen's¹⁵⁷ geochronological data overlap
58 with the 30 ka interval, it is more likely that this part of the Hudson Bay Lowlands was ice-
59 free closer to the 40 ka interval, as supported by various radiocarbon dates¹⁵⁹. To be
60 conservative, the best-estimate for the CIS and ice in NE Asia at 30 ka is the same as the
61 minimum.

62 **Robustness scores for the 30 ka ice-sheet reconstruction**

63 EIS 4 (empirical outlines constrain much of the ice margin)
64 LIS 5 (ice-sheet-wide empirical outlines)
65 CIS 1 (modelled outlines)
66 NE Asia 1 (modelled outlines)
67 Mean robustness score: 2.75

68

Supplementary Note 3: 35 ka

69 The reader should refer to [Supplementary Figure 2c](#) for a map of previously published
70 data on ice-sheet extent at 35 ka, [Supplementary Figure 2d](#) for a map of the maximum,
71 minimum and best-estimate ice-sheet reconstructions, and [Supplementary Table 2](#) for details
72 of the data sources used to inform these reconstructions.

73 **Maximum estimate of the 35 ka ice-sheet extent**

74 For the maximum European Ice Sheet (EIS) at 35 ka, the empirical outlines of
75 Houmark-Nielsen³, Obst *et al.*³⁵ and Marks⁷ in northern Germany and Poland are merged
76 with the outline of Olsen *et al.*⁸ in Scandinavia and the LGM ice extent in the Barents-Kara
77 Sea. The maximum MIS 4 ice extent is used for the Putorana Plateau in central Siberia. Ice in
78 Greenland and Iceland is shown at the present-day shelf break. For the maximum LIS, ice is
79 shown at the shelf break along the northern and eastern margin. The empirically derived late
80 MIS 3 outline of Kleman *et al.*⁵ is used to the south. The western LIS margin is the modelled
81 outline of Ganopolski and Calov¹¹, which keeps the LIS and CIS separate during this time¹⁶⁰.
82 The LGM ice extent is used for the CIS, and the maximum Quaternary ice-extent
83 template^{55,156} is used for NE Asia (see [Methods](#)).

84 **Minimum estimate of the 35 ka ice-sheet extent**

85 For the minimum EIS at 35 ka, the larger of the two empirically derived outlines
86 provided by Hughes *et al.*⁴ for the period 34–38 ka is used. Ice in Greenland and Iceland is
87 shown at the coastline. A schematic ice cap is shown over Scotland, which is based on the
88 minimum modelled ice extent in Britain during MIS 4¹⁸. The empirically derived late MIS 3
89 outline of Kleman *et al.*⁵ is used for the minimum LIS at 35 ka, but is not allowed to extend
90 beyond the detailed empirical reconstruction of Dyke *et al.*² for 30 ka. The minimum ice
91 extent was further reduced in west-central Canada by ~200 km to account for the possibility
92 of an ice-free interval in the Hudson Bay Lowlands as indicated by thermoluminescence
93 work on non-glacial sediments¹⁵⁷. The minimum LIS extent was also reduced in the Ungava
94 Peninsula, Canada, by ~200 km to account for the possibility of an ice-free interval as
95 indicated by various radiocarbon ages on non-glacial sediments¹⁶¹. Because of an absence of
96 data, only coastal mountain glaciers are shown for the CIS and no ice is shown in NE Asia.

97 **Best-estimate of the 35 ka ice-sheet extent**

98 To be conservative, the minimum ice-sheet extents over Britain and Iceland are used
99 for the 35 ka best-estimate. The tentative outlines of Obst *et al.*³⁵, Marks⁷ and Olsen *et al.*⁸,
100 which show the EIS extending into northern Germany, Poland and Finland during this time,
101 are not included. Instead, the ice sheet is shown following the present-day coastline around
102 Norway and Sweden, in agreement with the empirical reconstruction of Houmark-Nielsen³
103 and IRD records off southern and western Norway^{21,26}. Ice in Greenland is shown in a mid-
104 shelf position, following Funder *et al.*⁸², who suggest that the ice sheet was on the continental
105 shelf during this time. The minimum LIS at 35 ka is used as the best-estimate in most areas.
106 This outline is based on the empirically derived late MIS 3 outline of Kleman *et al.*⁵ and the
107 detailed empirical reconstruction of Dyke *et al.*² for 30 ka. Although the 1-sigma errors on
108 Berger and Nielsen's¹⁵⁷ geochronological data overlap with the 35 ka interval, it is more
109 likely that these sites in the Hudson Bay Lowlands were ice-free closer to the 40 ka interval,
110 as supported by various radiocarbon dates¹⁵⁹. The Ungava Peninsula in Canada is shown as
111 ice-covered. Although there is no evidence to rule out the possibility that this region was ice-
112 free at 35 ka, Guyard *et al.*¹⁶¹ suggest that their radiocarbon ages may represent a minimum
113 age estimate owing to the suspected mixing of older and younger carbon in the sample. To be
114 conservative, the best-estimate 30 ka ice extent is used for the CIS¹⁶, and the LGM of Barr
115 and Clark¹⁵⁶ is used for NE Asia.

116 **Robustness scores for the 35 ka ice-sheet reconstruction**

117 EIS 3 (regional empirical outlines of contrasting extent)

118 LIS 3 (single broad-scale empirical outline)

119 CIS 1 (modelled outlines)

120 NE Asia 1 (modelled outlines)

121 Mean robustness score: 2

122

123

124

125

126

Supplementary Note 4: 40 ka

127 The reader should refer to [Supplementary Figure 3a](#) for a map of previously published
128 data on ice-sheet extent at 40 ka, [Supplementary Figure 3b](#) for a map of the maximum,
129 minimum and best-estimate ice-sheet reconstructions, and [Supplementary Table 3](#) for details
130 of the data sources used to inform these reconstructions.

131 **Maximum estimate of the 40 ka ice-sheet extent**

132 For the maximum EIS at 40 ka, the maximum modelled ice extent over Europe is
133 used, because the outline of Arnold *et al.*³³ is a minimum estimate and the outline of
134 Houmark-Nielsen³ depicts ice at 34–46 ka. The modelled outlines selected are not allowed to
135 be larger than at the LGM. This means that the LGM limit is used everywhere except for
136 Britain and the North Sea¹⁰, Poland^{10, 18} and western Russia¹⁸. Ice in Greenland and Iceland is
137 shown at the present-day shelf break. Ice is also shown at the shelf break for the northern and
138 eastern margin of the LIS. For the southern LIS margin, the largest modelled outline is used¹⁸
139 but is not allowed to be larger than at the LGM. The modelled outline of Ganopolski and
140 Calov¹¹ is used for the western LIS margin because it keeps the LIS and CIS separate¹⁶⁰.
141 Because of an absence of empirical data, the LGM extent⁹³ is used for the CIS. For NE Asia,
142 the maximum Quaternary ice-extent template (based on Glushkova⁵⁵ and Barr and Clark¹⁵⁶),
143 is used to account for the large ice-sheet outline of Barr and Solomina⁴¹.

144 **Minimum estimate of the 40 ka ice-sheet extent**

145 For the minimum EIS at 40 ka, ice is not shown in Britain, as in Hughes *et al.*⁴. The
146 outline of Houmark-Nielsen³ is combined with the maximum outline of Hughes *et al.*⁴ (34–38
147 ka) over Scandinavia. The present-day ice cover is used for the islands of the Barents and
148 Kara seas, and ice is shown to the coastline for Greenland and Iceland. For the LIS,
149 hypothesis 2 of Dredge and Thorleifson⁴² is used, which shows small ice-dispersal areas. This
150 minimum ice extent is supported by geochronological data from the Hudson Bay Lowlands,
151 Canada, which show the development of peatlands and boreal forests in this region at ~40
152 ka¹⁵⁹. Coastal mountain glaciers are shown for the CIS, and the LGM extent of Barr and
153 Clark¹⁵⁶ is used for NE Asia.

154 **Best-estimate of the 40 ka ice-sheet extent**

155 We note that the 40 ka interval immediately preceded a time of rapid ice growth in the
156 NH^{162,163}. For the best-estimate EIS at 40 ka, the empirical outlines of Houmark-Nielsen³,
157 Hughes *et al.*⁴ and van Andel and Tzedakis⁴³ are used but are not allowed to extend beyond
158 the 35 ka best-estimate along the eastern margin. The ice sheet is shown on the continental
159 shelf off southern and western Norway, in agreement with IRD records^{21,26} and suggestions
160 that the southern Fennoscandian Ice Sheet (FIS) extended beyond the coastline around 42
161 ka^{43,164,165}. To be conservative, the minimum ice extent is followed in the Barents and Kara
162 seas and Iceland. As a mid-point between our minimum and maximum reconstructions, a
163 schematic ice cap is placed over Scotland, which is based mainly on the minimum modelled
164 ice extent in Britain during MIS 4¹⁸. Ice is extended onto the continental shelf to the north of
165 Scotland, as suggested by Lekens *et al.*²⁶. However, it is worth noting that Hughes *et al.*⁴ do
166 not include any ice over Britain in their reconstruction for 34–38 ka. Ice in Greenland is
167 shown in a mid-shelf position, following Funder *et al.*⁸² who suggest that the ice sheet was on
168 the continental shelf during this time.

169 Over North America, the minimum outline, based on hypothesis 2 of Dredge and
170 Thorleifson⁴², is used for the LIS. This ice extent is supported by geochronological data from
171 the Hudson Bay Lowlands, Canada, showing the development of peatlands and boreal forests
172 in this region at ~40 ka¹⁵⁹. Recently, the feasibility of such a reduced ice extent was
173 demonstrated by reconciling geological data from the Hudson Bay Lowlands with estimates
174 of sea level and isostatic adjustment for this area¹⁶⁶. Deglaciation of Hudson Bay at ~40 ka is
175 also supported by 8 radiocarbon dates on shells from Wager Bay¹⁶⁷. The 30 ka ice-extent
176 template (see [Methods](#)) is used for the CIS¹⁶, and the Quaternary maximum ice-extent
177 template is used in NE Asia^{55,156}.

178 **Robustness scores for the 40 ka ice-sheet reconstruction**

179 EIS 3 (ice-sheet-wide empirical outlines of contrasting extent)
180 LIS 3 (ice-sheet-wide empirical outlines of contrasting extent)
181 CIS 1 (modelled outlines)
182 NE Asia 3 (regional empirical outline and modelled outlines).
183 Mean robustness score: 2.5

184

Supplementary Note 5: 45 ka

185 The reader should refer to [Supplementary Figure 3c](#) for a map of previously published
186 data on ice-sheet extent at 45 ka, [Supplementary Figure 3d](#) for a map of the maximum,
187 minimum and best-estimate ice-sheet reconstructions, and [Supplementary Table 4](#) for details
188 of the data sources used to inform these reconstructions.

189 **Maximum estimate of the 45 ka ice-sheet extent**

190 The maximum limit of the empirical data is used for the maximum EIS at 45 ka. It
191 should be noted that, due to the spread of the ages, some of these outlines^{3,35,48} probably
192 relate to MIS 4 rather than the peak warmth of MIS 3. This maximum outline accounts for the
193 possibility of a second Weichselian glaciation in Finland at 40–45 ka¹⁶⁸. A schematic ice cap
194 is shown over Scotland, which is based on the minimum modelled ice extent in Britain during
195 MIS 4¹⁸. Ice in Greenland and Iceland is shown at the shelf break.

196 Over North America, the best-estimate LIS at 35 ka, which is based on the empirically
197 derived late MIS 3 outline of Kleman *et al.*⁵ and the detailed empirical reconstruction of
198 Dyke *et al.*² for 30 ka, is used for the maximum LIS at 45 ka. This outline is extended by
199 around 150 km in the northwest and southeast to include areas covered by ice in hypothesis 2
200 of Dredge and Thorleifson⁴². The LGM outline of Ehlers *et al.*⁹³ is used for the CIS. Because
201 of an absence of empirical data, the maximum Quaternary ice-extent template (derived from
202 Glushkova⁵⁵ and Barr and Clark¹⁵⁶) is used for NE Asia.

203 **Minimum estimate of the 45 ka ice-sheet extent**

204 The present-day ice cover is used as the minimum ice extent over Europe, Greenland,
205 the North American Cordillera and NE Asia at 45 ka. Hypothesis 2 of Dredge and
206 Thorleifson⁴², which shows small ice-dispersal centres, is used for the LIS. These minimal ice
207 outlines are supported by geochronological work (radiocarbon, OSL) on sub-till sediments
208 from the Hudson Bay Lowlands¹⁵⁹.

209 **Best-estimate of the 45 ka ice-sheet extent**

210 For the best-estimate EIS at 45 ka, we include small ice caps over high areas of
211 Norway and Svalbard. We note that our reconstruction tries to capture the peak warmth of
212 MIS 3, whereas some of the empirical outlines shown for 45 ka may relate to MIS 4^{3,35,48} or
213 the suggested expansion of the FIS around 42 ka⁸. Ice in Greenland is shown in a mid-shelf

214 position, following Funder *et al.*⁸² who suggest that the ice sheet was on the continental shelf
215 during this time. Ice in Iceland is shown at the present-day coastline.

216 Over North America, the minimum LIS extent, which is based on hypothesis 2 of
217 Dredge and Thorleifson⁴² is used as the best-estimate. This minimum ice extent is supported
218 by geochronological data from the Hudson Bay Lowlands, Canada, which show the
219 development of peatlands and boreal forests in this region at ~40 ka¹⁵⁹. Recently, the
220 feasibility of such a reduced ice extent was demonstrated by reconciling geological data from
221 the Hudson Bay Lowlands with estimates of sea level and isostatic adjustment for this area¹⁶⁶.
222 Coastal mountain glaciers are shown for the CIS, and the LGM ice-extent template of Barr
223 and Clark¹⁵⁶ is used for NE Asia ([Methods](#)).

224 **Robustness scores for the 45 ka ice-sheet reconstruction**

225 EIS 3 (ice-sheet-wide empirical outlines of contrasting extent)

226 LIS 3 (ice-sheet-wide empirical outlines of contrasting extent)

227 CIS 1 (modelled outlines)

228 NE Asia 1 (modelled data)

229 Mean robustness score: 2

230

Supplementary Note 6: MIS 4 (58–72 ka)

231 The reader should refer to [Supplementary Figure 4a](#) for a map of previously published
232 data on ice-sheet extent during MIS 4, [Supplementary Figure 4b](#) for a map of the maximum,
233 minimum and best-estimate ice-sheet reconstructions, and [Supplementary Table 5](#) for details
234 of the data sources used to inform these reconstructions.

235 **Maximum estimate of the MIS 4 (58–72 ka) ice-sheet extent**

236 The maximum empirical data extent is used for the maximum EIS during MIS 4. Ice
237 in Greenland, Iceland and northern Britain is shown at the shelf break. The reconstruction of
238 Helmens⁴⁷ is used for the southern margin of the British Irish Ice Sheet (BIIS). Over North
239 America, as the empirical reconstruction of Kleman *et al.*⁵ is extrapolated from flow lines and
240 topography, the maximum modelled outline is used for the southern LIS, which is based on
241 Stokes *et al.*¹⁷. The western margin of the LIS is the same as the maximum reconstruction for
242 MIS 6. The MIS 6 outline is derived from the empirical data of Barendregt *et al.*⁸⁸ (modified
243 from Barendregt and Duk-Rodkin¹³⁸), the empirically derived outline of Jackson *et al.*⁹⁹ and
244 the modelled outlines of Peltier¹⁰⁸ and de Boer *et al.*¹⁰. This reconstruction leaves Edmonton
245 ice free during MIS 4, as suggested by Young *et al.*¹⁶⁰. The maximum Quaternary ice-extent
246 template is used for the maximum CIS during MIS 4. This uses the pre-Reid limit of
247 Kaufman *et al.*⁵⁷ in Alaska, the pre-Reid limit of Turner *et al.*⁶⁴ in the Yukon, and the MIS 6
248 modelled outline of Ganopolski and Calov¹¹ for the southern CIS (see [Methods](#)). The
249 Quaternary maximum ice extent of Glushkova⁵⁵ and Barr and Clark¹⁵⁶ is used in NE Asia,
250 and extensive grounded ice is shown in the Arctic Ocean^{100,105}.

251 **Minimum estimate of the MIS 4 (58–72 ka) ice-sheet extent**

252 For the minimum EIS during MIS 4, the minimum empirical ice extent is followed
253 over Scandinavia⁵⁹ and the Barents-Kara Sea⁴⁸. Ice is not included in the North Sea, and
254 northwest Denmark is left ice-free after Houmark-Nielsen³. The smallest modelled ice
255 extent¹⁸ is shown over Scotland. Ice in Greenland and Iceland is shown to the present-day
256 coastline. The empirically derived outline of Kleman *et al.*⁵ is broadly used for the LIS. This
257 minimum ice extent was further reduced in central and eastern Canada by 500–1000 km to
258 account for the possibility of an ice-free interval in these areas. Optically stimulated
259 luminescence dating, uranium-thorium dating and thermoluminescence dating of non-glacial
260 deposits in eastern Canada allow for the possibility that these areas were ice-free during MIS

261 4¹⁶⁹⁻¹⁷⁴. The minimum ice extent was further reduced in the Hudson Bay Lowlands by 500–
262 1000 km to account for the possibility of an ice-free interval in that area as indicated by
263 optically stimulated luminescence and uranium-thorium dating on non-glacial materials^{175,176}.
264 The LGM ice-extent template is used for the CIS⁹³ (see [Methods](#)). The Quaternary maximum
265 ice-extent template is used for NE Asia, which includes the empirically derived outline of
266 Glushkova⁵⁵ for MIS 4.

267 **Best-estimate of the MIS 4 (58–72 ka) ice-sheet extent**

268 The outline of Svendsen *et al.*⁶², which is based on a compilation of empirical data, is
269 broadly used for the best-estimate EIS in its northern and western margins during MIS 4. This
270 may correspond with the Ristinge Advance of around 50 ka into eastern Denmark^{3,35,48}. Ice is
271 shown in northeast Germany in the best-estimate, as suggested by Möller⁶⁰, but we note that
272 this is an area of uncertainty. Where there is a difference between the outlines of Svendsen *et*
273 *al.*⁶² and Mangerud *et al.*³⁴ in northwest Russia, we follow the more detailed, less extensive
274 reconstruction of Svendsen *et al.*⁶². Glaciation of the Urals^{52,62} is included in the MIS 4 best-
275 estimate. The tentative outline of Carr *et al.*⁵⁴ is used for the southern margin of the BIIS. The
276 BIIS is extended to the shelf break beyond Scotland as suggested by offshore evidence for
277 ice-sheet expansion during this time^{24,71}. Ice is shown in the North Sea^{47,54,72}. To be
278 conservative, ice in Greenland is shown in a mid-shelf position, and ice in Iceland is shown at
279 the present-day coastline.

280 For North America, the empirically derived outline of Kleman *et al.*⁵ is used as the
281 best-estimate for the LIS. Empirical data from the Hudson Bay Lowlands are not
282 incorporated into the best-estimate because of low precision of these ages, which leaves the
283 possibility that they may reflect ice-free conditions during MIS 3 or MIS 5a¹⁷⁶. The Reid ice-
284 extent template of suggested MIS 4/MIS 6 age is used in Alaska (Kaufman *et al.*⁵⁷) and
285 Yukon (Turner *et al.*⁶⁴) ([Methods](#)). The Quaternary maximum ice-extent template is used for
286 NE Asia^{55,156}. To be conservative, extensive grounded ice is not shown in the Arctic Ocean,
287 but we note that grounded ice may have been present on bathymetric highs^{100,105}.

288 **Robustness scores for the MIS 4 (58–72 ka) ice-sheet reconstruction**

289 EIS 4 (ice-sheet-wide empirical outlines with some differences in ice extent)
290 LIS 2 (single broad-scale empirical outline)
291 CIS 3 (regional empirical outlines)
292 NE Asia 3 (regional empirical outlines)

293 Mean robustness score: 3.

294

295

296

297

298

299

300

301

302

303

304

305

306

307

308

309

310

311

312

313

314

315

316

317

318

319

320

321

322

323

Supplementary Note 7: MIS 5a (72–86 ka)

324

325

326

327

The reader should refer to [Supplementary Figure 4c](#) for a map of previously published data on ice-sheet extent during MIS 5a, [Supplementary Figure 4d](#) for a map of the maximum, minimum and best-estimate ice-sheet reconstructions, and [Supplementary Table 6](#) for details of the data sources used to inform these reconstructions.

328

Maximum estimate of the MIS 5a (72–86 ka) ice-sheet extent

329

330

331

332

333

334

335

336

337

338

For the maximum EIS during MIS 5a, the maximum modelled outline is used but is not allowed to be larger than the best-estimate reconstruction for MIS 5b or 5d. We note that this outline is probably unrealistically extensive. Ice is shown on the continental shelf beyond Scotland to account for the suggestion that ice may have reached beyond the coastline around 80 ka²⁶. To cover the maximum scenario, ice is shown to the shelf break beyond Greenland and Iceland. For the maximum LIS during MIS 5a, the modelled outline of Stokes *et al.*¹⁷ is combined with hypothesis 2 of Dredge and Thorleifson⁴² for MIS 3. The 30 ka ice-extent template¹⁶ is used for the CIS, and the Quaternary maximum ice-extent template is used for NE Asia^{55,156} (see [Methods](#)). Extensive grounded ice (following the empirically derived outlines for MIS 6^{89,100,105}) is shown in the Arctic Ocean.

339

Minimum estimate of the MIS 5a (72–86 ka) ice-sheet extent

340

341

342

343

There is some evidence that global sea level during MIS 5a was close to that of the present-day¹⁷⁸. To capture this uncertainty, the present-day ice cover is used for the minimum MIS 5a ice extent in Eurasia, Greenland, Iceland and North America. An ice cap, based on hypothesis 2 of Dredge and Thorleifson⁴², is also included over Baffin Island.

344

Best-estimate of the MIS 5a (72–86 ka) ice-sheet extent

345

346

347

348

349

350

351

352

For the best-estimate EIS during MIS 5a, the empirically derived outline of Mangerud *et al.*³⁴ over Norway is combined with the best-estimate 30 ka ice extent (based on Hughes *et al.*⁴) for the islands of the Barents-Kara Sea. To be conservative, no ice is shown in Britain; it is possible that IRD evidence for shelf glaciation during this time²⁶ may relate to a colder period within MIS 4 or 5. Ice in Greenland and Iceland is shown at the present-day coastline. Hypothesis 2 of Dredge and Thorleifson⁴², which is also used as the best-estimate for 45 ka, is followed for the best-estimate LIS during MIS 5a. This ice extent is supported by geochronological data that suggest that large areas of North America were ice-free at this

353 time^{170,171,175}. A schematic outline showing coastal mountain glaciation is used in the North
354 American Cordillera, and the LGM ice-extent template is suggested in NE Asia¹⁵⁶.

355 **Robustness scores for the MIS 5a (72–86) ka ice-sheet reconstruction**

356 EIS 2 (two empirical outlines and modelled outlines)

357 LIS 1 (modelled outlines; uses ice-sheet extent at 45 ka)

358 CIS 1 (modelled outlines)

359 NE Asia 1 (modelled outlines)

360 Mean robustness score: 1.25

361

362

363

364

365

366

367

368

369

370

371

372

373

374

375

376

377

Supplementary Note 8: MIS 5b (86–92 ka)

378 The reader should refer to [Supplementary Figure 5a](#) for a map of previously published
379 data on ice-sheet extent during MIS 5b, [Supplementary Figure 5b](#) for a map of the maximum,
380 minimum and best-estimate ice-sheet reconstructions, and [Supplementary Table 7](#) for details
381 of the data sources used to inform these reconstructions.

382 **Maximum estimate of the MIS 5b (86–92 ka) ice-sheet extent**

383 The maximum empirical outline^{8,34,53,62,81} is used for the maximum EIS during MIS
384 5b. Ice is extended to the shelf break in the western Barents Sea, as suggested by Eccleshall
385 *et al.*⁶⁷. A schematic ice cap, based on the minimum modelled ice extent in Britain during
386 MIS 4¹⁸, is shown in Scotland. To cover the maximum scenario, ice in Greenland and Iceland
387 is shown at the shelf break. For the LIS, the maximum modelled outline, which was derived
388 by combining Zweck and Huybrechts¹⁸ and Ganopolski and Calov¹¹, is used, but is not
389 allowed to be larger than the best-estimate for MIS 4. This is because the global benthic $\delta^{18}\text{O}$
390 stack shows MIS 5b to have been significantly warmer than MIS 4⁷⁹. The northwest margin
391 of the LIS is further reduced from the MIS 4 extent in the Mackenzie Delta region, following
392 work that suggests that there were only two ice-sheet advances into this region (probably
393 during either the LGM and MIS 4, or the LGM and MIS 6¹⁷⁹). The LGM extent of Ehlers *et*
394 *al.*⁹³ is shown for the CIS and the maximum Quaternary ice-extent template^{55,156} is used for
395 NE Asia. Extensive grounded ice (following the empirically derived outlines for MIS
396 6^{89,100,105}) is shown in the Arctic Ocean.

397 **Minimum estimate of the MIS 5b (86–92 ka) ice-sheet extent**

398 For the minimum EIS during MIS 5b, the minimum empirical outline is used over
399 Europe, and the present-day ice extent is used for Greenland and Iceland. The empirically
400 derived MIS 5b/5d outline of Kleman *et al.*⁵ is used for the LIS, together with the present-day
401 ice extent in the islands of the Canadian Arctic. The minimum LIS extent was further reduced
402 in the Gulf of Saint Lawrence and off the coast of Nova Scotia by ~100 to ~200 km to
403 account for the possibility of an ice-free interval in this area as indicated by optically
404 stimulated luminescence and uranium-thorium dating of non-glacial sediments^{170,174}. Coastal
405 mountain glaciers are shown for the CIS, and the LGM extent of Barr and Clark¹⁵⁶ is used for
406 NE Asia.

407 **Best-estimate of the MIS 5b (86–92 ka) ice-sheet extent**

408 The empirical outlines of Svendsen *et al.*⁶² and Astakhov *et al.*⁵³ are used for the best-
409 estimate EIS during MIS 5b. The exception is on the western margin of Svalbard, where the
410 ice limit is extended to the shelf break, as suggested by the work of Eccleshall *et al.*⁶⁷. Ice in
411 Greenland is shown in an inner- to mid-shelf position, following the work of Funder *et al.*⁸²
412 who suggest that the eastern GIS extended to the Kap Brewster ridge off Scoresby Sund
413 during MIS 5b. Ice in Iceland is extended to the present-day coastline. The minimum ice-
414 sheet reconstruction for MIS 5b is used for the best-estimate in North America. The
415 maximum ice-extent template is used for NE Asia, as suggested by IRSL dates of 80–90 ka
416 on a moraine in this region⁵⁰. To be conservative, grounded ice is not shown in the Arctic
417 Ocean, but we note that grounded ice may have been present on bathymetric highs^{100,105}.

418

419 **Robustness scores for the MIS 5b (86–92 ka) ice-sheet reconstruction**

- 420 EIS 5 (ice-sheet-wide empirical outlines)
- 421 LIS 3 (single broad-scale empirical outline)
- 422 CIS 1 (modelled outlines)
- 423 NE Asia 1 (modelled outlines)
- 424 Mean robustness score: 2.5

425

Supplementary Note 9: MIS 5c (92–108 ka)

426 The reader should refer to [Supplementary Figure 5c](#) for a map of previously published
427 data on ice-sheet extent during MIS 5c, [Supplementary Figure 5d](#) for a map of the maximum,
428 minimum and best-estimate ice-sheet reconstructions, and [Supplementary Table 8](#) for details
429 of the data sources used to inform these reconstructions.

430 **Maximum estimate of the MIS 5c (92–108 ka) ice-sheet extent**

431 The maximum empirical outlines in Europe are used for the maximum EIS during
432 MIS 5c. The modelled ice extent of Zweck and Huybrechts¹⁸ for MIS 5a is used for the
433 maximum ice extent on the Putorana Plateau during MIS 5c. This limit is slightly larger than
434 their modelled outline for MIS 5c, and therefore captures a greater range of uncertainty. Ice
435 in Greenland and Iceland is shown to the shelf break. For the maximum LIS, the modelled
436 outline of Stokes *et al.*¹⁷ is combined with hypothesis 2 of Dredge and Thorleifson⁴² for MIS
437 3. The 30 ka ice-extent template¹⁶ is used for the CIS, and the Quaternary maximum ice-
438 extent template^{55,156} is used for NE Asia (see [Methods](#)). Extensive grounded ice (following
439 the empirically derived outlines for MIS 6^{89,100,105}) is shown in the Arctic Ocean.

440 **Minimum estimate of the MIS 5c (92–108 ka) ice-sheet extent**

441 The present-day ice cover is used for the minimum MIS 5c ice extent in Eurasia,
442 Greenland, Iceland and North America. An ice cap, based on hypothesis 2 of Dredge and
443 Thorleifson⁴², is also included over Baffin Island.

444 **Best-estimate of the MIS 5c (92–108 ka) ice-sheet extent**

445 The best-estimate for MIS 5a (which uses the MIS 5a empirical outline of Mangerud
446 *et al.*³⁴ in Norway and the 30 ka ice extent of Hughes *et al.*⁴ in the Barents-Kara Sea) is used
447 for the best-estimate EIS during MIS 5c. Ice in Greenland and Iceland is shown at the
448 present-day coastline. Hypothesis 2 of Dredge and Thorleifson⁴², which is also used for the
449 best-estimate of 45 ka and MIS 5a, is used for the best-estimate LIS during MIS 5c. This ice
450 extent is supported by geochronological data that suggest that parts of eastern Canada^{170,174}
451 and the Hudson Bay Lowlands^{175,180} were ice-free during this time. Coastal mountain
452 glaciation is shown in the North American Cordillera, and the LGM ice-extent template¹⁵⁶ is
453 suggested for NE Asia ([Methods](#)).

- 454 **Robustness scores for the MIS 5c (92–108 ka) ice-sheet reconstruction**
- 455 EIS 3 (ice-sheet-wide empirical outlines of contrasting extent)
- 456 LIS 1 (modelled outlines; uses ice-sheet extent during 45 ka)
- 457 CIS 1 (modelled outlines)
- 458 NE Asia 1 (modelled outlines)
- 459 Mean robustness score: 1.5

460

Supplementary Note 10: MIS 5d (108–117 ka)

461

462

463

464

The reader should refer to [Supplementary Figure 6a](#) for a map of previously published data on ice-sheet extent during MIS 5d, [Supplementary Figure 6b](#) for a map of the maximum, minimum and best-estimate ice-sheet reconstructions, and [Supplementary Table 9](#) for details of the data sources used to inform these reconstructions.

465

Maximum estimate of the MIS 5d (108–117 ka) ice-sheet extent

466

467

468

469

470

471

472

473

474

475

476

477

For the maximum EIS during MIS 5d, the maximum empirical data over western Scandinavia⁵⁹ are combined with the maximum modelled outline in eastern Europe and western Siberia^{11,76}. This outline is extended slightly farther south in Russia to account for the Kormuzhikhantskaya moraine, which has a suggested age of 100–117 ka^{85,181,182}. Ice is shown on the continental shelf beyond Scotland to account for the suggestion that ice may have reached beyond the coastline during this time²⁶. To cover the maximum scenario, ice in Greenland and Iceland is shown at the shelf break. For the LIS, the maximum modelled outline, which was derived by combining Ganopolski and Calov¹¹ and de Boer *et al.*¹⁰, is used, but is not allowed to be larger than the best-estimate for MIS 4. The LGM ice-extent template⁹³ is shown for the CIS, and the maximum Quaternary ice-extent template^{55,156} is used for NE Asia (see [Methods](#)). Extensive grounded ice (following the empirically derived outlines for MIS 6^{89,100,105}) is shown in the Arctic Ocean.

478

Minimum estimate of the MIS 5d (108–117 ka) ice-sheet extent

479

480

481

482

483

484

485

486

487

For the minimum EIS during MIS 5d, the smallest empirical outline⁴⁷ is used over Scandinavia. The MIS 5c outline of Larsen *et al.*⁴⁸, adjusted to incorporate the MIS 5d outline of Möller *et al.*⁶⁰, is used for the Barents-Kara Sea. The present-day ice extent is used for Greenland and Iceland. The MIS 5b/5d empirically derived outline of Kleman *et al.*⁵ is used for the LIS. The minimum LIS extent was further reduced in the Gulf of Saint Lawrence and off the coast of Nova Scotia by ~100 to 200 km to account for the possibility of an ice-free interval in that area as indicated by optically stimulated luminescence and uranium-thorium dating of non-glacial sediments^{170,174}. Coastal mountain glaciers are shown for the CIS, and the LGM ice-extent template¹⁵⁶ is used for NE Asia ([Methods](#)).

488 **Best-estimate of the MIS 5d (108–117 ka) ice-sheet extent**

489 For the best-estimate ice sheet in the Barents-Kara Sea, the MIS 5d minimum estimate
490 is combined with the outline of Möller *et al.*⁶⁰ for MIS 5d and Astakhov *et al.*⁵³ for MIS 5b.
491 The ice extent over Scandinavia follows the maximum of the empirical outlines for MIS
492 5d^{8,34,47,59}. To be conservative, the ice sheet is not extended to the Kormuzhikhantskaya
493 moraine in Russia^{85,181,182}, and no ice is shown in Britain. Ice in Greenland is shown in an
494 inner- to mid-shelf position, following the work of Funder *et al.*⁸² who suggest that the
495 eastern GIS extended to the Kap Brewster ridge off Scoresby Sund during MIS 5d. Ice in
496 Iceland is extended to the present-day coastline. The minimum ice-sheet reconstruction for
497 MIS 5d is used for the best-estimate in North America. The maximum ice-extent
498 template^{55,156} is used for NE Asia. To be conservative, grounded ice is not shown in the
499 Arctic Ocean, but we note that grounded ice may have been present on bathymetric
500 highs^{105,183}.

501 **Robustness scores for the MIS 5d (108–117 ka) ice-sheet reconstruction**

502 EIS 3 (ice-sheet-wide empirical outlines of contrasting extent)

503 LIS 3 (single broad-scale empirical outline)

504 CIS 1 (modelled outlines)

505 NE Asia 1 (modelled outlines)

506 Mean robustness score: 2

507

Supplementary Note 11: MIS 6 (132–190 ka)

508 The reader should refer to [Supplementary Figure 6c](#) for a map of previously published
509 data on ice-sheet extent during MIS 6, [Supplementary Figure 6d](#) for a map of the maximum,
510 minimum and best-estimate ice-sheet reconstructions, and [Supplementary Table 10](#) for details
511 of the data sources used to inform these reconstructions.

512 **Maximum estimate of the MIS 6 (132–190 ka) ice-sheet extent**

513 The maximum empirical data limit is used to define most of the maximum EIS during
514 MIS 6. The empirically derived Samarovo limit of Astakhov *et al.*⁵³ in eastern Siberia is also
515 included because of uncertainty about the timing of this event (MIS 6 or 8). Ice in Greenland
516 and Iceland is shown at the shelf edge.

517 Over North America, the southern margin of the LIS is based on the empirical
518 outlines of Balco and Rovey⁸⁷ and Curry *et al.*⁹¹. The western margin of the LIS is defined by
519 the empirical data of Barendregt *et al.*⁸⁸ (modified from Barendregt and Duk-Rodkin¹³⁸) the
520 empirically derived outline of Jackson *et al.*⁹⁹ and the modelled outlines of Peltier¹⁰⁸ and de
521 Boer *et al.*¹⁰. This reconstruction leaves Edmonton ice free during this time, as suggested by
522 Young *et al.*¹⁶⁰. The Quaternary maximum ice-extent templates are used for the CIS⁵⁷ and NE
523 Asia^{55,156} (see [Methods](#)). Extensive grounded ice is shown in the Arctic Ocean^{89,100,105,118,183}.

524 **Minimum estimate of the MIS 6 (132–190 ka) ice-sheet extent**

525 The minimum empirical data limit is used for the minimum EIS during MIS 6. The
526 Urdachsk and Sampesa moraine limits on the Taymyr Peninsula⁶⁰ are not included as these
527 may have been formed during MIS 5b–d. Ice in Greenland and Iceland is shown at the
528 present-day coastline. For the LIS, the empirical outlines of Balco and Rovey⁸⁷, Curry *et al.*⁹¹
529 and Jackson *et al.*⁹⁹, are combined with the empirical outline of Barendregt *et al.*⁸⁸ (modified
530 from Barendregt and Duk-Rodkin¹³⁸). The LGM ice-extent template is used for the CIS. The
531 Quaternary maximum ice-extent template in NE Asia^{55,156} is used to account for the extensive
532 empirically derived ice-sheet outline of Barr and Solomina⁴¹ on the Kamchatka Peninsula.
533 Grounded ice is shown in the Eastern Siberian Sea⁸⁹.

534 **Best-estimate of the MIS 6 (132–190 ka) ice-sheet extent**

535 For the best-estimate EIS during MIS 6, the detailed empirical outlines of Ehlers *et*
536 *al.*⁹³, Marks¹⁰², Marks *et al.*¹⁰⁴ and Astakhov *et al.*⁵³ are used, which broadly agree with the

537 coarser outlines of Svendsen *et al.*⁶² and Hughes and Gibbard⁹⁸. The Samarovo limit is not
538 included, since this is more likely to have been reached during MIS 8⁵³. The depiction of the
539 GIS at the shelf break is in agreement with work that has inferred extensive glaciation of East
540 Greenland during MIS 6^{82,116}. Shelf-break glaciation is also inferred beyond Britain^{26,71},
541 Iceland and the Canadian Arctic Archipelago.

542 Over North America, the empirical data of Balco and Rovey⁸⁷, Curry *et al.*⁹¹ and
543 Jackson *et al.*⁹⁹, are combined with the coarse ice-sheet outline of Barendregt *et al.*⁸⁸
544 (modified from Barendregt and Duk-Rodkin¹³⁸) for the southern and western LIS margin.
545 The LIS is extended to the shelf break at its southeastern and eastern margin, which is in
546 agreement with modelled outlines^{10,11}. For the CIS, the Reid ice-extent template of suggested
547 MIS 4/MIS 6 age is used in Alaska⁵⁷ and Yukon⁶⁴ (**Methods**). The maximum Quaternary ice-
548 extent template is used in NE Asia^{55,156} to account for the large ice sheet suggested by Barr
549 and Solomina⁴¹ for MIS 6. The maximum inferred extent of grounded ice is shown in the
550 Arctic Ocean^{89,100,105,118,183}.

551 **Robustness scores for the MIS 6 (132–190 ka) ice-sheet reconstruction**

552 EIS 5 (ice-sheet-wide empirical outlines)

553 LIS 4 (detailed regional empirical outlines and coarse ice-sheet-wide outline)

554 CIS 3 (detailed regional empirical outline and coarse ice-sheet-wide outline)

555 NE Asia 3 (regional empirical outline)

556 Mean robustness score: 3.75

557

Supplementary Note 12: MIS 8 (243–279 ka)

558 The reader should refer to [Supplementary Figure 7a](#) for a map of previously published
559 data on ice-sheet extent during MIS 8, [Supplementary Figure 7c](#) for a map of the maximum,
560 minimum and best-estimate ice-sheet reconstructions, and [Supplementary Table 11](#) for details
561 of the data sources used to inform these reconstructions.

562 **Maximum estimate of the MIS 8 (243–279 ka) ice-sheet extent**

563 For the maximum EIS during MIS 8, the available empirical outlines in eastern
564 Russia^{53,98} are combined with the best-estimate ice-sheet extent during MIS 6 in western
565 Russia and the Barents-Kara Sea. Further to the west, the maximum ice limit includes the
566 Krznanian limit of Marks¹⁰³ in Poland, the data of Roskosch *et al.*¹⁰⁶, who suggest two
567 Saalian (MIS 6 and 8) advances into the Leine Valley in Germany, and the data of Beets *et*
568 *al.*¹²³ in the North Sea. The maximum Quaternary ice-sheet extent (Anglian Stage limit of
569 MIS 12⁹⁵) is used for Britain, which encompasses the MIS 8 limit suggested by White *et*
570 *al.*^{121, 122}. Shelf-break glaciation is shown for Greenland and Iceland.

571 Over North America, the northern margin of the LIS is shown at the present-day shelf
572 break. For the southern LIS margin, the maximum of the two modelled outlines of
573 Ganopolski and Calov¹¹ and de Boer *et al.*¹⁰ is extended to account for the outline of Balco
574 and Rovey⁸⁷ that has been suggested for 0.2–0.75 Ma. The maximum reconstruction for MIS
575 6 is used for the western LIS, which keeps the LIS and CIS separate following the work of
576 Young *et al.*¹⁶⁰. The maximum Quaternary ice-extent templates are used for the CIS⁵⁷ and NE
577 Asia^{55,156} ([Methods](#)). Extensive grounded ice (following the empirically derived outlines for
578 MIS 6^{89,100,105}) is shown in the Arctic Ocean.

579 **Minimum estimate of the MIS 8 (243–279 ka) ice-sheet extent**

580 For the minimum EIS during MIS 8, the Samarovo glaciation limit of Astakhov *et*
581 *al.*⁵³ is used in western Siberia and otherwise the minimum estimate for MIS 4 is followed
582 (because of the similar benthic $\delta^{18}\text{O}$ records for MIS 4 and 8⁷⁹). To be conservative, this
583 outline is reduced further over Finland and Sweden. Because of uncertainty about the timing
584 of these events, the tentative MIS 8 limits of White *et al.*^{121, 122}, Marks¹⁰³ and Roskosch *et*
585 *al.*¹⁰⁶ are not included in the minimum reconstruction, and ice is not shown in Britain or in
586 the North Sea. Ice in Greenland and Iceland is shown at the present-day coastline. The

587 minimum ice-sheet extent for MIS 4 is used for the LIS. Because of an absence of empirical
588 data, the 30 ka ice-extent template¹⁶ is used for the CIS, and no ice is shown in NE Asia.

589 **Best-estimate of the MIS 8 (243–279 ka) ice-sheet extent**

590 Our best-estimate ice-sheet extents for MIS 8 have high uncertainty. They should not
591 be used to indicate the position of the ice-sheet margin, only as an indication of the likely
592 amount of ice present in the NH during this time. For the best-estimate EIS during MIS 8, the
593 empirically derived Samarovo limit of Astakhov *et al.*⁵³ is used in eastern Europe. Ice is
594 extended to Vologda city, Russia, where it may correlate with the Vologda glaciation⁹⁸. Ice is
595 shown to the shelf break in the Barents-Kara Sea and on the mid-Norwegian shelf¹¹⁵.

596 The extent of ice in Britain during MIS 8 is controversial; some researchers suggest
597 that the BIIS reached a similar position to that during the LGM^{121,122}, whereas others suggest
598 that no unequivocal physical evidence of glaciation during MIS 8 has been identified from
599 the UK⁹⁸. In our best-estimate reconstruction, we show an intermediate-sized ice sheet over
600 Britain that extends to the shelf break beyond Scotland⁷¹ and covers part of the North
601 Sea^{72,123,130}. The modelled outline of Ganopolski and Calov¹¹ is used for the southern and
602 western BIIS margin. To be conservative, ice is not shown extending into central Germany
603 and Poland^{103,106} during this time. Ice in Greenland is shown in an intermediate, mid-shelf
604 position, with the exception of part of the western Greenland margin where shelf-break
605 glaciation has been suggested during this time¹¹⁹. The minimum ice extent is used for Iceland.

606 Over North America, for the LIS, the best-estimate for MIS 4 is used (because of the
607 similar benthic $\delta^{18}\text{O}$ records for MIS 4 and 8⁷⁹), but this is not allowed to be larger than the
608 maximum MIS 8 limit. The exception is the northwest margin of the LIS, where the best-
609 estimate for MIS 6 is used to prevent ice from extending into the Mackenzie Delta region.
610 The range of ages provided for the southern LIS margin by Balco and Rovey⁸⁷ span MIS 8,
611 but the three ice advances that are proposed between 0.2 and 0.75 Ma most likely occurred in
612 MIS 6, 12 and 16 because these were the most extensive glaciations in this time span
613 according to the benthic $\delta^{18}\text{O}$ record⁷⁹. To be conservative, the 30 ka ice-extent template¹⁶ is
614 used for the CIS (although Huscroft *et al.*¹⁸⁴ suggest that the Reid glaciation may date to MIS
615 8 in some areas). The LGM ice-extent template¹⁵⁶ is used for NE Asia.

616 **Robustness scores for the MIS 8 (243–279 ka) ice-sheet reconstruction**

617 EIS 3 (regional empirical outlines and point-source data)

618 LIS 2 (small-scale empirical outline; uses ice-sheet extent during MIS 4)

619 CIS 1 (modelled outline)
620 NE Asia 1 (modelled outline)
621 Mean robustness score: 1.75
622
623
624
625
626
627
628
629
630
631
632
633
634
635
636
637
638
639

640

Supplementary Note 13: MIS 10 (337–365 ka)

641 The reader should refer to [Supplementary Figure 7c](#) for a map of previously published
642 data on ice-sheet extent during MIS 10, [Supplementary Figure 7d](#) for a map of the maximum,
643 minimum and best-estimate ice-sheet reconstructions, and [Supplementary Table 12](#) for details
644 of the data sources used to inform these reconstructions.

645 **Maximum estimate of the MIS 10 (337–365 ka) ice-sheet extent**

646 The maximum EIS during MIS 10 includes the empirical data points in western
647 Europe^{30,94 97,106}. The maximum reconstruction for MIS 8 is used in Poland, Belarus and
648 western Russia, to account for the suggestion that ice in MIS 10 could have extended as far as
649 the northern foreland of the South Polish Uplands¹⁸⁵. As the ice-sheet extent during MIS 10
650 has been suggested to have been smaller than during both MIS 6 and 8⁹⁸, the smaller of the
651 best-estimates for MIS 6 and 8 is followed in eastern Europe. Ice in Greenland and Iceland is
652 shown at the present-day shelf break.

653 Over North America, for the LIS, the maximum modelled extent for MIS 10 is
654 combined with the outline of Balco and Rovey⁸⁷. Ice is shown to the shelf break along the
655 northern and eastern margin of the LIS, as suggested by the modelled outlines of Ganopolski
656 and Calov¹¹ and de Boer *et al.*¹⁰. The best-estimate for MIS 12 was followed over
657 Pennsylvania to account for suggestions that this region was ice-covered during either MIS
658 10 or 12¹⁸⁶⁻¹⁹⁰. The rest of the southern LIS margin is the maximum modelled ice extent for
659 MIS 10 combined with the empirically derived outline of Balco and Rovey⁸⁷. The maximum
660 reconstruction for MIS 6 is used for the western LIS, which keeps the LIS and CIS separate
661 following the work of Young *et al.*¹⁶⁰. The maximum Quaternary ice-extent templates are
662 used for the CIS⁵⁷ and NE Asia^{55,156} (**Methods**). Extensive grounded ice (following the
663 empirically derived outlines for MIS 6^{89,100,107}) is shown in the Arctic Ocean.

664 **Minimum estimate of the MIS 10 (337–365 ka) ice-sheet extent**

665 For the minimum EIS during MIS 10, the minimum reconstruction for MIS 8 is used
666 in Scandinavia and Britain, and the minimum reconstruction for MIS 4 is applied elsewhere.
667 We note that the eastern EIS extent is probably unrealistically small. Ice in Greenland and
668 Iceland is shown at the present-day coastline. The minimum outline for MIS 4 is used for the
669 LIS. The 30 ka ice-extent template¹⁶ is used for the CIS and no ice is shown in NE Asia.

670 **Best-estimate of the MIS 10 (337–365 ka) ice-sheet extent**

671 Because of a lack of empirical data, our best-estimate ice-sheet extents for MIS 10 are
672 highly uncertain. As a result, they should not be used to indicate the position of the ice-sheet
673 margin, only as an indication of the likely amount of ice present in the NH during this time.
674 For the best-estimate EIS reconstruction for MIS 10, the best-estimate for MIS 8 is used for
675 the northern and western limits. To be conservative, ice is not shown extending into central
676 Germany and Poland during this time^{94,103,106}. We note that these areas are shown as ice-
677 covered in the maximum reconstruction. In eastern Europe and western Siberia, due to an
678 absence of information, an approximate mid-point between the best-estimates for MIS 8 and
679 4 is used.

680 The extent of ice in Britain during MIS 10 is controversial; some researchers have
681 suggested that the BIIS during MIS 10 reached a similar position as during the Elsterian
682 glaciation (MIS 12)^{90,97}, whereas others have questioned these data, largely because the
683 relationships between dated sand deposits and glacial extents can be ambiguous⁹⁸. In our
684 best-estimate reconstruction, we show an intermediate sized ice sheet over Britain that
685 extends to the shelf break beyond Scotland⁷¹ and covers part of the North Sea⁷². The
686 modelled outline of Ganopolski and Calov¹¹ is used for the southern and western BIIS
687 margin. Ice in Greenland is shown in a mid-shelf position, with the exception of part of the
688 western Greenland margin where shelf-break glaciation has been suggested during this
689 time¹¹⁹. The minimum ice extent is used for Iceland.

690 Over North America, the best-estimate for MIS 4 is used for the LIS. This is because
691 MIS 4 and MIS 10 have broadly similar values in the benthic $\delta^{18}\text{O}$ stack⁷⁹, although we note
692 that MIS 10 has a lower value than both MIS 4 and MIS 8 and therefore had more ice. The
693 exception is the NW margin of the LIS, where we use the best-estimate for MIS 6 to prevent
694 ice from extending into the Mackenzie Delta region. The range of ages provided for the
695 southern LIS margin by Balco and Rovey⁸⁷ spans MIS 10, but the three ice advances that are
696 suggested to have occurred between 0.2 and 0.75 Ma most likely occurred in MIS 6, 12 and
697 16 because these were the most extensive glaciations in this time span according to the
698 benthic $\delta^{18}\text{O}$ record⁷⁹. The 30 ka ice-extent template¹⁶ is used for the CIS, and the LGM ice-
699 extent template¹⁵⁶ is used for NE Asia ([Methods](#)).

700 **Robustness scores for the MIS 10 (337–365 ka) ice-sheet reconstruction**

701 EIS 2 (regional empirical outlines, point-source data and modelled outlines)

702 LIS 2 (regional empirical outline and modelled outlines; uses ice-sheet extent during MIS 4)

- 703 CIS 1 (modelled outlines)
- 704 NE Asia 1 (modelled outlines)
- 705 Mean robustness score: 1.5

706

Supplementary Note 14: MIS 12 (429–477 ka)

707

708

709

710

The reader should refer to [Supplementary Figure 8a](#) for a map of previously published data on ice-sheet extent during MIS 12, [Supplementary Figure 8b](#) for a map of the maximum, minimum and best-estimate ice-sheet reconstructions, and [Supplementary Table 13](#) for details of the data sources used to inform these reconstructions.

711

Maximum estimate of the MIS 12 (429–477 ka) ice-sheet extent

712

713

714

715

716

717

718

719

720

721

The maximum empirical outlines over Europe are followed for the maximum EIS during MIS 12. The outline of Eissmann⁹⁴, which shows part of the Don lobe as MIS 12, is included. The southern limit, between the Urals and the empirical outline of Astakhov *et al.*⁵³, is the all-time Quaternary maximum, which, in this region, is the maximum reconstruction of MIS 8. Ice is extended to the shelf break in the Barents-Kara Sea, off Norway and beyond Greenland and Iceland. For the LIS, the maximum reconstruction for MIS 6 is used, which includes the empirically derived outline of Balco and Rovey⁸⁷. The maximum Quaternary ice-extent templates are used for the CIS⁵⁷ and NE Asia^{55,156} ([Methods](#)). Extensive grounded ice (following the empirically derived outlines for MIS 6^{89,100,105}) is shown in the Arctic Ocean.

722

Minimum estimate of the MIS 12 (429–477 ka) ice-sheet extent

723

724

725

726

727

For the minimum EIS and LIS during MIS 12, empirical outlines^{87,93,95,96,101,104} are used where available and the minimum reconstruction of MIS 6 is used where there are gaps in empirical data coverage. Ice in Greenland and Iceland is shown at the present-day coastline. The 30 ka ice-extent template¹⁶ is used for the CIS, and the LGM ice-extent template¹⁵⁶ is used in NE Asia ([Methods](#)).

728

Best-estimate of the MIS 12 (429–477 ka) ice-sheet extent

729

730

731

732

733

734

735

The detailed empirical outlines of Gibbard and Clark⁹⁵ in Britain, Laban and van der Meer¹⁰¹ in the Netherlands, and Ehlers *et al.*⁹³ in Germany are followed for the best-estimate EIS during MIS 12. The empirical outlines of Marks *et al.*¹⁰⁴ and Gozhik *et al.*⁹⁶ are adopted in eastern Europe, and the outline of Astakhov *et al.*⁵³ is followed in central Siberia. Due to the lack of empirical data between these regions, the best-estimate of MIS 6 is used to delimit the southern margin of the EIS. Ice in Greenland and Iceland is shown at the shelf break. The best-estimate for MIS 6 is used for the LIS, which includes the outline of Balco and Rovey⁸⁷.

736 The LGM ice-extent template is used for the CIS, and the maximum Quaternary ice-extent
737 template^{55,156} is used for NE Asia ([Methods](#)).

738 **Robustness scores for the MIS 12 (429-477 ka) ice-sheet reconstruction**

739 EIS 4 (many regional empirical outlines)

740 LIS 2 (regional empirical outline; uses ice-sheet extent from MIS 6)

741 CIS 1 (modelled outline; LGM empirically derived template)

742 NE Asia 1 (modelled outline)

743 Mean robustness score: 2

744

Supplementary Note 15: MIS 16 (622–677 ka)

745 The reader should refer to [Supplementary Figure 8c](#) for a map of previously published
746 data on ice-sheet extent during MIS 16, [Supplementary Figure 8d](#) for a map of the maximum,
747 minimum and best-estimate ice-sheet reconstructions, and [Supplementary Table 14](#) for details
748 of the data sources used to inform these reconstructions.

749 **Maximum estimate of the MIS 16 (622–677 ka) ice-sheet extent**

750 For the maximum EIS during MIS 16, the maximum empirical data^{53,96,98} are used for
751 the southern ice-sheet margin. The maximum reconstruction for MIS 12 is used for Britain,
752 western Scandinavia and the Barents-Kara Sea because of the similar benthic $\delta^{18}\text{O}$ records for
753 MIS 16 and 12⁷⁹. This incorporates the empirical data of Hamblin *et al.*⁹⁷ in Britain, and the
754 suggestion of shelf-break glaciation on the mid-Norwegian margin¹¹⁵. Ice is shown at the
755 shelf break beyond Greenland and Iceland. Ice is also shown at the shelf break along the
756 northern and eastern margin of the LIS. The southern LIS follows the empirical data for MIS
757 16^{87,128}, and the western margin uses the maximum reconstructed ice limit for MIS 6. The
758 maximum Quaternary ice-extent templates are used for the CIS⁵⁷ and NE Asia^{55,156}
759 (**Methods**). Extensive grounded ice (following the empirically derived outlines for MIS
760 6^{89,100,105}) is shown in the Arctic Ocean.

761 **Minimum estimate of the MIS 16 (622–677 ka) ice-sheet extent**

762 For the minimum EIS during MIS 16, we use the empirically derived outlines of
763 Olsen *et al.*⁸ in Scandinavia and the Barents-Kara Sea, Toucanne *et al.*¹³⁰ in Denmark,
764 Germany and Poland, and Astakhov *et al.*⁵³ in Russia. Note that our minimum reconstruction
765 for the EIS in Siberia shows virtually no ice, which is likely to be unrealistic even for a
766 minimum estimate. To be conservative in our minimum estimate, grounded ice is not
767 included in the North Sea. Schematic ice caps are shown over Scotland and Ireland, as in the
768 minimum reconstruction for MIS 20–24. Ice in Greenland and Iceland is shown at the
769 present-day coastline. For the minimum LIS during MIS 16, the minimum empirical data¹²⁹ is
770 used where they are available, and the minimum of MIS 6 is used where empirical data for
771 MIS 16 are lacking. Owing to a lack of data, the 30 ka ice-extent template¹⁶ is used for the
772 CIS, and the LGM ice-extent template¹⁵⁶ is used in NE Asia (**Methods**).

773 **Best-estimate of the MIS 16 (622–677 ka) ice-sheet extent**

774 For the best-estimate EIS for MIS 16, the empirically derived outlines of Toucanne *et*
775 *al.*¹³⁰, Gozhik *et al.*⁹⁶, Astakhov *et al.*⁵³ and Marks *et al.*¹⁰⁴ are used for the southern limit in
776 Europe. East of the Urals, in western Siberia, the best-estimate of MIS 6 is used to provide a
777 realistic ice-sheet extent given the relatively extensive glaciation of Russia during MIS 16⁵³.
778 The EIS is extended to the shelf break on the mid-Norwegian margin¹¹⁵. Further, our best-
779 estimate for MIS 16 shows the EIS extending into the central North Sea, as in the best-
780 estimate for MIS 20–24. The EIS and BIIS are not joined during this time, following the
781 suggestion of Toucanne *et al.*¹³⁰. Ice in Greenland and Iceland is shown at the shelf break.

782 To produce the best-estimate of MIS 16 ice over North America for the LIS, the
783 empirical outlines of Aber¹²⁸ and Colgan¹²⁹ are used to delimit the southern extent. For the
784 remainder, the best-estimate from MIS 6 is used. In western North America, the LGM ice-
785 extent template is used for the CIS⁹³, and the maximum Quaternary ice-extent template^{55,156} is
786 adopted for NE Asia ([Methods](#)).

787 **Robustness scores for the MIS 16 (622–677 ka) ice-sheet reconstruction**

788 EIS 4 (regional empirical outlines; uses ice-sheet extents from MIS 6 and 12)

789 LIS 4 (regional empirical outlines; uses ice-sheet extents from MIS 6 and 12)

790 CIS 0 (no data)

791 NE Asia 0 (no data)

792 Mean robustness score: 2

793

Supplementary Note 16: MIS 20–24 (790–928 ka)

794 The reader should refer to [Supplementary Figure 9a](#) for a map of previously published
795 data on ice-sheet extent during MIS 20–24, [Supplementary Figure 9b](#) for a map of the
796 maximum, minimum and best-estimate ice-sheet reconstructions, and [Supplementary Table](#)
797 [15](#) for details of the data sources used to inform these reconstructions.

798 **Maximum estimate of the MIS 20–24 (790–928 ka) ice-sheet extent**

799 For the maximum EIS during MIS 20–24, tentative empirical outlines for the
800 Nidanian glaciation^{96,103} are merged with the maximum estimates of MIS 8 and 10 combined
801 (because of the similar benthic $\delta^{18}\text{O}$ values for MIS 8, 10 and 20–24⁷⁹). Ice in Greenland and
802 Iceland is shown to the shelf break. Over North America, for the LIS, the outline of Balco
803 and Rovey⁸⁷ is combined with the maximum estimate for MIS 8 and 10. Over western North
804 America and NE Asia, to capture the maximum scenario, the maximum Quaternary ice-extent
805 templates are used for the CIS⁵⁷ and in NE Asia^{55,156} (see [Methods](#)). Finally, extensive
806 grounded ice (following the empirically derived outlines for MIS 6^{89,100,105}) is shown in the
807 Arctic Ocean.

808 **Minimum estimate of the MIS 20–24 (790–928 ka) ice-sheet extent**

809 For the minimum EIS during MIS 20–24, we use the same ice-sheet extent as for the
810 minimum ice-sheet reconstruction for the early Matuyama magnetic Chron (1.78–2.6 Ma).
811 The minimum reconstruction for the early Matuyama Chron follows the smaller of the two
812 empirically derived reconstructions of Knies *et al.*¹⁴¹ over the Barents-Kara Sea, and the
813 minimum of the empirical outlines^{132,139,141} for the early Matuyama Chron over Scandinavia.
814 Schematic ice caps are shown over Scotland and Ireland to account for IRD evidence for
815 marine-terminating glaciers during this time¹³⁷. Ice in Greenland and Iceland is shown at the
816 present-day coastline. Over North America, the reconstruction of Andriashek and
817 Barendregt¹³¹ is used for the LIS, and the 30 ka ice-extent template¹⁶ is used for the CIS.
818 Finally, no ice is shown in NE Asia or the Arctic Ocean.

819 **Best-estimate of the MIS 20–24 (790–928 ka) ice-sheet extent**

820 Our MIS 20–24 time-slice spans part of the Mid-Pleistocene Transition, which was a
821 time of generally expanded NH ice sheets. In our MIS 20–24 best-estimate reconstruction,
822 the EIS is extended into central Europe to incorporate the suggested outlines for the Nidanian

823 glaciation of around 0.9 Ma^{96,103}. At this time, we also interpolate an ice margin between
824 Scandinavia and central Europe, linking the limit of Olsen *et al.*⁸ with those of Gozhik *et al.*⁹⁶
825 and Marks¹⁰³. The expansion of the EIS into central Europe around 1 Ma has been inferred to
826 have led to excavation of the Baltic Basin, causing the Baltic (Eridanos) river system, which
827 had operated in the Miocene, Pliocene and Early Pleistocene, to lose its connection to the
828 Scandinavian and Baltic headwaters^{191,192}. The empirically derived outline of Olsen *et al.*⁸ is
829 used for the best-estimate ice sheet in the Barents-Kara Sea. The EIS is extended to the shelf
830 break off western Norway¹¹⁵ and into the central North Sea^{132,133,136}. We note that there is
831 also evidence for the FIS extending into the central North Sea slightly earlier, around 1.1–1.2
832 Ma^{193,194}. To be conservative, ice in Iceland is shown at the present-day coastline, and the
833 minimum ice-sheet extent is used for Britain and Ireland. The reconstruction of the GIS at the
834 shelf break during MIS 20–24 is in agreement with an increase in IRD at around 0.8 Ma¹³⁴,
835 and seismic evidence for multiple cross-shelf glaciations between 0.78 and 1.77 Ma¹³⁵.

836 To produce the best-estimate reconstruction of MIS 20–24 ice over North America,
837 the LIS reconstruction of Andriashek and Barendregt¹³¹ is combined with the best-estimate
838 for MIS 8 at the southeast and northeast ice-sheet margin. This is because the reconstruction
839 of Andriashek and Barendregt¹³¹ is a schematic outline around sites that they interpret to have
840 been covered by ice as suggested by palaeo-magnetic dating, and is therefore a minimum
841 extent. Our best-estimate of MIS 20–24 ice also smooths an irregular ice margin in the
842 southwest by extending the outline by about 100 km. The minimum reconstruction is
843 followed for the northwest LIS in the Mackenzie Delta region. To account for the relatively
844 large empirically derived outline of Andriashek and Barendregt¹³¹, the Reid ice-sheet
845 template of MIS 4/6 is used for the CIS^{57,64}. Finally, the LGM ice-extent template¹⁵⁶ is shown
846 in NE Asia ([Methods](#)) and no ice is shown in the Arctic Ocean.

847 **Robustness scores for the MIS 20–24 (790–928 ka) ice-sheet reconstruction**

848 EIS 3 (regional empirical outlines of contrasting extent)

849 LIS 3 (regional empirical outline and coarse ice-sheet-wide outline; uses ice-sheet extent
850 from MIS 8)

851 CIS 3 (coarse ice-sheet-wide outline and empirical data points)

852 NE Asia 0 (no data)

853 Mean robustness score: 2.25

854 **Supplementary Note 17: Early Matuyama palaeomagnetic Chron**
855 **(1.78–2.6 Ma)**

856 The reader should refer to [Supplementary Figure 9c](#) for a map of previously published
857 data on ice-sheet extent during the early Matuyama palaeomagnetic Chron, [Supplementary](#)
858 [Figure 9d](#) for a map of the maximum, minimum and best-estimate ice-sheet reconstructions,
859 and [Supplementary Table 16](#) for details of the data sources used to inform these
860 reconstructions.

861 **Maximum estimate of the early Matuyama palaeomagnetic Chron (1.78–2.6 Ma) ice-**
862 **sheet extent**

863 Our reconstructions aim to show the *maximum* extent of the NH ice sheets within the
864 long (0.8 Ma) period of the early Matuyama Chron ([Methods](#)). For the maximum EIS during
865 this period, the best-estimate reconstruction for MIS 20–24 is used in most cases; this
866 includes the proposed extent of the Narewian glaciation of Germany and Poland¹⁰³, which has
867 been suggested to be *c.* 1.4 Ma in age, because of uncertainty in dating older sediments.
868 However, the maximum outline differs from the MIS 20–24 reconstruction in the North Sea.
869 For the maximum ice extent in the early Matuyama Chron, we show the EIS extending
870 westward into the northern North Sea, but it is not merged with the BIIS because the central
871 North Sea was a deep basin during the Early Pleistocene¹³³. We also show an ice sheet over
872 Scotland and Ireland to account for IRD and seismic evidence for marine-terminating glaciers
873 during this time^{137,142}. Ice in Greenland and Iceland is shown to the shelf break.

874 Over North America, for the LIS, the empirical data of Balco and Rovey⁸⁷ is
875 combined with the maximum reconstruction for MIS 6. Over western North America, the
876 lack of available evidence means that the maximum Quaternary ice-extent templates are used
877 for the CIS⁵⁷ and NE Asia^{55,156} ([Methods](#)). Finally, extensive grounded ice (following the
878 empirically derived outlines for MIS 6^{89,100,105}) is shown in the Arctic Ocean.

879 **Minimum estimate of the early Matuyama palaeomagnetic Chron (1.78–2.6 Ma) ice-**
880 **sheet extent**

881 For the minimum EIS during the early Matuyama magnetic Chron, the smaller of the
882 two empirically derived outlines of Knies *et al.*¹⁴¹ is used for the islands of the Barents-Kara
883 Sea. The minimum empirical outlines^{132,139,141} are used over Scandinavia, which show the ice
884 sheet extending to the present-day coastline. Schematic ice caps are shown over Scotland and

885 Ireland to account for IRD evidence for marine-terminating glaciers during this time¹³⁷. Ice in
886 Greenland and Iceland is shown at the present-day coastline. Over North America, for the
887 LIS, the empirically derived outlines of Balco and Rovey⁸⁷ and Barendregt *et al.*⁸⁸ (modified
888 from Barendregt and Duk-Rodkin¹³⁸) are used. The 30 ka ice-extent template¹⁶ is used for the
889 CIS and no ice is shown in NE Asia ([Methods](#)).

890 **Best-estimate of the early Matuyama palaeomagnetic Chron (1.78–2.6 Ma) ice-sheet** 891 **extent**

892 For the best-estimate EIS during the early Matuyama Chron, we use the larger of the
893 two empirically derived outlines of Knies *et al.*¹⁴¹ in the Barents-Kara Sea and northern
894 Scandinavia. This follows evidence that the Barents-Kara Ice Sheet developed to a moderate
895 size during a transitional growth phase between around 2.4 and 1 Ma^{141,146,150,195-197}. The
896 outlines of Knies *et al.*¹⁴¹, Ottesen *et al.*¹³³ and Rea *et al.*¹⁴² are followed in southern
897 Scandinavia and the North Sea. Ice is extended to the present-day shelf break on the mid-
898 Norwegian margin, although we note that the shelf break has prograded several tens of
899 kilometres in a seaward direction through the Quaternary¹¹⁵. To be conservative, the
900 minimum ice-sheet extent is used over Britain, which shows ice in Scotland and Ireland
901 reaching sea level¹³⁷.

902 The GIS is shown at the shelf break in our best-estimate reconstruction for the early
903 Matuyama Chron. This follows seismic stratigraphic investigations and modelling studies
904 that suggest that the GIS extended to the shelf break during the Late Pliocene to Early
905 Pleistocene, between around 2.5 and 3 Ma^{116,134,143,145,148,150,198,199}. An expanded GIS during
906 this time is also suggested from IRD records^{144,149}. The GIS probably advanced to the shelf
907 break during several glacial periods within the early Matuyama palaeo-magnetic Chron¹³⁵.
908 Although our best-estimate reconstruction aims to capture the *maximum* ice-sheet extent
909 within this long timeslice, we note that there is evidence for a reduced GIS during an Early
910 Pleistocene warm period around 2.4 Ma^{200,201}.

911 Over North America, for the LIS, we adopt the best-estimate for MIS 4 combined
912 with the empirical outlines of Balco and Rovey⁸⁷ and Barendregt *et al.*⁸⁸ (modified from
913 Barendregt and Duk-Rodkin¹³⁸). The maximum Quaternary ice-extent template is used for the
914 CIS⁵⁷, following suggestions that the CIS reached its maximum extent during the early
915 Matuyama palaeo-magnetic Chron^{88,138}. Because of the lack of data for NE Asia during this
916 time-slice, the best-estimate uses the LGM ice-sheet template¹⁵⁶, which is a mid-point
917 between our minimum and maximum reconstructions.

- 918 **Robustness scores for the early Matuyama palaeomagnetic Chron (1.78–2.6 Ma) ice-**
919 **sheet reconstruction**
- 920 EIS 3 (regional empirical outlines of contrasting extent)
- 921 LIS 3 (regional empirical outline and coarse ice-sheet-wide empirical outline; uses ice-sheet
922 extent of MIS 4)
- 923 CIS 3 (coarse ice-sheet-wide outline and empirical data points)
- 924 NE Asia 0 (no data)
- 925 Mean robustness score: 2.25

926 **Supplementary Note 18: Late Gauss palaeomagnetic Chron (2.6–3.59 Ma)**

927 The reader should refer to [Supplementary Figure 10a](#) for a map of previously
928 published data on ice-sheet extent during the late Gauss palaeomagnetic Chron,
929 [Supplementary Figure 10b](#) for a map of the maximum, minimum and best-estimate ice-sheet
930 reconstructions, and [Supplementary Table 17](#) for details of the data sources used to inform
931 these reconstructions.

932 **Maximum estimate of the late Gauss palaeomagnetic Chron (2.6–3.59 Ma) ice-sheet** 933 **extent**

934 In this section, it should be noted that we show the *maximum* ice extent during the late
935 Gauss magnetic Chron (2.6–3.59 Ma) that probably dates to around 2.6 Ma, when NH
936 glaciations became more extensive. Over northern Europe and the Barents-Kara Sea, the
937 larger of the hypothesised outlines of Knies *et al.*¹⁴¹ are used. Our maximum ice outline for
938 Scandinavia is also extended westward into the northern North Sea, following evidence that
939 the FIS had a marine-terminating margin since around 2.7 Ma¹³³. An ice sheet is shown over
940 Scotland and Ireland to account for IRD evidence for marine-terminating glaciers¹³⁷. Ice in
941 Greenland and Iceland is shown to the shelf break.

942 Over North America, for the LIS, the generalised schematic outline of Kleman *et al.*⁵
943 for 35 ka and 40 ka is used for this maximum outline. Also included in this outline are the
944 empirical data from hypothesis 2 of Dredge and Thorleifson⁴² for MIS 3, which show ice
945 cover over Nova Scotia and northwestern Canada. For the CIS, because of an absence of
946 empirical data, the maximum Quaternary ice-extent template is used, which is based mainly
947 on Kaufman *et al.*⁵⁷ and Turner *et al.*⁶⁴ (**Methods**), to account for the large empirically
948 derived outline of Barendregt *et al.*⁸⁸ (modified from Barendregt and Duk-Rodkin¹³⁸). The
949 maximum Quaternary ice-extent template is used in NE Asia^{55,156}. Finally, the maximum
950 reconstruction shows extensive grounded ice (following the empirically derived outlines for
951 MIS 6^{89,100,105}) in the Arctic Ocean.

952 **Minimum estimate of the late Gauss palaeomagnetic Chron (2.6–3.59 Ma) ice-sheet** 953 **extent**

954 For the minimum EIS during the late Gauss palaeo-magnetic Chron, the present-day
955 ice extent is combined with schematic ice caps in Norway and the Barents-Kara Sea (based
956 on Hughes *et al.*⁴ for 35 ka). The present-day ice extent is also adopted for Greenland,

957 Iceland and the LIS. The 30 ka ice-extent template¹⁶ is used for the CIS and no ice is shown
958 in NE Asia or the Arctic Ocean.

959 **Best-estimate of the late Gauss palaeomagnetic Chron (2.6–3.59 Ma) ice-sheet extent**

960 For the best-estimate EIS during the late Gauss palaeo-magnetic Chron, the minimum
961 reconstruction of Knies *et al.*¹⁴¹ is used in northern Norway and the Barents-Kara Sea. This
962 outline is adjusted slightly to cover our minimum reconstruction for the late Gauss
963 palaeomagnetic Chron, which is based on the schematic ice caps of Hughes *et al.*⁴ for 35 ka.
964 Following seismic and IRD evidence for a marine-terminating ice margin at around 2.7
965 Ma^{149,202}, we also extend this ice margin to the coastline of mid-Norway. The FIS is also
966 extended into the northern North Sea, following evidence of a marine-terminating ice margin
967 from around 2.7 Ma¹³³. This evidence includes features interpreted as glacigenic debris-flow
968 deposits on palaeo-slope surfaces^{132,203}, IRD in sediment cores^{202,204}, and iceberg
969 ploughmarks preserved on early Quaternary surfaces^{139,142}. Our best-estimate FIS is shown at
970 the former shelf break in the northern North Sea, which was located around 80 km beyond
971 the present-day coastline during the Late Pliocene/ Early Pleistocene when the North Sea was
972 a deep basin¹³³. The best-estimate reconstruction also shows ice caps over Scotland and
973 Ireland to account for IRD evidence for marine-terminating glaciers during this time¹³⁷.

974 The GIS is shown at the shelf break in our best-estimate reconstruction. This is in
975 agreement with empirical and modelling work that suggests that the GIS extended to the shelf
976 break during the Late Pliocene to Early Pleistocene, between around 2.5 and 3 Ma<sup>116,134,143,145,
977 148,150,198,199</sup>. An expanded GIS during this time is also suggested from IRD records^{144,149}. It is
978 noted that the late Gauss palaeo-magnetic Chron spans a period of Early Pliocene warmth
979 (5.5–3 Ma), during which there is evidence for a reduced GIS²⁰⁵⁻²⁰⁷. To be conservative, the
980 present-day ice extent is shown for Iceland.

981 Over North America, for the LIS, the best-estimate for 45 ka is used (based on
982 hypothesis 2 of Dredge and Thorleifson⁴²) and shows the main ice dispersal centres. Due to
983 suggestions of an extensive CIS during this time^{88,138,147}, the maximum Quaternary ice-extent
984 template⁵⁷ is used for the CIS. The LGM ice-extent template¹⁵⁶ is used for NE Asia, which is
985 a mid-point between our maximum and minimum reconstructions, and accounts for IRD
986 evidence that glaciers on the Kamchatka Peninsula reached at least sea level around 2.6
987 Ma^{125,208}.

988 **Robustness scores for the late Gauss palaeomagnetic Chron (2.6–3.59 Ma) ice-sheet**
989 **reconstruction**

990 EIS 2 (regional empirical outlines)
991 LIS 0 (no data)
992 CIS 3 (coarse ice-sheet-wide outline and empirical data points)
993 NE Asia 0 (no data)
994 Mean robustness score: 1.25

Supplementary References

- 996 1. Amante, C. & Eakins, B. W. ETOPO1 1 Arc-Minute Global Relief Model:
997 Procedures, Data Sources and Analysis. *NOAA Technical Memorandum NESDIS*
998 *NGDC-24*. National Geophysical Data Center, NOAA (2009).
- 999 2. Dyke, A. S., Andrews, J. T., Clark, P. U., England, J. H., Miller, G. H., Shaw, J. &
1000 Veillette, J. J. The Laurentide and Innuitian ice sheets during the Last Glacial
1001 Maximum. *Quat. Sci. Rev.* **21**, 9–31 (2002).
- 1002 3. Houmark-Nielsen, M. Extent, age and dynamics of Marine Isotope Stage 3 glaciations
1003 in the southwestern Baltic Basin. *Boreas* **39**, 343–359 (2010).
- 1004 4. Hughes, A. L. C., Gyllencreutz, R., Lohne, Ø. S., Mangerud, J. & Svendsen, J. I. The
1005 last Eurasian ice sheets—a chronological database and time-slice reconstruction,
1006 DATED-1. *Boreas* **45**, 1–45 (2016).
- 1007 5. Kleman, J., Jansson, K., De Angelis, H., Stroevem, A. P., Hättestrand, C., Alm, G. &
1008 Glasser, N. North American ice sheet build-up during the last glacial cycle, 115-21
1009 kyr. *Quat. Sci. Rev.* **29**, 2036–2051 (2010).
- 1010 6. Larsen, N. K., Knudsen, K. L., Krohn, C. F., Knoborg, C., Murray, A. S. & Nielsen,
1011 O. B. Late Quaternary ice sheet, lake and sea history of southwest Scandinavia – a
1012 synthesis. *Boreas* **38**, 732–761 (2009).
- 1013 7. Marks, L. Timing of the Late Vistulian (Weichselian) glacial phases in Poland. *Quat.*
1014 *Sci. Rev.* **44**, 81–88 (2012).
- 1015 8. Olsen, L., Sveian, H., Bergstrøm, B., Ottesen, D. & Rise, L. Quaternary glaciations
1016 and their variations in Norway and on the Norwegian continental shelf. In: Olsen, L.,
1017 Fredin, O. & Olesen, O. (Eds.) Quaternary Geology of Norway, *Geological Survey of*
1018 *Norway Special Publication* **13**, 27–78 (2013).
- 1019 9. Bonelli, S., Charbit, S., Kageyama, M., Woillez, M. -N., Ramstein, G., Dumas, C. &
1020 Quiquet, A. Investigating the evolution of major NH ice sheets during the last
1021 interglacial cycle. *Clim. Past* **5**, 329–345 (2009).
- 1022 10. de Boer, B., Stocchi, P. & van de Wal, R. S. W. A fully coupled 3-D ice-sheet–sea-
1023 level model: algorithm and applications. *Geosci. Model Dev.* **7**, 2141–2156 (2014).
- 1024 11. Ganopolski, A. & Calov, R. The role of orbital forcing, carbon dioxide and regolith in
1025 100 kyr glacial cycles. *Clim. Past* **7**, 1415–1425 (2011).

- 1026 **12.** Heinemann, M., Timmermann, A., Timm, O. E., Saito, F. & Abe-Ouchi, A. Deglacial
1027 ice sheet meltdown: orbital pacemaking and CO₂ effects. *Cim. Past* **10**, 1567–1579
1028 (2014).
- 1029 **13.** Hubbard, A., Bradwell, T., Golledge, N., Hull, A., Patton, H., Sugden, D., Cooper, R.
1030 & Stoker, M. Dynamic cycles, ice streams and their impact on the extent, chronology
1031 and deglaciation of the British-Irish ice sheet. *Quat. Sci. Rev.* **28**, 758–776 (2009).
- 1032 **14.** Lambeck, K., Purcell, A., Zhao, J. & Svendsen, N-O. The Scandinavian Ice Sheet;
1033 from MIS 4 to the end of the Last Glacial Maximum. *Boreas* **39**, 410–435 (2010).
- 1034 **15.** Patton, H., Hubbard, A., Bradwell, T. & Schomacker, A. The configuration,
1035 sensitivity and rapid retreat of the Late Weichselian Icelandic ice sheet. *Earth-Sci.*
1036 *Rev.* **166**, 223–245 (2017).
- 1037 **16.** Seguinot, J., Rogozhina, I., Stroeven, A. P., Margold, M. & Kleman, J. Numerical
1038 simulations of the Cordilleran ice sheet through the last glacial cycle. *Cryosphere* **10**,
1039 639–664 (2016).
- 1040 **17.** Stokes, C. R., Tarasov, L. & Dyke, A. S. Dynamics of the North American Ice Sheet
1041 complex during its inception and build-up to the Last Glacial Maximum. *Quat. Sci.*
1042 *Rev.* **50**, 86–104 (2012).
- 1043 **18.** Zweck, C. & Huybrechts, P. Modeling of the NH ice sheets during the last glacial
1044 cycle and glaciological sensitivity. *J. Geophys. Res.* **110**, D07103 (2005).
- 1045 **19.** Abramowski, U., Bergau, A., Seebach, D., Zech, R., Glaser, B., Sosin, P., Kubin, P.
1046 W. & Zech, W. Pleistocene glaciations of Central Asia: results from ¹⁰Be surface
1047 exposure ages of erratic boulders from the Pamir (Tajikistan), and the Alay-Turkestan
1048 range (Kyrgyzstan). *Quat. Sci. Rev.* **25**, 1080–1096 (2006).
- 1049 **20.** Arzhannikhov, S. G., Braucher, R., Jolivet, M. & Arzhannikova, A. V. Late
1050 Pleistocene glaciations in southern East Sayan and detection of MIS 2 terminal
1051 moraines based on beryllium (¹⁰Be) dating of glacier complexes. *Russ. Geol.*
1052 *Geophys.* **56**, 1509–1521 (2015).
- 1053 **21.** Baumann, K-H., Lackschewitz, K. S., Mangerud, J., Spielhagen, R. F., Wolf-welling,
1054 T. C. W., Henrich, R. & Kassens, H. Reflection of Scandinavian Ice Sheet
1055 fluctuations in Norwegian Sea sediments during the past 150,000 years. *Quat. Res.*
1056 **43**, 185–197 (1995).
- 1057 **22.** Chevalier, M-L., Hilley, G., Tapponnier, P., Van Der Woerd, J., Liu-Zeng, J., Finkel,
1058 R. C., Ryerson, F. J., Li, H. & Liu, X. Constraints on the late Quaternary glaciations

- 1059 in Tibet from cosmogenic exposure ages of moraine surfaces. *Quat. Sci. Rev.* **30**, 528–
1060 554 (2011).
- 1061 **23.** Hall, A. M. The last glaciation of Shetland: local ice cap or invasive ice sheet?
1062 *Norwegian Journal of Geology* **93**, 229–242 (2013).
- 1063 **24.** Hibbert, F. D., Austin, W. E. N., Leng, M. J. & Gatliff, R. W. British Ice Sheet
1064 dynamics inferred from North Atlantic ice-rafted debris records spanning the last 175
1065 000 years. *J. Quat. Sci.* **25**, 461–482 (2010).
- 1066 **25.** Lehmkühl, F. Quaternary glaciations in central and western Mongolia. *Quaternary*
1067 *Proceedings* **6**, 153–167 (1998).
- 1068 **26.** Lekens, W. A. H., Haflidason, H., Sejrup, H. P., Nygard, A., Richter, T., Vogt, C. &
1069 Frederichs, T. Sedimentation history of the northern North Sea Margin during the last
1070 150 ka. *Quat. Sci. Rev.* **28**, 469–483 (2009).
- 1071 **27.** Li, Y. *et al.* Timing and extent of Quaternary glaciations in the Tianger Range, eastern
1072 Tian Shan, China, investigated using ¹⁰Be surface exposure dating. *Quat. Sci. Rev.* **98**,
1073 7–23 (2014).
- 1074 **28.** Owen, L. A. & Dortch, J. M. Nature and timing of Quaternary glaciation in the
1075 Himalayan-Tibetan orogen. *Quat. Sci. Rev.* **88**, 14–54 (2014).
- 1076 **29.** Owen, L. A., Yi, C., Finkel, R. C. & Davis, N. K. Quaternary glaciation of Gurla
1077 Mandhata (Naimon’anyi). *Quat. Sci. Rev.* **29**, 1817–1830 (2010).
- 1078 **30.** Stein, R., Nam, S., Grobe, H. & Hubberten, H. Late Quaternary glacial history and
1079 short-term ice-rafted debris fluctuations along the East Greenland continental margin.
1080 *Geological Society, London, Special Publications* **111**, 135–151 (1996).
- 1081 **31.** Stübner, K., Grin, E., Hidy, A. J., Schaller, M., Gold, R. D., Ratschbacher, L. &
1082 Ehlers, T. Middle and Late Pleistocene glaciations in the southwestern Pamir and their
1083 effects on topography. *Earth Planet. Sci. Lett.* **466**, 181–194 (2017).
- 1084 **32.** Thackray, G. D. Varied climatic and topographic influences on Late Pleistocene
1085 mountain glaciation in the western United States. *J. Quat. Sci.* **23**, 671–681 (2008).
- 1086 **33.** Arnold, N. S., van Andel, T. H. & Valen, V. Extent and dynamics of the Scandinavian
1087 Ice Sheet during Oxygen Isotope Stage 3 (65,000–25,000 yr B.P.) *Quat. Res.* **57**, 38–
1088 48 (2002).
- 1089 **34.** Mangerud, J., Gyllencreutz, R., Lohne, Ø. & Svendsen, J. I. Glacial History of
1090 Norway. In: Ehlers, J., Gibbard, P. L. & Hughes, P. D. (eds). *Quaternary Glaciation*
1091 *Extent and Chronology: a closer look. Developments in Quaternary Science* **15**,
1092 Elsevier, Amsterdam (2011).

- 1093 35. Obst, K., Nachtweide, C. & Müller, U. Late Saalian and Weichselian glaciations in
1094 the German Baltic Sea documented by Pleistocene successions at the southeastern
1095 margin of the Arkona Basin. *Boreas* **46**, 18–33 (2017).
- 1096 36. Murton, D. K. Late Pleistocene palaeoenvironmental change in the Vale of York and
1097 Humber gap. PhD thesis, University of Cambridge (2017).
- 1098 37. Owen, L., Finkel, R. C., Haizhou, M., Spencer, J. Q., Derbyshire, E., Barnard, P. L. &
1099 Caffee, M. W. Timing and style of Late Quaternary glaciation in northeastern Tibet.
1100 *Geol. Soc. Am. Bull.* **115**, 1356–1364 (2003).
- 1101 38. Owen, L. A., Robinson, R., Benn, D. I., Finkel, R. C., Davis, N. K., Yi, C., Putkonen,
1102 J., Li, D. & Murray, A. S. Quaternary glaciation of Mount Everest. *Quat. Sci. Rev.* **28**,
1103 1412–1433 (2009).
- 1104 39. Rother, H., Lehmkuhl, F., Fink, D. & Nottebaum, V. Surface exposure dating reveals
1105 MIS-3 glacial maximum in the Khangai Mountains of Mongolia. *Quat. Res.* **82**, 297–
1106 308 (2014).
- 1107 40. Syvitski, J. P., Jennings, A. E. & Andrews, J. T. High-resolution seismic evidence for
1108 multiple glaciation across the Southwest Iceland shelf. *Arct. Antarct. Alp. Res.* **31**, 50–
1109 57 (1999).
- 1110 41. Barr, I. D. & Solomina, O. Reprint of ‘Pleistocene and Holocene glacier fluctuations
1111 upon the Kamchatka Peninsula’. *Glob. Planet. Change* **134**, 155–165 (2015).
- 1112 42. Dredge, L. A. & Thorleifson, L. H. The Middle Wisconsinan history of the Laurentide
1113 Ice Sheet. *Géographie physique et Quaternaire* **41**, 215–235 (1987).
- 1114 43. Van Andel, T. H. & Tzedakis, P. C. Palaeolithic landscapes of Europe and environs,
1115 150,000–25,000 years ago: An overview. *Quat. Sci. Rev.* **15**, 481–500 (1996).
- 1116 44. Marshall, S. J., Tarasov, L., Clarke, G. K. C. & Peltier, W. R. Glaciological
1117 reconstruction of the Laurentide Ice Sheet: physical processes and modelling
1118 challenges. *Can. J. Earth Sci.* **37**, 769–793 (2000).
- 1119 45. Zhao, J., Liu, S., He, Y. & Song, Y. Quaternary glacial chronology of the
1120 Ateoyinake River Valley, Tianshan Mountains, China. *Geomorphology* **103**, 276–
1121 284 (2009).
- 1122 46. Zhao, J., Yin, X., Harbor, J. M., Lai, Z., Liu, S. & Li, Z. Quaternary glacial
1123 chronology of the Kansas River valley, Altai Mountains, China. *Quat. Int.* **311**, 44–53
1124 (2013).

- 1125 **47.** Helmens, K. F. The Last Interglacial-Glacial cycle (MIS 5-2) re-examined based on
1126 long proxy records from central and northern Europe. *Quat. Sci. Rev.* **86**, 115–143
1127 (2014).
- 1128 **48.** Larsen, E. *et al.* Late Pleistocene glacial and lake history of northwestern Russia.
1129 *Boreas* **35**, 394–424 (2006).
- 1130 **49.** Owen, L. A., Caffee, M. W., Bovard, K. R., Finkel, R. C. & Sharma, M. C. Terrestrial
1131 cosmogenic nuclide surface exposure dating of the oldest glacial successions in the
1132 Himalayan orogen: Ladakh Range, northern India. *Geol. Soc. Am. Bull.* **118**, 383–392
1133 (2006).
- 1134 **50.** Stauch, G. & Lehmkuhl, F. Quaternary glaciations in the Verkhoyansk Mountains,
1135 Northeast Siberia. *Quat. Res.* **74**, 145–155 (2010).
- 1136 **51.** Ward, B. C., Bond, J. D. & Gosse, J. C. Evidence for a 55-50 ka (early Wisconsin)
1137 glaciation of the Cordilleran Ice Sheet, Yukon Territory, Canada. *Quat. Res.* **68**, 141–
1138 150 (2007).
- 1139 **52.** Astakhov, V. I. Late Quaternary glaciation of the northern Urals: a review and new
1140 observations. *Boreas* **47**, 379–389 (2018).
- 1141 **53.** Astakhov, V., Shkatova, V., Zastrozhnov, A. & Chuyko, M. Glaciomorphological
1142 Map of the Russian Federation. *Quat. Int.* **420**, 4–14 (2016).
- 1143 **54.** Carr, S. R., Holmes, R., van der Meer, J. J. M. & Rose, J. The Last Glacial Maximum
1144 in the North Sea Basin: micromorphological evidence of extensive glaciation. *J. Quat.*
1145 *Sci.* **21**, 131–153 (2006).
- 1146 **55.** Glushkova, O. Y. Late Pleistocene glaciations in North-East Asia. In: Ehlers, J.,
1147 Gibbard, P. L. & Hughes, P. D. (eds). Quaternary Glaciation Extent and Chronology:
1148 a closer look. *Developments in Quaternary Science* **15**, Elsevier, Amsterdam (2011).
- 1149 **56.** Hjort, C. A glacial chronology for northern East Greenland. *Boreas* **10**, 259-274
1150 (1981).
- 1151 **57.** Kaufman, D. S., Young, N. E., Briner, J. P. & Manley, W. F. Alaska palaeo-glacier
1152 atlas (version 2). In: Ehlers, J., Gibbard, P. L. & Hughes, P. D. (eds). Quaternary
1153 Glaciation Extent and Chronology: a closer look. *Developments in Quaternary*
1154 *Science* **15**, Elsevier, Amsterdam (2011).
- 1155 **58.** Kleman, J., Fastook, J., Ebert, K., Nilsson, J. & Caballero, R. Pre-LGM NH ice sheet
1156 topography. *Clim. Past* **9**, 2365–2378 (2013).

- 1157 **59.** Lundqvist, J. Glacial history of Sweden. In: Ehlers, J. & Gibbard, P. L. (eds.)
1158 Quaternary Glaciations – Extent and Chronology, Volume 2. *Developments in*
1159 *Quaternary Science* **2**, Elsevier, Amsterdam (2004).
- 1160 **60.** Möller, P., Alexanderson, H., Funder, S. & Hjort, C. The Taimyr Peninsula and the
1161 Severnaya Zemlya archipelago, Arctic Russia: a synthesis of glacial history and
1162 palaeo-environmental change during the Last Glacial cycle (MIS 5e-2). *Quat. Sci.*
1163 *Rev.* **107**, 149–181 (2015).
- 1164 **61.** Rolfe, C. J., Hughes, P. H., Fenton, C. R., Schnabel, C., Xu, S. & Brown, A. G. Paired
1165 ^{26}Al and ^{10}Be exposure ages from Lundy: new evidence for the extent and timing of
1166 Devensian glaciation in the southern British Isles. *Quat. Sci. Rev.* **43**, 61–73 (2012).
- 1167 **62.** Svendsen, J. I. *et al.* Late Quaternary ice sheet history of northern Eurasia. *Quat. Sci.*
1168 *Rev.* **23**, 1229–1271 (2004).
- 1169 **63.** Svendsen, J. I., Krüger, L. C., Mangerud, J., Astakhov, V. I., Paus, A., Nazarov, D. &
1170 Murray, A. Glacial and vegetation history of the Polar Ural Mountains in northern
1171 Russia during the Last Ice Age, Marine Isotope Stages 5-2. *Quat. Sci. Rev.* **92**, 409–
1172 428 (2014).
- 1173 **64.** Turner, D. G., Ward, B. C., Froese, D. G., Lamothe, M., Bond, J. D. & Bigelow, N.
1174 H. Stratigraphy of Pleistocene glaciations in the St Elias Mountains, southwest
1175 Yukon, Canada. *Boreas* **45**, 521–536 (2016).
- 1176 **65.** Kleman, J., Fastook, J. & Stroeven, A. P. Geologically and geomorphologically
1177 constrained numerical model of Laurentide Ice Sheet inception and build-up. *Quat.*
1178 *Int.* **95–96**, 87–98 (2002).
- 1179 **66.** Davies, B. J. British and Fennoscandian Ice-Sheet interactions during the Quaternary.
1180 PhD thesis, University of Durham (2008).
- 1181 **67.** Eccleshall, S. V., Hormes, A., Hovland, A. & Preusser, F. Constraining the
1182 chronology of Pleistocene glaciations on Svalbard: Kapp Ekholm re-visited. *Boreas*
1183 **45**, 790–803 (2016).
- 1184 **68.** Grin, E., Ehlers, T. A., Schaller, M., Sulaymonova, V., Ratschbacher, L. & Gloaguen,
1185 R. ^{10}Be surface-exposure age dating of the Last Glacial Maximum in the northern
1186 Pamir (Tajikistan). *Quat. Geochronol.* **34**, 47–57 (2016).
- 1187 **69.** Hall, R. D. & Shroba, R. R. Soil evidence for a Glaciation Intermediate between the
1188 Bull Lake and Pinedale Glaciations at Fremont Lake, Wind River Range, Wyoming,
1189 U.S.A. *Arct. Antarct. Alp. Res.* **27**, 89–98 (1995).

- 1190 **70.** Sejrup, H. P., Larsen, E., Landvik, J., King, E. L., Haflidason, H., Nesje, A.
1191 Quaternary glaciations in southern Fennoscandia: evidence from southwestern
1192 Norway and the northern North Sea region. *Quat. Sci. Rev.* **19**, 667–685 (2000).
- 1193 **71.** Sejrup, H. P. *et al.* Pleistocene glacial history of the NW European continental
1194 margin. *Mar. Petrol. Geol.* **22**, 1111–1129 (2005).
- 1195 **72.** Stewart, M. A. & Lonergan, L. Seven glacial cycles in the middle-late Pleistocene of
1196 northwest Europe: Geomorphic evidence from buried tunnel valleys. *Geology* **39**,
1197 283–286 (2011).
- 1198 **73.** Winkelmann, D., Schafer, C., Stein, R. & Mackensen, A. Terrigenous events and
1199 climate history of the Sophia Basin, Arctic Ocean. *Geochem. Geophys. Geosyst.* **9**,
1200 Q07023 (2008).
- 1201 **74.** Zech, W., Zech, R., Zech, M., Leiber, K., Dippold, M., Frechen, M., Bussert, R. &
1202 Andreev, A. Obliquity forcing of Quaternary glaciation and environmental changes in
1203 NE Siberia. *Quat. Int.* **234**, 133–145 (2011).
- 1204 **75.** Zech, R., Röhringer, I., Sosin, P., Kabgov, H., Merchel, S., Akhmadaliev, S. & Zech,
1205 W. Late Pleistocene glaciations in the Gissar Range, Tajikistan, based on ¹⁰Be surface
1206 exposure dating. *Palaeogeogr., Palaeoclimatol., Palaeoecol.* **369**, 253–261 (2013).
- 1207 **76.** Lambeck, K., Purcell, A., Funder, S., Kjær, K. H., Larsen, E. & Möller, P. Constraints
1208 on the Late Saalian to early Middle Weichselian ice sheet of Eurasia from field data
1209 and rebound modelling. *Boreas* **35**, 539–575 (2006).
- 1210 **77.** Blomdin, R. *et al.* Evaluating the timing of former glacier expansions in the Tian
1211 Shan: A key step towards robust spatial correlations. *Quat. Sci. Rev.* **153**, 78–96
1212 (2016).
- 1213 **78.** Fu, P., Stroeven, A. P., Harbor, J. M., Hättstrand, C., Heyman, J., Caffee, M. W. &
1214 Zhou, L. Paleoglaciation of Shaluli Shan, southeastern Tibetan Plateau. *Quat. Sci.*
1215 *Rev.* **64**, 121–135 (2013).
- 1216 **79.** Lisiecki, L. E. & Raymo, M. E. A Pliocene-Pleistocene stack of 57 globally
1217 distributed benthic $\delta^{18}\text{O}$ records. *Paleoceanography and Paleoclimatology* **20**,
1218 PA1003 (2005).
- 1219 **80.** Zhao, J., Wang, J., Harbor, J. M., Liu, S., Yin, X. & Wu, Y. Quaternary glaciations
1220 and glacial landform evolution in the Tailan River valley, Tianshan Range, China.
1221 *Quat. Int.* **358**, 2–11 (2015).
- 1222 **81.** Astakhov, V. Middle Pleistocene glaciations of the Russian North. *Quat. Sci. Rev.* **23**,
1223 1285–1311 (2004).

- 1224 **82.** Funder, S., Hjort, C., Landvik, J. Y., Nam, S-I., Reeh, N. & Stein, R. History of a
1225 stable ice margin – East Greenland during the Middle and Upper Pleistocene. *Quat.*
1226 *Sci. Rev.* **17**, 77–123 (1998).
- 1227 **83.** Chadwick, O. A., Hall, R. D. & Phillips, F. M. Chronology of Pleistocene glacial
1228 advances in the central Rocky Mountains. *Geol. Soc. Am. Bull.* **109**, 1143–1452
1229 (1997).
- 1230 **84.** Funder, S. The Baffin Bay Region During the Last Interglaciation: Evidence from
1231 Northwest Greenland. *Géographie physique at Quaternaire* **43**, 255–262 (1989).
- 1232 **85.** Karabanov, E. B., Prokopenko, A. A., Williams, D. F. & Colman, S. M. Evidence
1233 from Lake Baikal for Siberian Glaciation during Oxygen-Isotope Substage 5d. *Quat.*
1234 *Res.* **50**, 46–55 (1998).
- 1235 **86.** Phillips, F. M., Zreda, M. G., Gosse, J. C., Klein, J., Evenson, E. B., Hall, R. D.,
1236 Chadwick, O. A. & Sharma, P. Cosmogenic ^{36}Cl and ^{10}Be ages of Quaternary glacial
1237 and fluvial deposits of the Wind River Range, Wyoming. *Geol. Soc. Am. Bull.* **109**,
1238 1453–1463 (1997).
- 1239 **87.** Balco, G. & Rovey II, C. W. Absolute chronology for major Pleistocene advances of
1240 the Laurentide Ice Sheet. *Geology* **38**, 795–798 (2010).
- 1241 **88.** Barendregt, R. W., Andriashek, L. & Jackson, L. E. Evidence for Early Pleistocene
1242 glaciation obtained from borecores collected in East-Central Alberta, Canada.
1243 *American Geophysical Union Meeting*, GP13A-3574, San Francisco, USA (2014).
- 1244 **89.** Basilian, A. C., Nikolskiy, P. A. & Anisimov, M. A. Pleistocene glaciation of the
1245 New Siberian Islands - no more doubt. *IPY News* **12**, 7–9 (2008).
- 1246 **90.** Böse, M., Lüthgens, C., Lee, J. R. & Rose, J. Quaternary glaciations of northern
1247 Europe. *Quat. Sci. Rev.* **44**, 1–25 (2012).
- 1248 **91.** Curry, B. B., Grimley, D. A. & McKay III, E. D. Quaternary Glaciations in Illinois.
1249 In: Ehlers, J., Gibbard, P. L. & Hughes, P. D. (eds). Quaternary Glaciation Extent and
1250 Chronology: a closer look. *Developments in Quaternary Science* **15**, Elsevier,
1251 Amsterdam (2011).
- 1252 **92.** Ehlers, J. Reconstructing the dynamics of the North-west European Pleistocene ice
1253 sheets. *Quat. Sci. Rev.* **9**, 71–83 (1990).
- 1254 **93.** Ehlers, J., Gibbard, P. L. & Hughes, P. D. (eds). Quaternary Glaciation Extent and
1255 Chronology: a closer look. *Developments in Quaternary Science* **15**, Elsevier,
1256 Amsterdam (2011).

- 1257 **94.** Eissmann, L. Quaternary geology of eastern Germany (Saxony, Saxon-Anhalt, South
1258 Brandenburg, Thuringia), type area of the Elsterian and Saalian Stages in Europe.
1259 *Quat. Sci. Rev.* **21**, 1275–1346 (2002).
- 1260 **95.** Gibbard, P. L. & Clark, C. D. Pleistocene glaciation limits in Great Britain. In: Ehlers,
1261 J., Gibbard, P. L. & Hughes, P. D. (eds). Quaternary Glaciation Extent and
1262 Chronology: a closer look. *Developments in Quaternary Science* **15**, Elsevier,
1263 Amsterdam (2011).
- 1264 **96.** Gozhik, P., Lindner, L. & Marks, L. Late Early and early Middle Pleistocene limits of
1265 Scandinavian glaciation in Poland and Ukraine. *Quat. Int.* **271**, 31–37 (2010).
- 1266 **97.** Hamblin, R. J. O., Moorlock, B. S. P., Rose, J., Lee, J. R., Riding, J. B., Booth, S. J.
1267 & Pawley, S. M. Revised Pre-Devensian glacial stratigraphy in Norfolk, England,
1268 based on mapping and till provenance. *Neth. J. Geosci.* **84**, 77–85 (2005).
- 1269 **98.** Hughes, P. D. & Gibbard, P. L. Global glacier dynamics during 100 ka Pleistocene
1270 glacial cycles. *Quat. Res.* **90**, 222–243 (2018).
- 1271 **99.** Jackson, L. E., Andriashek, L. D. & Phillips, F. M. Limits of successive Middle and
1272 Late Pleistocene continental ice sheets, interior plains of southern and central Alberta
1273 and adjacent areas. In: Ehlers, J., Gibbard, P. L. & Hughes, P. D. (eds). Quaternary
1274 Glaciation Extent and Chronology: a closer look. *Developments in Quaternary
1275 Science* **15**, Elsevier, Amsterdam (2011).
- 1276 **100.** Jakobsson, M., Polyak, L., Edwards, M., Kleman, J. & Coakley, B. Glacial
1277 geomorphology of the Central Arctic Ocean: the Chukchi Borderland and the
1278 Lomonosov Ridge. *Earth Surf. Process. Landforms* **33**, 526–545 (2008).
- 1279 **101.** Laban, C. & van der Meer, J. J. M. Pleistocene Glaciation in The Netherlands. In:
1280 Ehlers, J., Gibbard, P. L. & Hughes, P. D. (eds). Quaternary Glaciation Extent and
1281 Chronology: a closer look. *Developments in Quaternary Science* **15**, Elsevier,
1282 Amsterdam (2011).
- 1283 **102.** Marks, L. Pleistocene glacial limits in the territory of Poland. *Przegląd Geologiczny*
1284 **53**, 988–993 (2005).
- 1285 **103.** Marks, L. Quaternary Glaciations in Poland. In: Ehlers, J., Gibbard, P. L. & Hughes,
1286 P. D. (eds). Quaternary Glaciation Extent and Chronology: a closer look.
1287 *Developments in Quaternary Science* **15**, Elsevier, Amsterdam (2011).
- 1288 **104.** Marks, L. *et al.* Revised limit of the Saalian ice sheet in central Europe. *Quat. Int.*
1289 **478**, 59–74 (2018).

- 1290 **105.** Niessen, F., Hong, J. K., Hegewald, A., Matthiessen, J., Stein, R., Kim, H., Kim, S.,
1291 Jensen, L., Jokat, W., Nam, S-I. & Kang, S-H. Repeated Pleistocene glaciation of
1292 the East Siberian continental margin. *Nat. Geosci.* **6**, 842–846 (2013).
- 1293 **106.** Roskosch, J., Winsemann, J., Polom, U., Brandes, C., Tsukamoto, S., Weitkamp, A.,
1294 Bartholomäus, W. A., Henningsen, D. & Frechen, M. Luminescence dating of ice-
1295 marginal deposits in northern Germany: evidence for repeated glaciations during the
1296 Middle Pleistocene (MIS 12 to MIS 6). *Boreas* **44**, 103–126 (2015).
- 1297 **107.** Colleoni, F., Wekerle, C., Näslund, J.-O., Brandefelt, J. & Masina, J. Constraint on
1298 the penultimate glacial maximum NH ice topography (= 140 kyrs BP). *Quat. Sci.*
1299 *Rev.* **137**, 97–112 (2016).
- 1300 **108.** Peltier, W. R. Global glacial isostasy and the surface of the ice-age Earth: The ICE-
1301 5G (VM2) model and GRACE. *Annu. Rev. Earth Planet. Sci.* **32**, 111–149 (2004).
- 1302 **109.** Anderson, R. S., Dühnforth, M., Colgan, W. & Anderson, L. Far-flung moraines:
1303 Exploring the feedback of glacial erosion on the evolution of glacier length.
1304 *Geomorphology* **179**, 269–285 (2012).
- 1305 **110.** Dahlgren, K. I. T., Vorren, T. O. & Laberg, J. S. Late Quaternary glacial
1306 development of the mid-Norwegian margin – 65 to 68°N. *Mar. Pet. Geol.* **19**, 1089–
1307 1113 (2002).
- 1308 **111.** Geirsdóttir, Á., Miller, G. H. & Andrews, J. T. Glaciation, erosion and landscape
1309 evolution of Iceland. *J. Geodyn.* **43**, 170–186 (2007).
- 1310 **112.** Hjelstuen, B. O., Sejrup, H. P., Haflidason, H., Nygård, A., Ceramicola, S. & Bryn,
1311 P. Late Cenozoic glacial history and evolution of the Storegga Slide area and
1312 adjacent slide flank regions, Norwegian continental margin. In: Solheim, A., Bryn,
1313 P., Berg, K., Sejrup, H. P. & Mienert, J. *Ormen Lange - an Integrated Study for Safe*
1314 *Field Development in the Storegga Submarine Area*, 57–69 (2005).
- 1315 **113.** Kuhle, M. The Pleistocene Glaciation (LGP and pre-LGP, Pre-LGM) of SE Iranian
1316 Mountains exemplified by the Kuh-i-Jupar, Kuh-i-Lalezar and Kuh-i-Hezar massifs
1317 in the Zagros. *Polarforschung* **77**, 71–88 (2007).
- 1318 **114.** Licciardi, J. M. & Pierce, K. L. Cosmogenic exposure-age chronologies of Pinedale
1319 and Bull Lake glaciations in greater Yellowstone and the Teton Range, USA. *Quat.*
1320 *Sci. Rev.* **27**, 814–831 (2008).
- 1321 **115.** Montelli, A., Dowdeswell, J. A., Ottesen, D. & Johansen, S. E. Ice-sheet dynamics
1322 through the Quaternary on the mid-Norwegian continental margin inferred from 3D
1323 seismic data. *Mar. Pet. Geol.* **80**, 228–242 (2017).

- 1324 **116.** Nielsen, T. & Kuijpers, A. Only 5 southern Greenland shelf edge glaciations since
1325 the early Pliocene. *Sci. Rep.* **3**, 1875 (2013).
- 1326 **117.** Nikolskiy, P. A., Basilyan, A. E. & Zazhigin, V. S. New data on the age of the
1327 glaciation in the New Siberian Islands (Russian Eastern Arctic). *Dokl. Earth Sci.*
1328 **475**, 748–752 (2017).
- 1329 **118.** O’Regan, M. *et al.* The De Long Trough: a newly discovered glacial trough on the
1330 East Siberian continental margin. *Clim. Past* **13**, 1269–1284 (2017).
- 1331 **119.** Strunk, A., Knudsen, M. F., Egholm, D. L., Jansen, J. D., Levy, L. B., Jacobsen, B.
1332 H. & Larsen, N. K. One million years of glaciation and denudation history in west
1333 Greenland. *Nat. Commun.* **8**, 14199 (2017).
- 1334 **120.** Vorren, T. O. & Laberg, J. S. Trough mouth fans – palaeoclimate and ice-sheet
1335 monitors. *Quat. Sci. Rev.* **16**, 865–881 (1997).
- 1336 **121.** White, T. S., Bridgland, D. R., Westaway, R., Howard, A. J. & White, M. J.
1337 Evidence from the Trent terrace archive, Lincolnshire, UK, for lowland glaciation of
1338 Britain during the Middle and Late Pleistocene. *P. Geologist. Assoc.* **121**, 141–153
1339 (2010).
- 1340 **122.** White, T. S., Bridgland, D. R., Westaway, R. & Straw, A. Evidence for late Middle
1341 Pleistocene glaciation of the British margin of the southern North Sea. *J. Quat. Sci.*
1342 **32**, 261–275 (2017).
- 1343 **123.** Beets, D. J., Meijer, T., Beets, C. J., Cleveringa, P., Laban, C. & van der Spek, A. J.
1344 F. Evidence for a Middle Pleistocene glaciation of MIS 8 age in the southern North
1345 Sea. *Quat. Int.* **133-134**, 7–19 (2005).
- 1346 **124.** Hodell, D. A., Channell, J. E. T., Curtis, J. H., Romero, O. E. & Röhl, U. Onset of
1347 ‘Hudson Strait’ Heinrich events in the eastern North Atlantic at the end of the
1348 middle Pleistocene transition (~640 ka)? *Paleoceanography* **23**, PA4218 (2008).
- 1349 **125.** Krissek, L. A. Late Cenozoic ice-rafting records from Leg 145 sites in the North
1350 Pacific: Late Miocene onset, Late Pliocene intensification, and Pliocene-Pleistocene
1351 events. In: Rea, D. K., Basov, I. A., Scholl, D. W. & Allan, J. F. (Eds.). *Proceedings*
1352 *of the Ocean Drilling Program, Scientific Results* **145** (1995).
- 1353 **126.** Spooner, I. S., Osborn, G. D., Barendregt, H. & Irving, E. A Middle Pleistocene
1354 (isotope stage 10) glacial sequence in the Stikine River valley, British Columbia.
1355 *Can. J. Earth Sci.* **33**, 1428–1438 (1996).

- 1356 **127.** Krzyszkowski, D., Wachecka-Kotkowska, L., Wieczorek, D. & Stoiński, A.
1357 Petrography of glacial tills in the Szczerców outcrop, central Poland – problems of
1358 stratigraphic interpretation. *Studia Quaternaria* **32**, 99–108 (2015).
- 1359 **128.** Aber, J. S. The glaciation of northeastern Kansas. *Boreas* **20**, 297–314 (1991).
- 1360 **129.** Colgan, P. M. Early middle Pleistocene glacial sediments (780000–620000 BP) near
1361 Kansas City, northeastern Kansas and northwestern Missouri, USA. *Boreas* **28**, 477–
1362 489 (1999).
- 1363 **130.** Toucanne, S. *et al.* A 1.2 Ma record of glaciation and fluvial discharge from the
1364 West European Atlantic margin. *Quat. Sci. Rev* **28**, 2974–2981 (2009).
- 1365 **131.** Andriashek, L. D. & Barendregt, R. W. Evidence for Early Pleistocene glaciation
1366 from borecore stratigraphy in north-central Alberta, Canada. *Can. J. Earth Sci.* **54**,
1367 445–460 (2017).
- 1368 **132.** Batchelor, C. L., Ottesen, D. & Dowdeswell, J. A. Quaternary evolution of the
1369 northern North Sea margin through glacial debris-flow and contourite deposition.
1370 *J. Quat. Sci.* **32**, 416–426 (2017).
- 1371 **133.** Ottesen, D., Batchelor, C. L., Dowdeswell, J. A. & Løseth, H. Morphology and
1372 pattern of Quaternary sedimentation in the North Sea Basin (52–62°N). *Mar. Petrol.*
1373 *Geol.* **98**, 836–859 (2018).
- 1374 **134.** Bierman, P. R., Shakun, J. D., Corbett, L. B., Zimmerman, S. R. & Rood, D. H. A
1375 persistent and dynamic East Greenland Ice Sheet over the past 7.5 million years.
1376 *Nature* **540**, 256–260 (2016).
- 1377 **135.** Laberg, J. S., Forwick, M., Husum, K. & Nielsen, T. A re-evaluation of the
1378 Pleistocene behaviour of the Scoresby Sund sector of the Greenland Ice Sheet.
1379 *Geology* **41**, 1231–1234 (2013).
- 1380 **136.** Sejrup, H. P., Aarseth, I. & Haflidason, H. The Quaternary succession in the
1381 northern North Sea. *Mar. Geol.* **101**, 103–111 (1991).
- 1382 **137.** Thierens, M. *et al.* Ice-rafting from the British-Irish ice sheet since the earliest
1383 Pleistocene (2.6 million years ago): Implications for long-term mid-latitude ice-
1384 sheet growth in the North Atlantic region. *Quat. Sci. Rev.* **44**, 229–240 (2012).
- 1385 **138.** Barendregt, R. W. & Duk-Rodkin, A. Chronology and extent of late Cenozoic ice
1386 sheets in North America: a magnetostratigraphic assessment. In: Ehlers, J., Gibbard
1387 P.L. & Hughes P.D. (eds.), *Quaternary Glaciations - Extent and Chronology, Part*
1388 *IV: a closer look*. *Developments in Quaternary Science* **15**, Elsevier, Amsterdam
1389 (2011).

- 1390 **139.** Dowdeswell, J. A. & Ottesen, D. Buried iceberg ploughmarks in the early
1391 Quaternary sediments of the central North Sea: a two-million-year record of glacial
1392 influence from 3D seismic data. *Mar. Geol.* **344**, 1–9 (2013).
- 1393 **140.** Kleman, J., Stroeven, A. P. & Lundqvist, J. Patterns of Quaternary ice sheet erosion
1394 and deposition in Fennoscandia and a theoretical framework for explanation.
1395 *Geomorphology* **97**, 73–90 (2008).
- 1396 **141.** Knies, J. *et al.* The Plio-Pleistocene glaciation of the Barents Sea-Svalbard region: a
1397 new model based on revised chronostratigraphy. *Quat. Sci. Rev.* **28**, 812–829 (2009).
- 1398 **142.** Rea, B. R. *et al.* Extensive marine-terminating ice sheets in Europe from 2.5 million
1399 years ago. *Sci. Adv.* **4**, eaar8327 (2018).
- 1400 **143.** Solgaard, A. M., Reeh, N., Japsen, P., Nielsen, T. Snapshots of the Greenland ice
1401 sheet configuration in the Pliocene to early Pleistocene. *J. Glaciol.* **57**, 871–880
1402 (2011).
- 1403 **144.** Bailey, I., Hole, G. M., Foster, G. L., Wilson, P. A., Storey, C. D., Trueman, C. N. &
1404 Raymo, M. E. An alternative suggestion for the Pliocene onset of major northern
1405 hemisphere glaciation based on the geochemical provenance of North Atlantic
1406 Ocean ice-rafted debris. *Quat. Sci. Rev.* **75**, 181–194 (2013).
- 1407 **145.** Berger, D. & Jokat, W. Sediment deposition in the northern basins of the North
1408 Atlantic and characteristic variations in shelf sedimentation along the East
1409 Greenland margin. *Mar. Pet. Geol.* **26**, 1321–1337 (2009).
- 1410 **146.** Butt, F. A., Elverhøi, A., Forsberg, C. F. & Solheim A. Evolution of the Scoresby
1411 Sund Fan, central East Greenland- evidence from ODP Site 987. *Norsk Geologisk*
1412 *Tidsskrift* **81**, 3–15 (2001).
- 1413 **147.** Hidy, A. J., Gosse, J. C., Froese, D. G., Bond, J. D., Rood, D. H. A latest Pliocene
1414 age for the earliest and most extensive Cordilleran Ice Sheet in northwest Canada.
1415 *Quat. Sci. Rev.* **61**, 77–84 (2013).
- 1416 **148.** Hofmann, J. C., Knutz, P. C., Nielsen, T. & Kuijpers, A. Seismic architecture and
1417 evolution of the Disko Bay trough-mouth fan, central West Greenland margin. *Quat.*
1418 *Sci. Rev.* **147**, 69–90 (2016).
- 1419 **149.** Jansen, E., Fronval, T., Rack, F. & Channel, J. E. T. Pliocene-Pleistocene ice rafting
1420 history and cyclicity in the Nordic Seas during the last 3.5 Myr. *Paleoceanogr.*
1421 *Paleoclimatol.* **15**, 709–721 (2000).
- 1422 **150.** Solheim, A., Faleide, J. I., Andersen, E. S., Elverhøi, A., Forsberg, C. F., Vanneste,
1423 K., Uenzelmann-Neben, G., Channell, J. E. T. Late Cenozoic seismic stratigraphy

- 1424 and glacial geological development of the East Greenland and Svalbard-Barents Sea
1425 continental margins. *Quat. Sci. Rev.* **17**, 155–184 (1998).
- 1426 **151.** Evans, J., Ó Cofaigh, C., Dowdeswell, J. A. & Wadhams, P. Marine geophysical
1427 evidence for former expansion and flow of the Greenland Ice Sheet across the north-
1428 east Greenland continental shelf. *J. Quat. Sci.* **24**, 279–293 (2009).
- 1429 **152.** Dowdeswell, J. A., Evans, J. & Ó Cofaigh, C. Submarine landforms and shallow
1430 acoustic stratigraphy of a 400 km-long fjord-shelf-slope transect, Kangerlussuaq
1431 margin, East Greenland. *Quat. Sci. Rev.* **29**, 3359–3369 (2010).
- 1432 **153.** Ó Cofaigh, C. *et al.* An extensive and dynamic ice sheet on the West Greenland
1433 shelf during the last glacial cycle. *Geology* **41**, 219–222 (2013).
- 1434 **154.** Shaw, J., Piper, D. J. W., Fader, G. B. J., King, E. L., Todd, B. J., Bell, T.,
1435 Batterson, M. J. & Liverman, D. G. E. A conceptual model of the deglaciation of
1436 Atlantic Canada. *Quat. Sci. Rev.* **25**, 2059–2081 (2006).
- 1437 **155.** Dyke, A. S., Moore, A. & Robertson, L. Deglaciation of North America, Scale
1438 1:7000000. Geological Survey of Canada, Open File 1574 (2003).
- 1439 **156.** Barr, I. D. & Clark, C. D. Late Quaternary glaciations in Far NE Russia; combining
1440 moraines, topography and chronology to assess regional and global glaciation
1441 synchrony. *Quat. Sci. Rev.* **53**, 72–87 (2012).
- 1442 **157.** Berger, G. W. & Nielsen, E. Evidence from thermoluminescence dating for Middle
1443 Wisconsinan deglaciation in the Hudson Bay Lowland of Manitoba. *Can. J. Earth*
1444 *Sci.* **28**, 240–249 (1991).
- 1445 **158.** Larsen, E., Sejrup, H. P., Janocko, J., Landvik, J. Y., Stalsberg, K. & Steinsund, P. I.
1446 Recurrent interaction between the Norwegian Channel Ice Stream and terrestrial-
1447 based ice across southwest Norway. *Boreas* **29**, 185–203 (2000).
- 1448 **159.** Dalton, A. S., Finkelstein, S. A., Barnett, P. J. & Forman, S. L. Constraining the
1449 Late Pleistocene history of the Laurentide Ice Sheet by dating the Missinaibi
1450 Formation, Hudson Bay Lowlands, Canada. *Quat. Sci. Rev.* **146**, 288–299 (2016).
- 1451 **160.** Young, R. R., Burns, J. A., Smith, D. G., Arnold, L. D. & Rains, R. B. A single, late
1452 Wisconsin, Laurentide glaciation, Edmonton area and southwestern Alberta.
1453 *Geology* **22**, 683–686 (1994).
- 1454 **161.** Guyard, H. *et al.* New insights into Late Pleistocene glacial and postglacial history
1455 of northernmost Ungava (Canada) from Pingualuit Crater Lake sediments. *Quat. Sci.*
1456 *Rev.* **30**, 3892–3907 (2011).

- 1457 **162.** Carlson, A. E., Tarasov, L. & Pico, T. Rapid Laurentide ice-sheet advance towards
1458 southern last glacial maximum limit during marine isotope stage 3. *Quat. Sci. Rev.*
1459 **196**, 118–123 (2018).
- 1460 **163.** Pico, T., Mitrovica, J. X., Braun, J. & Ferrier, K. L. Glacial isostatic adjustment
1461 deflects the path of the ancestral Hudson River. *Geology* **46**, 591–594 (2018).
- 1462 **164.** Mangerud, J., Løvlie, R., Gulliksen, S., Hufthammer, K-A., Larsen E. & Valen, V.
1463 Paleomagnetic correlations between Scandinavian Ice-Sheet fluctuations and
1464 Greenland Dansgaard-Oeschger events, 45,000-25,000 yr B.P. *Quat. Res.* **59**, 213–
1465 222 (2003).
- 1466 **165.** Sejrup, H. P. *et al.* Configuration, history and impact of the Norwegian Channel Ice
1467 Stream. *Boreas* **32**, 18–36 (2003).
- 1468 **166.** Dalton, A. S., Finkelstein, S. A., Forman, S. L., Barnett, P. J., Pico, T. & Mitrovica,
1469 J. X. Was the Laurentide Ice Sheet significantly reduced during Marine Isotope
1470 Stage 3? *Geology* **47**, 111–114 (2019).
- 1471 **167.** McMartin, I., Campbell, J. E. & Dredge, L. A. Middle Wisconsinan marine shells
1472 near Repulse Bay, Nunavut, Canada: implications for Marine Isotope Stage 3 ice-
1473 free conditions and Laurentide Ice Sheet dynamics in north-west Hudson Bay. *J.*
1474 *Quat. Sci.* **34**, 64–75 (2019).
- 1475 **168.** Johansson, P., Lunkka, J. P. & Sarala, P. The glaciation of Finland. In: Ehlers, J.,
1476 Gibbard, P. L. & Hughes, P. D. (eds). Quaternary Glaciation Extent and
1477 Chronology: a closer look. *Developments in Quaternary Science* **15**, Elsevier,
1478 Amsterdam (2011).
- 1479 **169.** Lamothe, M. Apparent thermoluminescence ages of St-Pierre sediments at
1480 Pierreville, Quebec, and the problem of anomalous fading. *Can. J. Earth Sci.* **21**,
1481 1406–1409 (1984).
- 1482 **170.** de Vernal, A., Causse, C., Hillaire-Marcel, C., Mott, R. J. & Occhietti, S.
1483 Palynostratigraphy and Th/U ages of upper Pleistocene interglacial and interstadial
1484 deposits on Cape Breton Island, eastern Canada. *Geology* **14**, 554–557 (1986).
- 1485 **171.** Berger, G. W. & Eyles, N. Thermoluminescence chronology of Toronto-area
1486 Quaternary sediments and implications for the extent of the midcontinent ice
1487 sheet(s). *Geology* **22**, 31–34 (1994).
- 1488 **172.** Karrow, P. F., Dreimanis, A. & Barnett, P. J. A proposed diachronic revision of Late
1489 Quaternary time-stratigraphic classification in the eastern and northern Great Lakes
1490 area. *Quat. Res.* **54**, 1–12 (2000).

- 1491 **173.** Munroe, J. S., Perzan, Z. M. & Amidon, W. H. Cave sediments constrain the latest
1492 Pleistocene advance of the Laurentide Ice Sheet in the Champlain Valley, Vermont,
1493 USA. *J. Quat. Sci.* **31**, 893–904 (2016).
- 1494 **174.** Rémillard, A. M., St-Onge, G., Bernatchez, P., Héту, B., Buylaert, J-P., Murray, A.
1495 S. & Lajeunesse, P. Relative sea-level changes and glacio-isostatic adjustment on the
1496 Magdalen Islands archipelago (Atlantic Canada) from MIS 5 to the late Holocene.
1497 *Quat. Sci. Rev.* **171**, 216–233 (2017).
- 1498 **175.** Allard, G., Roy, M., Ghaleb, B., Richard, P. J. H., Larouche, A. C., Veillette, J. J. &
1499 Parent, M. Constraining the age of the last interglacial-glacial transition in the
1500 Hudson Bay lowlands (Canada) using U-Th dating or buried wood. *Quat.*
1501 *Geochronol.* **7**, 37–47 (2012).
- 1502 **176.** Dalton, A. S., Finkelstein, S. A., Barnett, P. J., Väiliranta, M. & Forman, S. L. Late
1503 Pleistocene chronology, palaeoecology and stratigraphy at a suite of sites along the
1504 Albany River, Hudson Bay Lowlands, Canada. *Palaeogeogr., Palaeoclimatol.,*
1505 *Palaeoecol* **492**, 50–63 (2018).
- 1506 **177.** Ehlers, J. & Gibbard, P. L. Quaternary Glaciations – Extent and Chronology.
1507 *Developments in Quaternary Science 2*. Elsevier, Amsterdam (2004).
- 1508 **178.** Dorale, J. A., Onac, B. P., Fornós, J. J., Ginés, J., Ginés, A., Tuccimei, P. & Peate,
1509 D. W. Sea-level highstand 81,000 years ago in Mallorca. *Science* **327**, 860–863
1510 (2010).
- 1511 **179.** Batchelor, C. L., Dowdeswell, J. A. & Pietras, J. T. Variable history of Quaternary
1512 ice-sheet advance across the Beaufort Sea margin, Arctic Ocean. *Geology* **41**, 131–
1513 134 (2013).
- 1514 **180.** Dubé-Loubert, H., Roy, M., Allard, G., Lamothe, M. & Veillette, J. J. Glacial and
1515 nonglacial events in the eastern James Bay lowlands, Canada. *Can. J. Earth Sci.* **50**,
1516 379–396 (2013).
- 1517 **181.** Arkhipov, S. A. Pleistocene chronostratigraphy in northern Siberia. Proceedings of
1518 the First International Colloquium on Quaternary stratigraphy of Asia and Pacific
1519 Area, Osaka, 163–177 (1987).
- 1520 **182.** Arkhipov, S. A. Chronostratigraphy of Pleistocene in northern Siberia. *Russ. Geol.*
1521 *Geophys.* **6**, 13–21 (1989).
- 1522 **183.** Jakobsson, M. *et al.* Evidence for an ice shelf covering the central Arctic Ocean
1523 during the penultimate glaciation. *Nat. Commun.* **7**, 10365 (2016).

- 1524 **184.** Huscroft, C. A., Ward, B. C., Barendregt, R. W., Jackson, L. E. & Opdyke, N. D.
1525 Pleistocene volcanic damming of Yukon River and the maximum age of the Reid
1526 Glaciation, west-central Yukon. *Can. J. Earth Sci.* **41**, 151–164 (2004).
- 1527 **185.** Lindner, L., Bogucki, A., Chlebowski, R. & Gożik, P. The importance of glacial till
1528 occurrence in loess type sections of Poland and Ukraine. *Przegląd Geologiczny* **52**,
1529 331–335 (2004).
- 1530 **186.** Shepps, V. C., White, G. W., Droste, J. B. & Sitler, R. F. Glacial geology of
1531 northwestern Pennsylvania. *Pennsylvania Geological Survey, 4th Series, Bulletin G*
1532 **32**, 59 (1959).
- 1533 **187.** White, G. W. Pleistocene deposits of the north-western Allegheny Plateau, USA.
1534 *Quarterly Jour. Geo. Soc. London* **124**, 131–151 (1968).
- 1535 **188.** Marchand, D., Ciolkosz, E. J., Bucek, M. E. & Crowl, G. H. *Quaternary Deposits*
1536 *and Soils of the Central Susquehanna Valley of Pennsylvania*. Agronomy
1537 Department, Pennsylvania State University, University Park (1978).
- 1538 **189.** Braun, A., Kuo, C-Y., Shum, C. K., Wu, P., van der Wal, W. & Fotopoulos, G.
1539 Glacial isostatic adjustment at the Laurentide ice sheet margin: Models and
1540 observations in the Great Lake region. *J. Geodyn.* **46**, 165–173 (2008).
- 1541 **190.** Braun, D. D. The glaciation of Pennsylvania, USA. In: Ehlers, J., Gibbard, P. L. &
1542 Hughes, P. D. (eds). *Quaternary Glaciation Extent and Chronology: a closer look.*
1543 *Developments in Quaternary Science* **15**, Elsevier, Amsterdam (2011).
- 1544 **191.** Gibbard, P. L. The history of the great northwest European rivers during the past
1545 three million years. *Phil. Trans. Royal Soc. London* **318**, 559–602 (1988).
- 1546 **192.** Cohen, K. M., Gibbard, P. L. & Weerts, H. J. T. North Sea palaeogeographical
1547 reconstructions for the last 1 Ma. *Neth. J. Geosci.* **93**, 7–29 (2014).
- 1548 **193.** Sejrup, H. P., Aarseth, I., Haflidason, H., Løvlie, R., Bratten, Å., Tjøstheim, G. &
1549 Forsberg, C. F. Quaternary of the Norwegian Channel; paleoceanography and
1550 glaciation history. *Nor. Geol. Tidsskr.* **75**, 65–87 (1995).
- 1551 **194.** Reinardy, B. T. I., Hjelstuen, B. O., Sejrup, H. P., Augedal, H. & Jørstad, A. Late
1552 Pliocene-Pleistocene environments and glacial history of the northern North Sea.
1553 *Quat. Sci. Rev.* **158**, 107–126 (2017).
- 1554 **195.** Faleide, J. I., Solheim, A., Fiedler, A., Hjelstuen, B. O., Andersen, E. S. & Vanneste,
1555 K. Late Cenozoic evolution of the western Barents Sea-Svalbard continental margin.
1556 *Glob. Planet. Change* **12**, 53–74 (1996).

- 1557 **196.** Andreassen, K., Nilssen, L. C., Rafaelsen, B. & Kuilman, L. Three-dimensional
1558 seismic data from the Barents Sea margin reveal evidence of past ice stream and
1559 their dynamics. *Geology* **32**, 729–732 (2004).
- 1560 **197.** Andreassen, K., Glad Nilssen, E. & Ødegård, C.M. Analysis of shallow gas and
1561 fluid migration within the Plio-Pleistocene sedimentary succession of the SW
1562 Barents Sea continental margin using 3D seismic data. *Geo-Mar. Lett.* **27**, 155–171
1563 (2007).
- 1564 **198.** Knutz, P. C., Hopper, J. R., Gregersen, U., Nielsen T. & Japsen, P. A contourite drift
1565 system on the Baffin Bay–West Greenland margin linking Pliocene Arctic warming
1566 to poleward ocean circulation. *Geology* **43**, 907–910 (2015).
- 1567 **199.** Pérez, L. F., Nielsen, T., Knutz, P. C., Kuijpers, A. & Damm, V. Large-scale
1568 evolution of the central-east Greenland margin: new insights to the North Atlantic
1569 glaciation history. *Glob. Planet. Change* **163**, 141–157 (2018).
- 1570 **200.** Funder, S., Bennike, O., Böcher, J., Isrealson, C., Petersen, K. S. & Símonarson, L.
1571 A. Late Pliocene Greenland – the Kap København Formation in North Greenland.
1572 *Bull. Geol. Soc. Denmark* **48**, 117–134 (2001).
- 1573 **201.** Bennike, O., Knudsen, K. L., Abrahamsen, N., Böcher, J., Cremer, H. & Wagner, B.
1574 Early Pleistocene sediments on Store Koldewey, northeast Greenland. *Boreas* **39**,
1575 603–619 (2010).
- 1576 **202.** Ottesen, D., Rise, L., Andersen, E. S., Bugge, T. & Eidvin, T. Geological evolution
1577 of the Norwegian continental shelf between 61°N and 68°N during the last 3 million
1578 years. *Nor. J. Geol.* **89**, 251–265 (2009).
- 1579 **203.** Ottesen, D., Dowdeswell, J. A. & Bugge, T. Morphology, sedimentary infill and
1580 depositional environments of the Early Quaternary North Sea Basin (56°–62°N).
1581 *Mar. Petrol. Geol.* **56**, 123–146 (2014).
- 1582 **204.** Eidvin, T. & Rundberg, Y. Late Cainozoic stratigraphy of the Tampen area (Snorre
1583 and Visund fields) in the northern North Sea, with emphasis on the chronology of
1584 early Neogene sands. *Norsk Geologisk Tidsskrift* **81**, 119–160 (2001).
- 1585 **205.** Dowsett, H., Thompson, R., Barron, J., Cronin, T., Fleming, F., Ishman, S., Poore,
1586 R. Willard, D. & Holtz Jr., T. Joint investigations of the Middle Pliocene climate I:
1587 PRISM paleoenvironmental reconstructions. *Glob. Planet. Change* **9**, 169–195
1588 (1994).

- 1589 **206.** Salzmann, U., Haywood, A. M., Lunt, D. J. The past is a guide to the future?
1590 Comparing Middle Pliocene vegetation with predicted biome distributions for the
1591 twenty-first century. *Philos. Trans. Royal Soc. A.* **367** (2008).
- 1592 **207.** Haywood, A. M., Chandler, M. A., Valdes, P. J., Salzmann, U., Lunt, D. J. &
1593 Dowsett, H. J. Comparison of mid-Pliocene climate predictions produced by the
1594 HadAM3 and GCMAM3 General Circulation Models. *Glob. Planet. Change* **66**,
1595 208–224 (2009).
- 1596 **208.** McKelvey, B. C., Chen, W. & Arculus, R. J. Provenance of Pliocene-Pleistocene
1597 ice-rafted debris, Leg 145, Northern Pacific Ocean. In: D. K. Rea, I. A. Basov, D.
1598 W. Scholl and J. F. Allan (Eds.), *Proceedings of the Ocean Drilling Program*,
1599 *Scientific Results* **145**, 195–204 (1995).